ENHANCED SENSITIVITY TEMPERATURE SENSING BASED ON SECOND ORDER BRILLOUIN SLOW LIGHT

PANG WEN SHEAN

MASTER OF ENGINEERING SCIENCE

LEE KONG CHIAN FACULTY OF ENGINEERING & SCIENCE
UNIVERSITI TUNKU ABDUL RAHMAN
SEPTEMBER 2021

ENHANCED SENSITIVITY TEMPERATURE SENSING BASED ON SECOND ORDER BRILLOUIN SLOW LIGHT

By

PANG WEN SHEAN

A dissertation submitted to the Department of Electrical Engineering,
Lee Kong Chian Faculty of Engineering & Science,
Universiti Tunku Abdul Rahman,
in partial fulfillment of the requirements for the degree of
Master of Engineering Science
September 2021

ABSTRACT

ENHANCED SENSITIVITY TEMPERATURE SENSING BASED ON SECOND ORDER BRILLOUIN SLOW LIGHT

Pang Wen Shean

In the past few decades, fiber optic sensors emerged as a technology that had shown superior sensitivity, range, resolution and measurement speed. The incorporation of fiber optic sensors into communication systems enabled sensing in harsh environments. This is to resolve the issues with sparks, electromagnetic interference and long distance transmission, which is unachievable using electronic sensors.

In the recent few decades, there is an abundance of existing and ongoing researches on discrete optical sensing (FBG, interferometer and photonic crystal fiber) and distributed optical sensing (BOTDA, BOCDA, BOFDA and BOTDR). Distributed sensing is mainly based on the nonlinear stimulated Brillouin scattering (SBS) process. Alternatively, SBS can be used to produce slow light, which is used in slow light sensing. SBS slow light sensing should be explored because the cost, complexity of configuration and difficulty in data acquisition are potentially reduced compared to contemporary distributed sensing systems. Most of the distributed sensing systems required sophisticated signal processing in order to acquire the sensing parameters.

This dissertation shows the experimental studies on the characterization of SBS in optical fiber, with continuation of work in Brillouin slow light generation and characterization. Next, Brillouin slow light is used to perform temperature sensing. The configuration comprises of a seed signal generator and sensing region. Further improvement of the sensitivity is done by exploring higher order SBS slow light in the sensing system.

In SBS characterization, 2km, 5km and 10km fiber spools are used. For the first order setup, the BS1 threshold power are 101mW, 61mW and 26mW for lengths of 2km, 5km and 10km respectively. As for the second order setup, the BS2 threshold power are 124mW, 89mW and 53mW. Then, the relative Brillouin gains of first and second order setups are compared with the initial pump power of 13.19dBm. The delay increments with increasing Brillouin gain are 1.2ns/dB for first order and 6.67ns/dB for the second order setup. Finally, the first and second order SBS slow light temperature sensing systems are investigated and compared to show the sensitivity improvement. For the first order system, the sensitivity is 1.111ns/°C. Then, it is showed that the sensitivity almost doubled to a value of 1.918ns/°C for the second order system. This increase in sensitivity should prompt for a deeper research in higher order SBS sensing. With the enhanced sensitivity of fiber sensor system, it will definitely be potentially to be applied in sectors operating in harsh environment which need crucial monitoring.

ACKNOWLEDGEMENTS

I would like to thank everyone who had contributed to the successful completion of this project. I would like to express my gratitude to my research supervisors, Dr. Shee Yu Gang, Prof. Ts. Dr. Faidz bin Abd Rahman and Prof. Dr. Faisal Rafiq Mahamd Adikan for their invaluable advice, guidance and enormous patience throughout the development of the research.

In addition, I would also like to express my gratitude to my loving parents and friends who had helped and given me encouragement and support for this research.

APPROVAL SHEET

This dissertation/thesis entitled "**ENHANCED SENSITIVITY TEMPERATURE SENSING BASED ON SECOND ORDER BRILLOUIN SLOW LIGHT"** was prepared by PANG WEN SHEAN and submitted as partial fulfillment of the requirements for the degree of Master of Engineering Science at Universiti Tunku Abdul Rahman.

Approved by:

_____
(Dr. Shee Yu Gang)
Date:……..
Supervisor
Department of Electrical Engineering
Lee Kong Chian Faculty of Engineering & Science
Universiti Tunku Abdul Rahman

_____
(Prof. Ts. Dr. Faidz bin Abd Rahman)
Date:……..
Co-supervisor
Department of Electrical Engineering
Lee Kong Chian Faculty of Engineering & Science
Universiti Tunku Abdul Rahman

_____
(Prof. Dr. Faisal Rafiq Bin Mahamd Adikan)
Date:……..
Co-supervisor
School of Electrical and Electronic Engineering
Universiti Sains Malaysia

FACULTY OF ENGINEERING AND SCIENCE

UNIVERSITI TUNKU ABDUL RAHMAN

Date: 13/09/2021

SUBMISSION OF DISSERTATION

It is hereby certified that Pang Wen Shean (ID No: 17UEM06830) has completed this dissertation entitled "Enhanced Sensitivity Temperature Sensing Based On Second Order Brillouin Slow Light" under the supervision of Dr. Shee Yu Gang (Supervisor) from the Department of Electrical Engineering, Lee Kong Chian Faculty of Engineering & Science, Prof Ts. Dr. Faidz Bin Abd Rahman (Co-Supervisor) from the Department of Electrical Engineering, Lee Kong Chian Faculty of Engineering & Science and Prof Dr. Faisal Rafiq Mahamd Adikan (Co-Supervisor) from the School of Electrical and Electronic Engineering, Universiti Sains Malaysia.

I understand that University will upload softcopy of my dissertation in pdf format into UTAR Institutional Repository, which may be made accessible to UTAR community and public.

Yours truly,

(*Pang Wen Shean*)

DECLARATION

I hereby declare that the dissertation is based on my original work except for quotations and citations which have been duly acknowledged. I also declare that it has not been previously or concurrently submitted for any other degree at UTAR or other institutions.

Name _____PANG WEN SHEAN____

Date _____13 SEPTEMBER 2021__

LIST OF TABLES

Tables		Page
2.1	Thermocouple types and Characteristics (Szabó, Gontean and Lie, 2012)	10
4.1	Typical Values for SMF	61
4.2	Delay values for 20 iterations of the first order sensing setup	82
4.3	T test values for 20 iterations of the first order sensing setup	83
4.4	Delay values for 20 iterations of the second order sensing setup	84
4.5	T test values for 20 iterations of the second order sensing setup	84

LIST OF FIGURES

Figures		Page
2.1	FBG operating principle	13
2.2	Mach Zehnder Interferometer	16
2.3	Photonic Crystal FiberPhotonic Crystal Fiber	17
2.4	BOTDA setup (Lu et al., 2019)BOTDA setup (Lu *et al.*, 2019)	19
2.5	BOCDA setup (Lu et al., 2019)	21
2.6	Schematic of L-BOFDA (Wosniok et al., 2013)	24
2.7	Gain resonance spectral profile with refractive index dispersion profile	26
2.8	SBS slow light temperature sensing system (Wang et al., 2011)	35
2.9	(a) Heterodyned Brillouin gain spectrum for different temperature (b) Stokes frequency shift vs temperature	36
2.10	(a) Output pulses at different temperatures, 100m SMF (b) Time delay vs temperature at different gains (40dB, 30dB, 20dB)	37
2.11	(a) Output pulses at different temperatures, 2m SMF (b) Time delay vs temperature at 20dB gain	37
3.1	Research methodology chart	42
3.2	Fiber sensing classification	43
3.3	Operating setup for the generation of first order Brillouin Stokes	43
3.4	Flow chart for first order Brillouin Stokes	45
3.5	Operating concept for the generation of second order Brillouin Stokes	45
3.6	Flow chart for second order Brillouin Stokes	47

Figures		Page
3.7	General setup for first and second order Brillouin slow light	47
3.8	Flow chart for first order and second order Brillouin slow light	49
3.9	Flow chart for temperature sensing performance for the first and second order Brillouin slow light	50
4.1	Simplified Representation of the Slow Light Model	54
4.2	Tunable Laser Source Input Spectrum	58
4.3	First Order Brillouin Stokes for 2km Fiber Spool	58
4.4	First Order Brillouin Stokes for 5km Fiber Spool	59
4.5	First Order Brillouin Stokes for 10km Fiber Spool	59
4.6	Plotted BP and Stokes Peak Power	62
4.7	Second Order Brillouin Stokes for 2km Fiber Spool	63
4.8	Second Order Brillouin Stokes for 5km Fiber Spool	64
4.9	Second Order Brillouin Stokes for 10km Fiber Spool	64
4.10	Plotted BP and Stokes Peak Power	65
4.11	1st Order Slow Light with Increasing BP	67
4.12	2nd Order Slow Light with Increasing BP	68
4.13	Optical Delay Versus Relative Brillouin Gain for First and Second Order Slow Light	69
4.14	Sine Wave Modulation Frequencies at 10dBm BP power	70
4.15	Sine Wave Modulation Frequencies at 15dBm BP power	71

Figures		Page
4.16	Sine Wave Modulation Frequencies at 20dBm BP power	71
4.17	Square Wave Modulation Frequencies at 10dBm BP power	72
4.18	Square Wave Modulation Frequencies at 15dBm BP power	72
4.19	Square Wave Modulation Frequencies at 20dBm BP power	73
4.20	First order SBS slow light sensing setup	74
4.21	First Order Slow Light Oscilloscope Signal	75
4.22	Sensitivity of First Order Brillouin Slow Light Temperature Sensing	77
4.23	Second order SBS slow light sensing setup	78
4.24	Second Order Slow Light Oscilloscope Signal	79
4.25	Sensitivity of Second Order Brillouin Slow Light Temperature Sensing	80
4.26	Sensitivity of First and Second Order Brillouin Slow Light Temperature Sensing	81

LIST OF ABBREVIATIONS

5G	Fifth Generation
BFS	Brillouin frequency shift
BGS	Brillouin gain spectrum
BNC	Bayonet Neill–Concelman
BOCDA	Brillouin Optical Correlation Domain Analysis
BOFDA	Brillouin Optical Frequency-Domain Analysis
BOTDA	Brillouin Optical Time Domain Analysis
BOTDR	Brillouin Optical Frequency Domain Reflectometry
BP	Brillouin pump
BS1	First order Brillouin Stokes signal
BS2	Second order Brillouin Stokes signal
CCROW	Circled coupled resonator optical waveguides
CNN	Convolutional neural networks
CPO	Coherent population oscillation
CW	Continuous wave
DCF	Dispersion compensating fiber
DF	Degree of freedom
DGS	Dynamic grating spectrum
EDFA	Erbium-doped fiber amplifier
EIT	Electromagnetically induced transparency
EOM	Electro-optic modulator
FBG	Fiber Bragg gratings
FUT	Fiber under test

FWHM	Full width at half maximum
HVAC	Heating, ventilation, and air conditioning
IC	Integrated circuits
IM	Intensity modulator
NTC	Negative Temperature Coefficient
OSA	Optical spectrum analyzer
OTDR	Optical Time-domain Reflectrometry
PDMS	Polydimethylsiloxane
PMMA	Polymethyl methacrylate
PTC	Positive Temperature Coefficient
RTD	Resistance temperature detectors
SBS	Stimulated Brillouin scattering
SE	Standard error
SMA	SubMiniature version A
SMF	Single mode fiber
SNR	Signal-to-noise ratio
SRS	Stimulated Raman scattering
SSBM	Single sideband modulator
TCR	Temperature coefficient of resistance
TLS	Tunable laser source

TABLE OF CONTENTS

		Page
ABSTRACT		**ii**
ACKNOWLEDGEMENTS		**iv**
APPROVAL SHEET		**v**
DECLARATION		**vii**
LIST OF TABLES		**viii**
LIST OF FIGURES		**ix**
LIST OF ABBREVIATIONS		**xii**
CHAPTER		
1.0	**INTRODUCTION**	1
	1.1 Background	1
	1.2 Motivation	4
	1.3 Research Objectives	5
	1.4 Scope of Work	6
	1.5 Thesis Outline	6
2.0	**LITERATURE REVIEW**	8
	2.1 Introduction	8
	2.2 Electronic sensors	8
	2.3 Fiber Optic Sensors	11
	2.3.1 Discrete Sensing	12
	2.3.1.1 Fiber Bragg Grating	13
	2.3.1.2 Interferometer	16
	2.3.1.3 Photonic Crystal Fiber	17
	2.3.2 Distributed Sensing	18
	2.3.2.1 Brillouin Optical Time Domain Analysis (BOTDA)	19
	2.3.2.2 Brillouin Optical Correlation-Domain Analysis (BOCDA)	21
	2.3.2.3 Brillouin Optical Frequency-Domain Analysis (BOFDA)	23
	2.3.2.4 Brillouin Optical Time-Domain Reflectometry (BOTDR)	25
	2.4 Slow Light	26
	2.4.1 Slow Light Schemes	28
	2.4.2 Brillouin Slow Light	30
	2.4.3 Slow Light Sensing	34

2.5 Conclusion 39

3.0 **RESEARCH METHODOLOGY** 40
3.1 Introduction 40
3.2 Research Approach 41
3.3 Characterization of first order Brillouin Stokes 43
3.4 Characterization of Second Order Brillouin Stokes 45
3.5 Characterization of First and Second Order Brillouin Slow Light 47
3.6 Characterization of Temperature Sensing Performance for the First and Second Order Brillouin Slow Light 50
3.7 Conclusion 52

4.0 **GENERATION OF FIRST AND SECOND ORDER SLOW LIGHT BASED ON STIMULATED BRILLOUIN SCATTERING FOR TEMPERATURE SENSING** 53
4.1 Introduction 53
4.2 Brillouin Parameters Characterization 54
4.2.1 Brillouin Frequency Shift and Threshold Measurement 56
4.2.1.1 First Order Characterization 57
4.2.1.2 Second Order Characterization 62
4.3 Slow Light Characterization 66
4.3.1 First and Second Order Slow Light Delay Values by increasing Brillouin Pump 66
4.4 Comparison of Different Waveforms and Modulating Frequencies 70
4.5 First Order Temperature Sensing 74
4.6 Second Order Temperature Sensing 78
4.7 Reliability T-test 82
4.8 Conclusion 85

5.0 **CONCLUSION AND RECOMMENDATIONS FOR FUTURE WORKS** 86
5.1 Conclusion 86
5.2 Recommendations for Future Works 88

LIST OF REFERENCES 90
LIST OF PUBLICATIONS 108

CHAPTER 1

INTRODUCTION

1.1 Background

With the introduction of industrial revolution 4.0 and high speed 5G data transmission speeds, it is an undeniable fact that sensors are being increasingly more important in the acquisition of raw and/or refined data. In the near future, data will be acquired and uploaded at a high speed to the cloud, which then would be used for analysis and storage in order to improve commercial and industrial needs. High speed built-in sensors sending relevant data to the internet, which is processed by data analytical tools can provide valuable insight and information that is relayed throughout the life cycle of the product being used. On the other hand, in the industry, factory operations can be seamlessly controlled to ensure continuous equipment or production flow, worker safety can be enhanced by wearable accessories, equipment and environmental hazard detector (Al Mamun and Yuce, 2019). The consumer-producer gap will be greatly reduced, which brings about a supply chain which is more customer-centric (Thames and Schaefer, 2017). The automation work that is required is immense and creates a necessity that more precise, accurate and reliable sensors to be developed in order to rapidly detect anomalies.

In these few decades, fiber optics has emerged as a potential and reliable sensor technology due to its immunity to electromagnetic interference and operability in harsh environment. There are optical sensor applications in industries such as medical, motorsport, HVAC, agriculture, industrial, aerospace and automotive. Motors and computers have many components that need to be maintained at certain temperature so that they do not overheat. Maintenance of a specific temperature is important for medical drugs fabrication, liquid heating, or equipment cleaning. These applications require that the detection circuit to have a critical response time and accuracy for quality control. Therefore, different options have to be explored in order to find out suitable solutions for different sensing requirements and issues. The applications of fiber optic sensor have been explored in these few decades that showed low loss, long distance transmission and high speed, which makes it an excellent candidate in a rapid-connectivity network. Additionally, fiber optic sensing can be divided into distributed or point sensing. Point sensors, or called discrete sensors, are fiber optic sensors that can detect measurands at dedicated location where the sensors are mounted. Fiber Bragg gratings (FBG) sensors are discrete sensors which had been widely used in structural health monitoring, such as strain monitoring in towers (Bang, Kim and Lee, 2012; Guo *et al.*, 2012), bridges (Tong, Tham and Au, 2002; Xu *et al.*, 2010), tunnels (Li *et al.*, 2008) etc. Distributed sensors are fiber optic which are mounted on the structure and the whole length of fiber serves as sensors picking up signals from the sensing object. Through signal analysis and processing, fault localization is achievable. Various distributed sensing methods had been developed such as Brillouin Optical Time Domain Analysis

(BOTDA) (Horiguchi and Tateda, 1989; Zan and Horiguchi, 2012), Brillouin Optical Frequency Domain Reflectometry (BOTDR) (Yan and Chyan, 2010; F. Wang *et al.*, 2013) and Brillouin Optical Correlation Domain Analysis (BOCDA) (Yamauchi and Hotate, 2004; Matsumoto, Kishi and Hotate, 2014).

In relation to this, sensing can also be implemented by using slow light. Slow light occurs when a modulated optical carrier travels at lowered group velocity. The difference between phase and group velocity was distinguished by William Hamilton (Hamilton, 1839). Furthermore, the hypotheses and theories surrounding group velocity were established by Lord Rayleigh (Rayleigh, 1877), and the atomic vapour refractive index can be calculated as in the formulae provided in Theory of Electrons (Lorentz, 1916). On 1999, light was slowed down to 17 meters per second by Hau *et al*. by using electromagnetically induced transparency (EIT) (Hau *et al.*, 1999). This method maintains the nonlinear properties while keeping coherence in the quantum state, resulting in material transparency. The downside of this is that it requires ultracold controlled environments, which limited the use of slow light within practical applications. Stimulated Brillouin scattering (SBS) is an alternative methodology that can produce slow light through changing material resonance by applying an amplified optical field or using nonlinear effects to control the output of the optical pulse. The gain resonance caused by the pump field will produce a spectral variance of the material refractive index, leading to the slow light effect. Generally, the main advantage of sensing utilizing SBS is the compatibility with existing optical telecommunications infrastructure.

In recent years, slow light exhibited different potentials in applications such as optical switching, interferometry, optical regenerators, delay lines and buffers. In the industry, the transmission of delayed data pulses needs to be synchronized by optical regenerators. In research, it is found that the pump power that is required increases proportionally with increasing broadening SBS gain at a fixed normalized delay (Thévenaz, 2008) and a data packet is delayed by multiple pulse lengths (Krauss, 2008). Recently, the sensitivity in optical sensing is needed for precise temperature monitoring (Li *et al.*, 2019), and the spectral performance has been improved by a factor of 1.145 by using SBS slow light (Wang *et al.*, 2019). The delay increases proportionally with the pump, giving a value of 6.1ns/W and a maximum group delay of 11.2ns at 2W pump power. 1.57 times sensitivity improvement is shown by using a sine-modulated signal at 600 mV peak-to-peak and 1 kHz frequency (Qian *et al.*, 2019). The ongoing researches and underlying issues are considered to have value-added properties for the SBS slow light that significantly improved applications and motivated the progress of the field of optical sensing, therefore slow light has great potential as a candidate for optical sensing. However, current slow light generation techniques are limited to first order applications only. The higher order Brillouin slow light should be a subject of research to improve the sensitivity of the sensing systems even further.

1.2 Motivation

Slow light is known as the optical pulse propagation with lowered group velocity, which enhances the light-material interaction and gain

spectrum bandwidth (Zadok, Eyal and Tur, 2011). The transition of electrical to optical sensors took place due to reliability issues in electrically hostile environments, operability in harsh conditions and space constraint (Garret, 2012). In this context, SBS slow light sensing conforms to these requirements. The capability of slow light temperature sensing has venturing possibilities which is shown by Wang *et al.*(Wang *et al.*, 2011). The idea is further improved by dividing the sensing region into sections that acts as a distributed sensor (L. Wang *et al.*, 2013).

The first order slow light sensing system by Wang *et al.* showed the prospects in real life applications. For further improvement, higher order SBS slow light should be investigated. *S*econd order Brillouin Stokes signal can be generated by cascading the light source through a 4-port circulator and fiber spool. This is an enhancement of the slow light application, as the cascading effect causes the sensing region to have increased sensitivity as the temperature is being applied. Therefore, we believe that higher order SBS slow light can be explored to enhance the sensitivity of the sensing system.

1.3 Research Objectives

The primary focus of this research work is to generate and investigate stimulated Brillouin scattering slow light in optical fiber. The main purpose of this work is to characterize SBS slow light properties in a temperature sensing setup. The objectives are as follows:

1. To generate and characterize Brillouin slow light in optical fiber

2. To design and characterize a fiber optic temperature sensor based on brillouin slow light
3. To enhance the sensitivity of Brillouin slow light temperature sensing by using higher order Brillouin gain

1.4 Scope of Work

The work presented in this dissertation highlights the generation and characterization of first order and second order slow light based on SBS nonlinear effect due to the Kramers–Kronig relations. Temperature sensitivity of the first and second order SBS slow light is plotted as a function of the delays produced. An experimental design has been proposed and implemented which consist of two pathways: a fiber laser for the generation of probe signal and an amplified pump signal by an erbium-doped fiber amplifier (EDFA). The higher order Stokes signals are produced by the cascading of Brillouin effect in the Brillouin gain medium. All results are based on experimental work demonstrated in this study.

1.5 Thesis Outline

This dissertation shows the fundamentals and the generation of slow light based on SBS for temperature sensing. A short review on the future of telecommunications and slow light research is unveiled in Chapter 1, which included the motivation and objectives of this study. Chapter 2 shows the electrical and optical sensing technologies available, and addresses the

different signal parameters to explain the principles of slow light. Then, a review on slow light is described alongside the theory of stimulated Brillouin scattering. The research methodology chart and workflow are contained in Chapter 3. Chapter 4 displays the investigation of first and second order slow light based on SBS for temperature sensing. Manipulation of parameters such as the fiber spool length, BP power, modulating scheme and frequency are conducted to obtain the relevant optical spectrum analyzer (OSA) optical spectrum and oscilloscope electrical signal. A t-test was used to evaluate the reliability of the methodology being used. The first order slow light results are measured, recorded and then compared with the second order slow light results. This is a benchmark test for the results that are acquired from the second order SBS slow light setup. Chapter 5 concludes the dissertation and asserts some of the recommendation for future works.

CHAPTER 2

LITERATURE REVIEW

2.1 Introduction

In this chapter, various schemes of electronic and fiber optic sensors are discussed. Detailed explanation on slow light based on working principles, reported works, governing equations and history are also presented. SBS slow light generation methodologies and experimental works on slow light sensing are also reviewed.

2.2 Electronic sensors

A device or microchip that can detect physical changes and turn them into an electrical signal is called an electronic sensor (Fraden, 2004). The output of the sensor is computed and then provides data for measurement or triggers an action as a response. Generally the advantages of electronic sensors are low replacement costs, reliability, flexibility and integratability between different electronic systems.

Firstly, the thermistor is a device that gives out a reading for the temperature value using the varied electrical resistance in a material. Thermistors come in two variants: Negative Temperature Coefficient (NTC)

thermistors (de Györgyfalva and Reaney, 2001) and Positive Temperature Coefficient (PTC) thermistors (Baiatu, 2000). Applications in temperature sensing will commonly require NTC thermistors, whilist PTC thermistors are used in circuit breakers to limit the incoming current or provide surge protection.

Secondly, resistance temperature detectors (RTDs) use conductive material to determine the temperature. Platinum is used in RTDs due to stability and temperature range (Chauhan and Neelakantan, 2016) apart from copper and nickel. Specific materials selected for RTDs are determined by their temperature coefficient of resistance (TCR) (Turkani *et al.*, 2018). RTDs are either built as thin-film or wire wound type (Weber, Thiel and Bauschke, 2011). Using a constant voltage source, the resistance can also be obtained instead of using conventional method employing constant current source (Suthar and Gadit, 2012).

Thirdly, thermocouples are made by combining two wires with different metals together, which results in Seebeck Effect. The Seebeck Effect explains the phenomenon at which a temperature difference of conductors made from different materials produces a potential difference between the substances (MacDonald, 2006). This voltage potential is measured to calculate the temperature.

Types J, K, T, & E are base metal thermocouples and noble metal thermocouples are types R, S, and B, which describes their temperature range,

resistance to vibration, sensitivity, and applications. Table 2.1 below lists the various types of thermocouples and their metal composition.

Table 2.1: Thermocouple types and Characteristics (Szabó, Gontean and Lie, 2012)

Code type	Metal Composition	Sensing temperature	Sensitivity (μV/^{0}C)
E	Nickel Chromium/Constantan	-40 to 900°C	68
J	Iron/Constantan	-180 to 800°C	55
K	Nickel Chromium/Nickel Aluminum	-180 to 1300°C	41
N	Nicrosil/Nisil	-270 to 1300^{0}C	39
T	Copper/ Constantan	-250 to 400^{0}C	43
R/S	Copper/Copper Nickel Composition	-50 to 1750^{0}C	10
B	Platinum Rhodium	0 to 1820^{0}C	10

Next, semiconductor temperature sensors are integrated circuits (ICs) which include voltage output, current output, digital output, resistance output and diode, and are not suitable for high temperature applications. They produce a linear output, shows accuracy at 1°C to 5°C and has a temperature range of -70°C to 150°C. Semiconductor sensors are also extensively researched for their stretch-ability for strain sensing in moving units such as animals and robots (Kim, Thukral and Yu, 2018). The semiconductor uses π–π stacked poly(3-hexylthiophene-2,5-diyl) nanofibrils (P3HT-NFs) percolated in elastomer of silicon polydimethylsiloxane (PDMS) to yield a nanocomposite with great mechanical stretchability.

In general, power loss over longer distances, susceptibility towards interference and lower bandwidth are disadvantages of electronic sensors that makes optical sensing much more preferable compared to electronic sensing. Electrical signal which is exposed to flammable substances poses high risks in oil and gas industries.

2.3 Fiber Optic Sensors

Modern optical communications started in 1920s when hollow pipe arrays or translucent rods are used for fax and television. The first working laser was invented by Theodore Maiman in the year 1960 (Maiman, 1960; Lengyel, 1962). Until the year 1964, a theoretical specification for optical fiber was released for long range communications with a low loss of 10 to 20 dB by Dr. Charles K. Kao. Since then, the research of photonics became much more compact and advanced, prompting the growth of different groups of optical fiber sensing schemes. In the industry, devices used for measurements involving optical fibers are more often than not, named interrogators.

The earlier versions of optical sensing consist of colorimetric (Rush and Yoe, 1954; Rakow and Suslick, 2000) and interferometric sensors (Hocker, 1979; Shupe, 1980). The main types of interferometers are Mach-Zehnder, Fabry-Perot, and Sagnac interferometers. Up until now, ongoing studies are still being conducted to improve such systems, with different technologies being paired and tested (DeMiguel-Soto *et al.*, 2017; Hirsch *et al.*, 2017; Li, Askim and Suslick, 2018). The advantages of using fiber optics

is that they have higher bandwidth, lower power loss, smaller size, lightweight and higher tensile strength compared to electrical cables. Historically, lasers can enable information to travel far with low loss in long haul transmissions due to the invention of optical amplifiers in the 1980s that allow amplification without conversion of the signal to electrical signal. With all the advantages, sensing based on fiber optics provides environmental resilience, electrical immunity and also the capability of distributed sensing (Turner *et al.*, 1990). As the technology of fiber optic sensing becomes more and more refined, it is only a matter of time that it replaces the traditional sensor devices (Hisham, 2018). In comparison, the sensitivity, design flexibility and cost of optical sensors makes them better than their counterparts. Optical sensing can be in the form of discrete or distributed sensing.

2.3.1 Discrete Sensing

Discrete sensing consists of sensors that are manufactured and placed at points of interest to measure the changes in strain or temperature. The FBG is a simplistic low-cost filter with gratings which blocks out a specified wavelength. Interferometers merges different sources of light for interference to occur. Lastly, photonic crystal fibers have periodic microstructures along the fiber that confines light depending on their pattern, usually surrounded by a medium like air.

2.3.1.1 Fiber Bragg Grating

KO Hill *et al.* founded the FBG in the pursuit of the study on photosensitivity in optical fibers (Hill and Meltz, 1997). The gratings formed due to longitudinal optical resonances occurring from a compromised fiber using an argon-ion light as input. This modulated the refractive index and caused losses in the signal integrity (KERSEY, 2018). In FBG sensing, the parameter of strain is temperature dependent, and usually the temperature detected by the sensor has to be compensated to obtain the strain value, with exceptions (Zhu *et al.*, 2007).

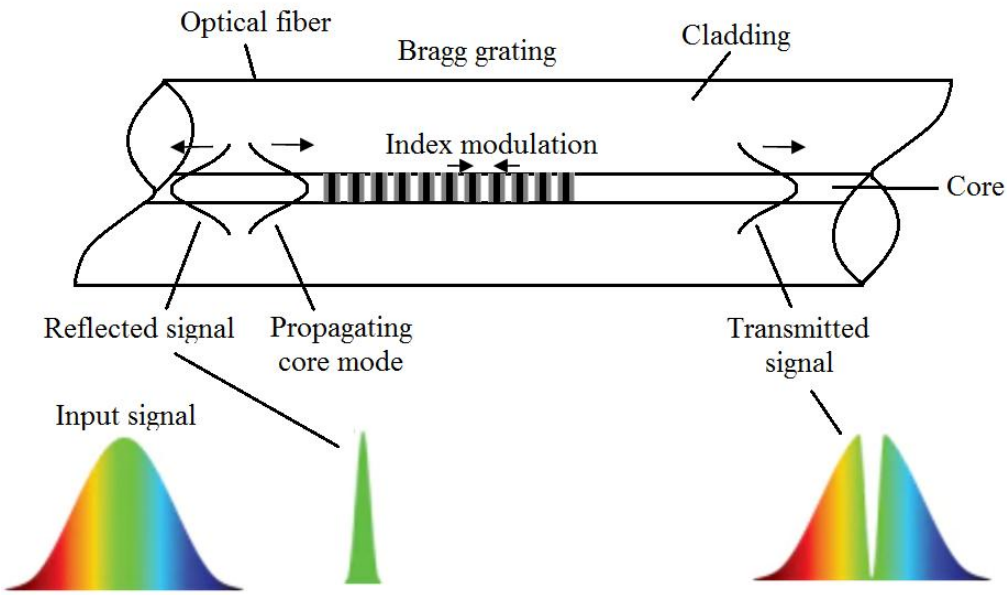

Figure 2.1: FBG operating principle

Despite being discovered by KO Hill *et al.*, the ability to write the FBG at any predetermined wavelength is manifested at the United

Technologies Research Center (Kersey, Berkoff and Morey, 1993). The formula governing the FBG's working principle is simple:

$$\lambda_B = 2\eta_{eff}\Lambda \tag{2.1}$$

where λ_B is the Bragg wavelength, η_{eff} is the effective refractive index and Λ is the periodic spacing (Alvarez-Botero *et al.*, 2017). In structural health monitoring, the most commonly required parameters are the temperature and strain, which is given by the differential formula below:

$$\lambda_B = 2\left[\eta_{eff}\frac{d\Lambda}{dT} + \Lambda\frac{d\eta_{eff}}{dT}\right]\Delta T + 2\left[\eta_{eff}\frac{d\Lambda}{dl} + \Lambda\frac{d\eta_{eff}}{dl}\right]\Delta l \tag{2.2}$$

where the first term of the equation describes the effect by temperature, while the second term describes the effect by strain.

The FBG played a major role in monitoring of civil structures like bridges (Tennyson *et al.*, 2001; Zhou *et al.*, 2003; Chan *et al.*, 2006), high-rise buildings (Li *et al.*, 2012), oilrig/offshore structures (Ren *et al.*, 2006; Qiao *et al.*, 2017) and also composite structures in wind turbines, marine and aircraft structural joints (Silva-Muñoz and Lopez-Anido, 2009; Chen *et al.*, 2012; Gupta *et al.*, 2013). These are all real-time results that can be monitored almost instantaneously using an interrogator. With scheduled maintenance and proper reviewing, the structural integrity could be kept at safe levels at all times. Besides providing real-time data, FBGs can be used to produce prediction models for early detection (Tam *et al.*, 2007; Tan *et al.*, 2016). The results produced by the prediction models are used for prevention measures so that disasters can be avoided.

In the recent years, research topics on FBG are focused on its commercialisation by usage of polymer material substitutes and femtosecond laser for fabrication (Zhou *et al.*, 2003). Testing and experimentation have been conducted to find out the most suitable material and methodology to produce FBG sensors that can withstand higher temperatures, harsh environments and are cheaper to produce. Companies such as Topas and Zeonex are promoting the usage of polymer-based FBG. Absorption of water is a primary attribute of polymethyl methacrylate (PMMA) polymer optical fibers, which meant that they can be used as humidity sensors (Woyessa *et al.*, 2016). However, the downside to this is measurement of strain and temperature will be affected by the surrounding humidity. Hence, the FBG polymer produced by Topas aims to overcome the humidity issue (Yuan *et al.*, 2011), and further competition by Zeonex produces their version of humidity insensitive FBGs (Woyessa *et al.*, 2017). The deliberate comparison made in Zeonex's paper judges both products based on ease of manufacturing, transmittance, temperature sensitivity and mechanical strength. For the femtosecond laser fabricated FBG, it brought more variability in terms of intensity threshold (type I and II), thermal stability up to 2000°C and fiber material (Liao and Wang, 2013). The femtosecond laser fabrication method is better than using ultraviolet light because it disregards the photosensitivity of the material and hydrogen loading treatment is not required. With that being said, competition in research accelerates the pace of which the technology is being evolved.

2.3.1.2 Interferometer

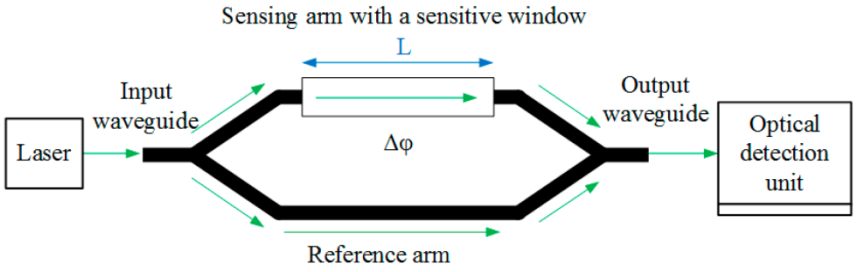

Figure 2.2: Mach Zehnder Interferometer

Interferometry is based on the principle of superposition. In an interferometer, the phase difference between the two beams, originated from the same source but going through different arms of the interferometer, is measured and plotted against the measurand that caused the phase difference. Thus, this property allows it to be an excellent sensor. Recently. the mid Infrared optical gas sensor is researched to solve problems such as size and alignment pertaining surface plasmon resonance sensors. Using Plasmonic waveguides, the sensitivity reaches 3695 nm/RIU at 730 nm wavelength (El Shamy, Khalil and Swillam, 2020). Then, cost reduction and tunability are also effectively implemented by following a set of design rules, dictated by the arm length difference (Xie, Zhang and Dai, 2020). In this experiment, a Mach-Zehnder interferometer is modified using high-frequency pulsed CO_2 laser to create a symmetrical double-grooved structure, which achieved sensitivity of 230 pm/°C and temperature range of 20 °C-90 °C with high repeatability (Dong *et al.*, 2020). The advantages of an interferometer are insensitivity of source lasing fluctuations, synchronized measurement and good dynamic accuracy.

2.3.1.3 Photonic Crystal Fiber

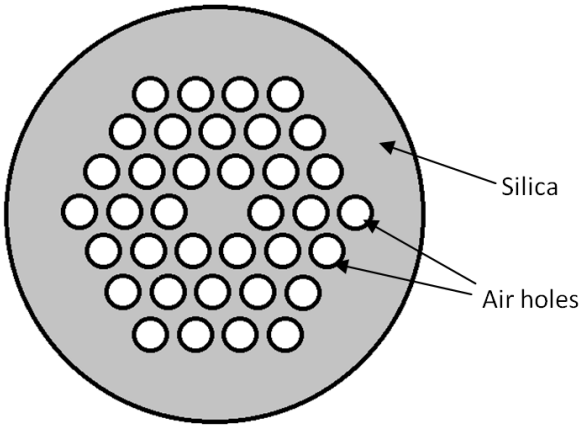

Figure 2.3: Photonic Crystal Fiber

A photonic crystal fiber is an optical fiber that has microstructured arrangement of material within another material with a refractive index difference. The background material, which is the material engulfing the other material along the fiber, is made out of undoped silica. Typically, the material within is filled with air, but exception arises in applications such as a copper-filled photonic crystal fiber in order to produce a broadband polarization filter (Azman *et al.,* 2019). By changing the diameter of the copper wire, the resonance wavelength of the filter can be varied from from 1390 to 1890 nm. Furthermore, due to the widespread of malaria disease in poverty-ridden countries, there are also increased effort to fabricate sensors that will assist in early detection that reduces the mortality rate. Photonic crystal fibers can serve as biosensor to detect malaria by arranging the microstructures in order to increase the sensitivity and quality factor (Mohammed *et al.,* 2020; Chaudhary, Kumar and Kumara, 2021; Shafkat *et al.*, 2021)

2.3.2 Distributed Sensing

Distributed sensing is the technology which allows incessant, synchronous measurements over the distance covered by a fiber optic line. In contrast to discrete sensors that measure at points where they are placed, distributed sensing utilises the optical fiber itself as the sensing element without transducers being added in the optical pathway. Distributed sensing interrogation is similar to a radar, where a pulse sequence is injected and the scattered wave that bounces back is plotted against time. Due to this operating principle, the distributed sensor can measure the points that are traversed by the wave along the fiber. The data that is acquired by distributed sensing are temperature, acoustic and strain. The backscattering of light in the fiber produces Stokes and anti-Stokes signal. The amplitudes and propagation speed are monitored, in order to determine the spatial localisation.

Generally, the distributed system is characterized by the spatial resolution and range. The spatial resolution is the minimum distance of which the sensor can detect the perturbations in the fiber, whereas the temperature resolution is the precision of the measured absolute value. The factors affecting the temperature resolution are the injected pulse repetition rate and time of measurement. The pulse width, amplitude and duration have to be controlled accurately because there is a trade-off in performance between the resolution, sensing range and measurement time.

2.3.2.1 Brillouin Optical Time Domain Analysis (BOTDA)

BOTDA is a distributed sensing method that employs Brillouin gain or loss spectroscopy. When temperature and strain applied to an optical fiber changes, changes to the refractive index and also the density could be observed. The change of the Brillouin shift will show the temperature and strain information along the fiber. Spatial distribution of the fiber can be obtained by transmitting a short optical pulse into the fiber. The time of flight of the backscattered pump pulse is plotted and reveals the distributed information over the sensing fiber. The difference that sets BOTDR and BOTDA systems apart is the requirement of the BOTDR to have only one end of the fiber, while BOTDA requires access to both ends of the fiber.

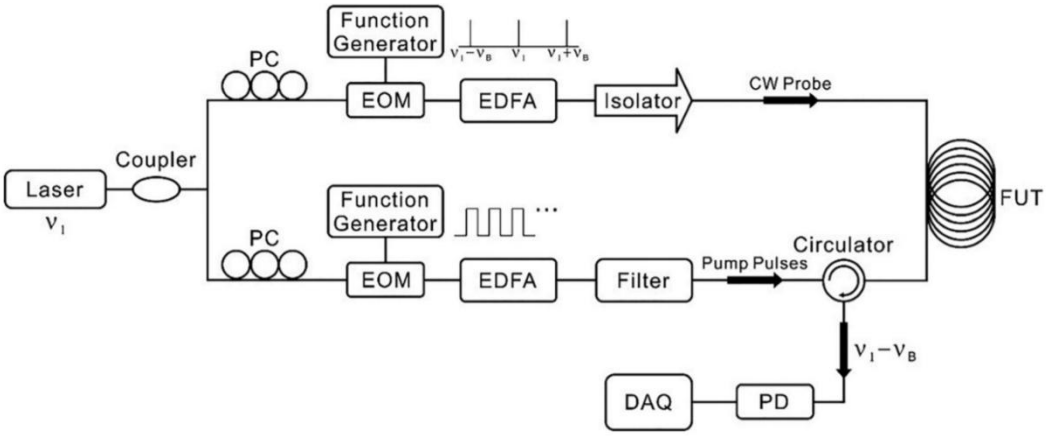

Figure 2.4: BOTDA setup (Lu *et al.*, 2019)

Horiguchi *et al.* explained the theory on BOTDA (Horiguchi and Tateda, 1989) and demonstrated a breakthrough in 1994 where an 1m spatial resolution over an 11km fiber is achieved (Horiguchi, Kurashima and Koyamada, 1994). The limiting factor of the BOTDA has also been set at the

spatial resolution whereby the pulse width of 10ns, corresponding to the 1m spatial resolution is a fixed value as nonlinearities of the fiber will produce unwanted noise due to pulse broadening, compromising the accuracy of the trace produced. There are papers that have presented sub-meter resolution for the BOTDA scheme (Dong *et al.*, 2012; Soto *et al.*, 2012), which have a 2cm and 25cm spatial resolution respectively. Nonetheless, the schemes proposed have either high cost and complexity in the experimental setup or have sacrificed the sensing range of the BOTDA or even both. Research is still being carried out to extend the sensing range and to reduce the spatial resolution of the BOTDA.

Lately, researchers combined methodologies for the improvement of the speed of acquisition for real-time applications, distinction of strain and temperature, simultaneous strain and temperature sensing, improvement of SNR, compensation of nonlocal effect, increment of sensing range and removal of the need of trace averaging. By deploying convolutional neural networks (CNN) (Hao Wu *et al.*, 2018), the processing time for the image denoising of BOTDA is shortened, as the CNN is trained to collect noise data from the photodetector by a large sample of data in real time. A channel estimation technique, complemented by pulse coding (Tang *et al.*, 2018) is also used to improve the SNR by obtaining a complex Brillouin gain spectrum (BGS) from the digital signal processing unit linked to the oscilloscope. Some methods added features to the BOTDA system, such as usage of a reference probe lightwave to assist with trace averaging (Guo *et al.*, 2018), replacing the modulator at the probe path with a Brillouin ring laser for tunability (Marini,

Iuliano, *et al.*, 2018; Marini, Rossi, *et al.*, 2018; Ruiz-Lombera *et al.*, 2018), support vector machine for extraction of temperature distribution in a DPP-BOTDA (Huan Wu *et al.*, 2018), and also swapping the fiber under test (FUT) from a conventional SMF to a dispersion compensating fiber (DCF) to discriminate temperature and strain (Li *et al.*, 2018).

2.3.2.2 Brillouin Optical Correlation-Domain Analysis (BOCDA)

The strain sensing system based on BOCDA scheme has been introduced as early as year 2005 (Hotate and Abe, 2005). The goal of having a BOCDA sensor is to overcome the limitations associated with the pulse-derived issues. The feature of a BOCDA sensor is that instead of using pulsed wave for sensing, continuous wave (modulated sinusoidally) is being deployed. Hence, the measurement time is reduced and the sensitivity of the typical Brillouin sensor is improved at the cost of increased complexity and reduced range (Hotate, 2014).

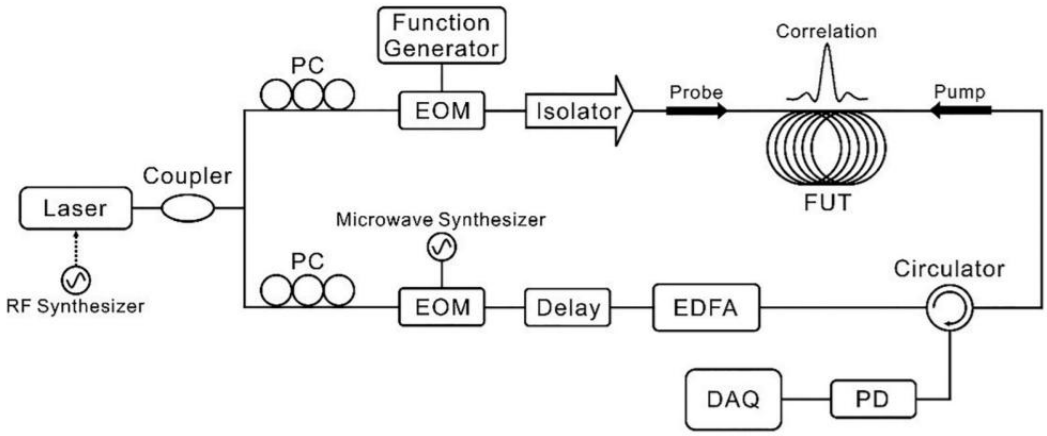

Figure 2.5: BOCDA setup (Lu *et al.*, 2019)

In the BOCDA system, spatial resolution Δz is given by (Song and Hotate, 2007b):

$$\Delta z = \frac{v_g \Delta v_B}{2\pi f_m \Delta f} \tag{2.3}$$

and the measurement range d_m:

$$d_m = \frac{v_g}{2f_m} \tag{2.4}$$

where v_g is the group velocity of light in the fiber, v_B is the Brillouin frequency, f_m is the modulating sinusoidal frequency and Δf is the modulation amplitude.

The concept of a orthogonally-polarized read path is introduced in addition to the existing pump and probe path to assist in the frequency sweeping process (Matsumoto, Kishi and Hotate, 2014). For the dynamic grating spectrum (DGS), the frequency difference between the pump-read is obtained. The function of having both BGS and DGS lies on their orthogonal relationship, whereby the y-polarized light (BGS) and x-polarized light (DGS) can be used to discriminatively measure strain and temperature in a single system. The DGS is produced by the dynamic grating of a polarization maintaining fiber (PMF). At the same time, the single sideband modulator (SSBM), microwave generator and intensity modulator (IM) are not required as in normal BOCDA schemes, through the usage of direct modulation of laser diode frequency.

2.3.2.3 Brillouin Optical Frequency-Domain Analysis (BOFDA)

The underlying principle of the Brillouin optical frequency-domain analysis (BOFDA) is the complex baseband transfer function that links the amplitude of pump travelling in the opposite direction and the Stokes wave (Garcus *et al.*, 1997). This transfer function is given by:

$$H(j\omega) = A(\omega)exp\left[j\Phi_{H(\omega)}\right] \tag{2.5}$$

where $A(\omega)$ and $j\Phi_{H(\omega)}$ are the amplitude and phase respectively. The maximum range d_m and spatial resolution Δz of the BOFDA is given by:

$$d_m = \frac{c}{2n} \cdot \frac{1}{\Delta f_m} \tag{2.6}$$

$$\Delta z = \frac{c}{2n} \cdot \frac{1}{f_{m,max} - f_{m,min}} \tag{2.7}$$

where $f_{m,max}$ and $f_{m,min}$ is the maximum and minimum modulation frequency.

Advantage of the BOFDA compared to the time-domain schemes is that it has improved signal strength. It offers narrow-bandwidth operation, which increases the signal-to-noise (SNR) ratio. By tuning the modulation frequency, the baseband transfer function is obtained at the frequency representing a fixed point which is measured by a network analyser. Different modulation frequencies are used to measure different points at the same time.

The latest progress in BOFDA has successfully improved the sensing range up to 63-km and 100-km respectively by the same team (Kapa, Schreier

and Krebber, 2018, 2019). Kapa *et al.* differentiated the fibers into transmission part and sensing part, whereby they measured the BGS of the sensing part. The transmission part also chosen to have different Brillouin frequency shift (BFS) values compared to the sensing part, so that the noise shifted to the transmission part, to increase the sensing range of the sensor . As the length of fiber is increased along with differentiated BFS values, higher pump power could be used before pump depletion occurs.

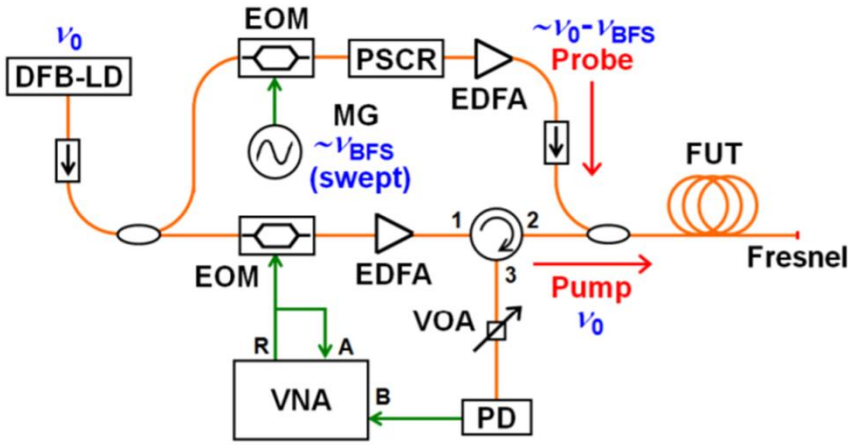

Figure 2.6: Schematic of L-BOFDA (Wosniok *et al.*, 2013)

Besides that, L-BOFDA has been developed (Wosniok *et al.*, 2013) which requires single end access to the sensing fiber. This is achieved by using the principle of Fresnel reflection of the probe wave on the other end of the fiber. This counterpropagating probe wave interacts with the pump wave on the way back and into the interrogator.

2.3.2.4 Brillouin Optical Time-Domain Reflectometry (BOTDR)

Optical Time-domain Reflectrometry (OTDR) is a method to obtain the information of an optical fiber using Rayleigh scattering. The methodology involves the attenuation, joint loss and the fiber length to confirm that the fiber is not broken. The working mechanism of an OTDR is that it uses one end of the fiber for the injection of a series of optical pulses. The Rayleigh backscattered signal, which is obtained at the very same end, has information such as the time of flight of the injected pulse. This time of flight is basically the time taken for the pulse to reach a specific length of the fiber. As such, the time of flight is a function of the length of the fiber, whereby the power of the received light is measured and plotted against time. If the fiber breaks, the OTDR can detect the breakage due to the strong reflection that occurs at the breaking point. The first publication on OTDR is at year 1977 (Barnoski *et al.*, 1977).

Since then, OTDR has also been used for distributed sensing. A novel method is proposed in (Gifford *et al.*, 2005) where the sweep based interferometry is being used. The concept of the distributed temperature sensor is by having a profile of the initial Rayleigh scatter signature, which is then compared with the fiber profile which has heat applied to it. The temperature resolution achieved by this paper is at 0.1°C with a 20m length fiber. A few years later, both strain and temperature measurements within the same OTDR is realised by (Koyamada *et al.*, 2009). The fiber being used is 8km and the technique achieved 0.01°C resolution and 1m spatial resolution. The biggest

drawback is that the measurement time takes too long, as the 40 traces that are measured required 3 hours, taking into account the time needed to adjust the laser and microwave power. This has restricted the number of data points that can be recorded and the real-time measurement regime has been deterred.

2.4 Slow Light

Slow light is the transmission of an optical carrier, either pulsed or modulated, at a lowered group velocity through a medium due to optical resonance. Applications using slow light include optical buffer, delay line, signal processor and equalizer (Boyd, Gauthier and Gaeta, 2006). Generally, the slow light effect occurring in a transparent medium is comparatively smaller for light pulse transmission through transparent medium. As the resonance interaction between the incoming light with the transition of particles take place, this effect will be enhanced. The parameters controlling the outcome of the slow light system is described in this section.

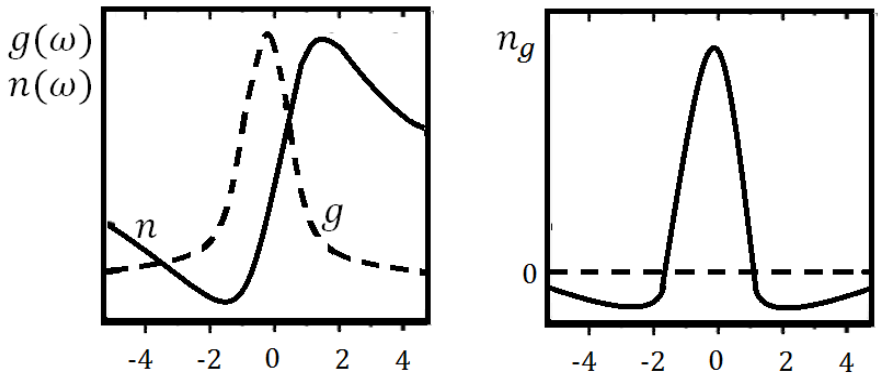

Figure 2.7: Gain resonance spectral profile with refractive index dispersion profile

In Figure 2.7, the group delay is at a maximum when n_g peaks at the centre line. However in experiments the delay is significant only when the gain is high, which will have other competing nonlinear effects that reduces the delay value instead (Basov *et al.*, 1966). In the 1990s, group velocity of 17 meters per second was achieved using nonlinear interactions (Hau *et al.*, 1999). The characteristics of this experiment is reduced absorption and resonance sharpness, which enhanced the group index and delay value.

SBS and stimulated Raman scattering (SRS) are the nonlinear methods used for generating slow light with the former being more preferred (Thévenaz, 2008). In SBS, the Stokes pulse which is frequency downshifted is to be delayed by transmitting the pulse through an optical fiber with a continuous wave (CW) sent in the opposite direction. The counterpropagating CW is used to assist the delay process, since parametric coupling occurred between pump and acoustic wave in the medium that is an amplified resonance gain profile (Kroll, 1965). Advantages of SBS slow light are compatibility with existing devices, tunable resonance by changing pump wavelength and room temperature operation. The drawback is that SBS spectral gain bandwidth is narrow at 120-200MHz for silica fiber (Agrawal, 2000).

2.4.1 Slow Light Schemes

The topics concerning slow light are varied due to the existing and emerging techniques that can be used to produce slow light. For now, the broad concept of producing slow light can be divided into two: nonlinear and structural slow light (Zhao, Qin and Wang, 2014).

The first general method is the interaction with medium in a specially-controlled environment such as EIT, SBS, SRS, soliton collision and coherent population oscillation (CPO); the second method is slow light material fabrication, i.e. Fabry-Perot interferometer, circled coupled resonator optical waveguides (CCROW), photonic crystal fiber/waveguide, microsphere and fiber Bragg grating (Zhao *et al.*, 2009; Digonnet *et al.*, 2012).

When EIT is mentioned, one could not help but inevitably think of the metamaterial research that is strongly based on EIT, which is first experimentally-proven in (Zhang *et al.*, 2008). Essentially, EIT is achieved during population trapping of the Λ-configuration, where coherence occurs between the two lower states, the ground and meta-stable states (Goldfarb *et al.*, 2009). Experimentally it is proven that EIT produced slow light with delays up to 200ns (Zhang, Hernandez and Zhu, 2008). Several photonic crystal gas sensors have also been established on slow light to be highly selective and sensitive (Zhao, Zhang and Wang, 2012; Kraeh *et al.*, 2018).

Slow light FBG has a much higher index modulation compared to the conventional ones (Arora *et al.,* 2018). At certain frequencies within the slow light FBG bandwidth, light travels to and fro along the FBG as in the Fabry-Perot interferometer. This phenomena increases the sensitivity of the FBG towards changes such as temperature or strain due to the shifting of the whole transmission spectra in the frequency space. This theory exhibits similar characteristics to the concept of our second order SBS slow light sensing system, where the repetition of light travel increased the sensitivity of sensor.

Last but not least, slow light can be made in optical fibers using SBS in room conditions. As far as we know, SBS interaction between the probe, pump and acoustic wave is a nonlinear process. Electrostriction produces an acoustic wave if the material density increases as the optical intensity increases (Khurgin and Tucker, 2008). The medium refractive index changes, induced by the acoustic wave. This will cause scattering of pump light, couples the three waves and amplification of the probe wave takes place. A first order SBS slow light sensing experiment is performed in (Wang *et al.*, 2011), and incorporation of SBS slow light theory in a fiber laser sensor for increased sensitivity (Qian *et al.*, 2019). Main differences between slow light and distributed sensing is that the latter has more sophisticated equipment and higher complexity in acquiring data, which both increased the cost of sensing.

2.4.2 Brillouin Slow Light

The SBS fundamental states that the resonance occurs at the Brillouin frequency v_B. The electrostriction process results from the density variation caused by two counter propagating waves in the z-plane, namely forward direction (+z) Stokes and backward direction (-z) pump wave. Both waves are described in the following equations:

$$E_s(z,t) = \frac{1}{2}[E_s(z,t)exp[-i(st - k_s z)] + c.c] \tag{2.8}$$

$$E_p(z,t) = \frac{1}{2}\left[E_p(z,t)exp[-i(pt + k_s z)] + c.c\right] \tag{2.9}$$

where (z,t) is the acoustic wave amplitude, $E_s(z,t)$ is the Stokes field amplitude, $E_p(z,t)$ is the pump field amplitude, s, k_s, p, k_p, are the frequencies and wave vectors and *c.c* is the complex conjugate.

For an isotropic medium (z,t) (Zeldovich *et al.*, 1985), the equation of the acoustic wave is:

$$\frac{\partial^2 \delta_\rho}{\partial t^2} - v^2\nabla^2\delta_\rho - A\nabla^2\frac{\partial \delta_\rho}{\partial t} = \rho_0\frac{\partial \varepsilon}{\partial \rho}\frac{1}{16\pi}\nabla^2|\mathrm{E(z,t)}|^2 \tag{2.10}$$

$$\frac{\partial^2 \delta_\rho}{\partial t^2} + \Omega^2{}_B\delta_\rho + \frac{\Gamma_B}{2}\frac{\partial \delta_\rho}{\partial t} = -\rho_0\frac{\partial \varepsilon}{\partial \rho}\frac{1}{8\pi}\frac{\partial^2}{\partial z^2}\left[\mathrm{E_p(z,t)E_s(z,t)}\right] \tag{2.11}$$

where the right-hand side of the equation is the driving force. The acoustic wave reflects the pump field to produce a new Stokes field, which in a cascading manner coincide with the pump and enhances the acoustic wave and so on. Hence, SBS gain is determined by the characteristics of the acoustic

wave such as reflectivity and spectrum dynamics. If the CW pump is not used up, the spatial growth of the signal over length *L* is:

$$\frac{\partial^2 E_S}{\partial z^2} - \frac{\varepsilon}{c^2}\frac{\partial^2 E_S}{\partial t^2} = \frac{1}{c^2}\frac{\partial \varepsilon}{\partial \rho}\frac{\partial^2}{\partial t^2}[\delta\rho(z,t)E_P(z,t)] \tag{2.12}$$

Eq (2.11) and (2.12) outlines SBS occurring in optical lossless media for small signal approximation. As Stokes amplitude, $E_S(z,t)$ and density, (z,t) changes minimally when acoustic wave exhibit strong attenuation, these equations are reduced to the first order relaxation equations:

$$\frac{\partial \rho}{\partial t} + \left(\frac{\Gamma_B}{2} + i\delta\Omega\right)\rho = -i\rho_0\frac{\partial \varepsilon}{\partial \rho}\frac{\Omega_B}{8\pi {v_s}^2}E_P {E_S}^*(z,t) \tag{2.13}$$

$$\frac{\partial E_S}{\partial z} + \frac{n}{c}\frac{\partial E_S}{\partial t} = -i\frac{\omega_s}{2cn}\frac{\partial \varepsilon}{\partial \rho}\rho^*(z,t)E_P t \tag{2.14}$$

which they describe the amplitude of the damped resonant oscillator (Eq 2.13) and partial differential equation $E_s(z,t)$ (Eq 2.14) respectively. The asterisk (*) in the equation is a complex conjugate and the RHS for Eq 2.14 is the Stokes emission source.

Now we will discuss about phase velocity and group velocity. The phase velocity (or equiphase surface propagation velocity) of a wave is the velocity of any point of the underlying wave, while group velocity (equiamplitude surface propagation velocity) of a wave is the velocity at which the enveloping wave's amplitude propagates. Phase and group velocities are different in a medium because a pulse is made up of different frequencies and the refractive index of the medium changes depending on the frequency of the incoming electromagnetic radiation. Both phase and group velocity are important variables that are used to describe a medium's dispersiveness.

Assuming we have two waves, E_1 and E_2 in the same direction of propagation, amplitude, but slightly different frequency and wave number ($\omega_1,k_1,\omega_2,k_2$) known as beating, and the initial phase is equals to zero:

$$E_1 = a\,cos(\omega_1 t - k_1 z) \tag{2.15}$$

$$E_2 = a\cos(\omega_2 t - k_2 z) \tag{2.16}$$

Summing the two waves, we get

$$E = E_1 + E_2 = a[cos(\omega_1 t - k_1 z) + cos(\omega_2 t - k_2 z)] \tag{2.17}$$

Using the triangular formula,

$$\cos(\alpha) + \cos(\beta) = 2\cos\left(\frac{\alpha+\beta}{2}\right)\cos\left(\frac{\alpha-\beta}{2}\right) \tag{2.18}$$

We obtain,

$$E = 2a\cos\frac{1}{2}[(\omega_1 - \omega_2)t - (k_1 - k_2)z]\cos\frac{1}{2}[(\omega_1 + \omega_2)t \tag{2.19}$$

With the annotation of mean angular frequency, $\bar{\omega}$, mean wave number, $\bar{k}$, modulation frequency, ω_m, and modulation wave number, k_m:

$$\bar{\omega} = \frac{1}{2}(\omega_1 + \omega_2) \tag{2.20}$$

$$\bar{k} = \frac{1}{2}(k_1 + k_2) \tag{2.21}$$

$$\omega_m = \frac{1}{2}(\omega_1 - \omega_2) \tag{2.22}$$

$$k_m = \frac{1}{2}(k_1 - k_2) \tag{2.23}$$

The superposed equation would be

$$E = 2a\cos(\omega_m t - k_m z)\cos\left(\bar{\omega}t - \bar{k}z\right)n_g \tag{2.24}$$

By definition,

$$v_g = \frac{\delta\omega}{\delta k} \tag{2.25}$$

and

$$v_p = \frac{dz}{dt} = \frac{\omega}{k} = \frac{c}{n} \tag{2.26}$$

Substituting (2.2) into (2.1),

$$v_g = \frac{\delta\omega}{\delta k} = \frac{\delta(kv_p)}{\delta k} = v_p + k\frac{dv_p}{dk} \tag{2.27}$$

$$k = \frac{2\pi}{\lambda} \tag{2.28}$$

Differentiating (2.4),

$$dk = -\frac{2\pi}{\lambda^2}d\lambda \tag{2.29}$$

$$v_g = v_p - \lambda\frac{dv_p}{d\lambda} \tag{2.30}$$

which also shows the relationship with the refractive index equation

$$n_g = n_p - \omega\frac{dn}{d\omega} \tag{2.31}$$

Thus, we obtain the relationship between phase and group velocity. Assume two monochromatic waves are travelling in vacuum, their phase velocity and group velocity are the same, which is *c*, the speed of light in free space. As they propagate in a dispersive medium, the phase and group velocities of these two waves will be different as they superpose with each other. When $dv_p/d\lambda > 0$, normal dispersion occurs; and if $dv_p/d\lambda < 0$, anomalous dispersion occurs. Also, the phase or group velocity can also be made to be zero, but the two waves have to coincide each other in the opposing direction.

The time delay in SBS slow light is given by (Agrawal, 2000; Khurgin and Tucker, 2008):

$$\Delta t = \Delta t_m \times \frac{1-\beta^2}{\left(1-\beta^2\right)^2} = \left(\frac{g_p dP_p}{\Gamma_B A_{eff}}\right)\frac{1-\beta^2}{\left(1-\beta^2\right)^2} \tag{2.32}$$

where the symbols represents the gain coefficient (g_p), the fiber distance (d), the pump power (P_p), the full width at half maximum (FWHM)/gain bandwidth ($\Gamma_B/2\pi$), the fiber effective mode area (A_{eff}). $\Delta t_m = g_p dP_p/(\Gamma_B A_{eff})$ is the maximum delay that occurs when the Brillouin gain value is at its highest. When Δt_m is a constant value, the β parameter will be the only determining factor of the time delay, expressed as

$$\beta = \frac{\Delta\Omega}{\left(\Gamma_B/2\right)} = \frac{2\alpha\left[MHz/°C\right]\times\left(T-T_0\right)\left[°C\right]}{\left(\Gamma_B/2\pi\right)\left[MHz\right]} \tag{2.33}$$

where the symbols represent the temperature coefficient (α), the sensing fiber temperature(T), and the room temperature (T_0). From Eq. (2.32) and Eq. (2.33), the temperature dependence of the delay can be obtained.

2.4.3 Slow Light Sensing

The Stokes shift is temperature dependent which equates to SBS slow light being affected by temperature changes. Thence, by measurement of the time delay, the temperature shift can be obtained. The slow light measurement system is advantageous due to the more straightforward approach of directly using the oscilloscope for detection. The equipment used in BOTDA, BOTDR, BOCDA and BOFDA is more costly and the configurations are also more complex.

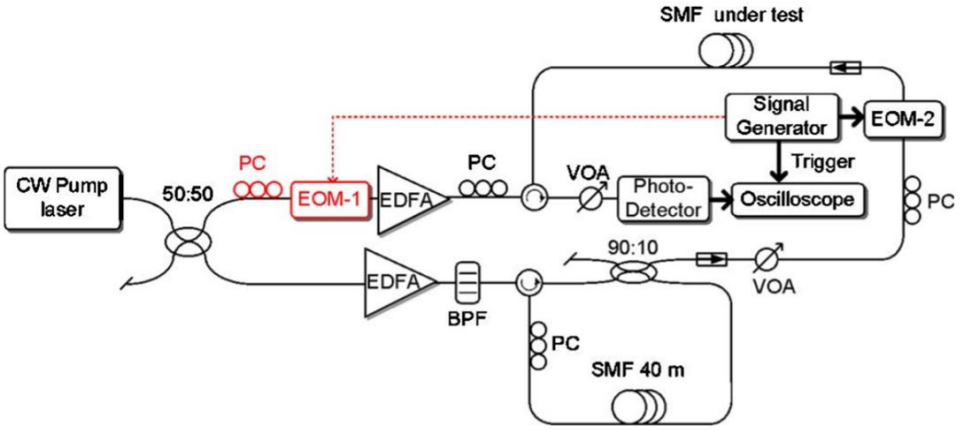

Figure 2.8: SBS slow light temperature sensing system (Wang et al., 2011)

In Figure 2.8, the experimental scheme produced by *Wang et al.* measured the probe pulse parameters to record the output of the system. They used an oscilloscope with resolution of ~1ps that can display high temperature sensitivity. In the setup, the pump laser is split into two paths: an upper path functions as the SBS slow light pump source; a lower path functions as the pump for the Brillouin fiber laser. The fiber laser output is downshifted by ~10GHz or the Stokes downshift frequency. This is to prime the process of SBS as mentioned in the SBS generation theory presented beforehand. Both the FUT and Brillouin laser fiber are the same type so that the probe frequency is the same as the Stokes downshift frequency. Electrostriction occurs in the fiber and produces acoustic waves that scatter the pump light, delaying the pump light pulse due to the slow light effect. In Figure 2.9 (a), the gain spectra reduced slightly as temperature increases. The gain of the system should be high enough as to obtain a delay value that is significant. Based on the Stokes frequency shift in Figure 2.9(b), the sensitivity obtained is 1.07MHz/^{0}C.

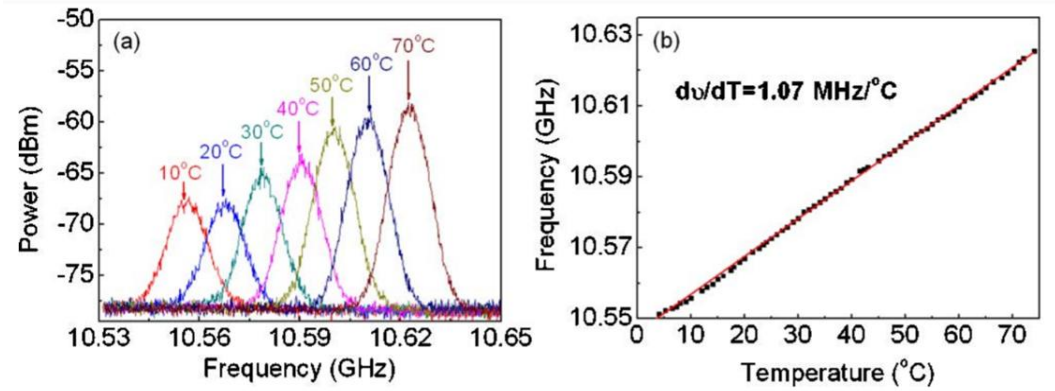

Figure 2.9: (a) Heterodyned Brillouin gain spectrum for different temperature (b) Stokes frequency shift vs temperature

Wang et al. used a 100m SMF as the FUT to test the performance of the system, and later on replaced it with a 2m SMF to serve as a benchmarking. The comparison test is important to be issued so that the hypothesis can be proven. The CW pump for the Brillouin fiber laser is amplified by EDFA through a 40m SMF. Then, the fiber laser output is filtered by a bandpass filter for noise reduction. A 50ns probe pulse is modulated using an electro-optic modulator. The downshifted Stokes pulse coincides with the CW pump and detected using a photodetector. In Figure 2.10, the measurement range is from 23.0^{0}C to 41.0^{0}C. The Brillouin gain spectra determines the temperature sensing range. As the temperature increases, the pulse becomes more distorted because of gain reduction and bandwidth limit. The maximum delay achieved is 29.90ns as shown in Figure 2.10(a). For Figure 2.10(b), it is observed that higher SBS gain provided higher temperature sensitivity as the gain is increased from 20dB to 40dB.

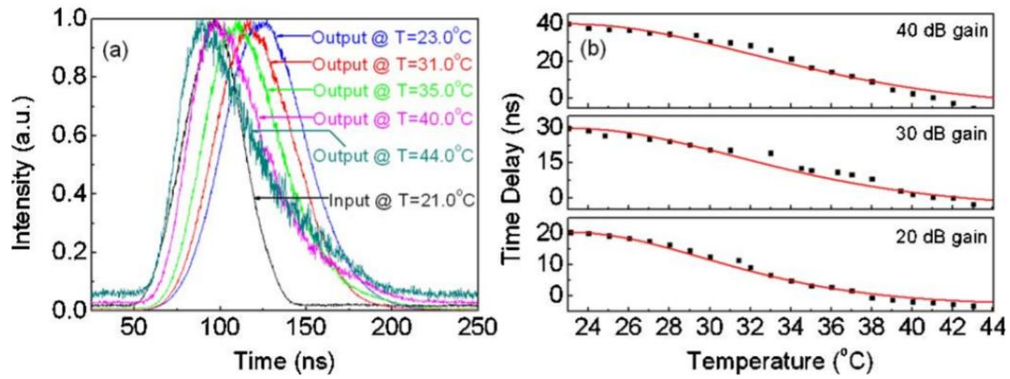

Figure 2.10: (a) Output pulses at different temperatures, 100m SMF (b) Time delay vs temperature at different gains (40dB, 30dB, 20dB)

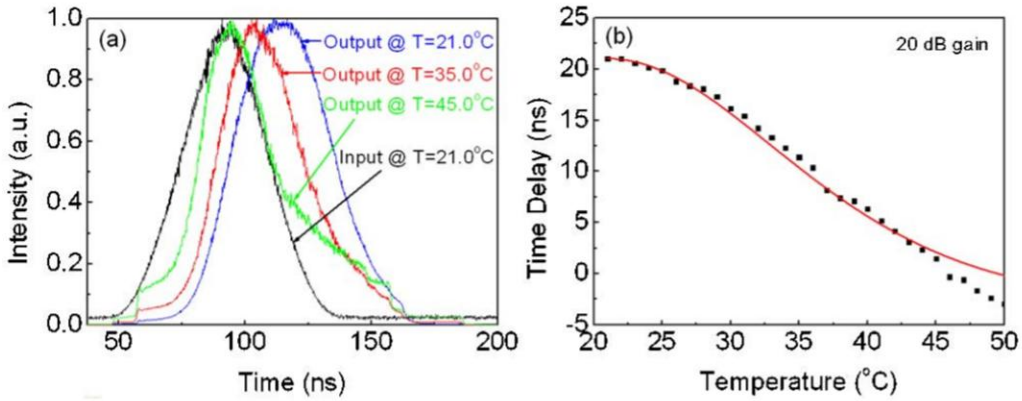

Figure 2.11: (a) Output pulses at different temperatures, 2m SMF (b) Time delay vs temperature at 20dB gain

The comparison test results are shown in Figure 2.11. A pulsed pump is used for higher peak power for slow light effect to take place. The obtained maximum delay is 21.00ns, while the sensitivity is 0.90ns/^{0}C. The difference of this experiment from the previous one is the increase of the sensing range, which is 21.0^{0}C to 46.0^{0}C. The spectral width of the pump pulse is negligible for the case of 100m experiment as the SBS gain bandwidth is around 40MHz. For the 2m experiment, the spectral width of the pump pulse is around 10MHz which is about the same order as the SBS gain bandwidth. This means that the

SBS gain bandwidth obtained from the pump spectrum convolution and intrinsic gain spectrum is at around 50MHz, which explains the increase in sensing range.

.

The positive or negative change in temperature can be determined by modifying the parameters to offset the Brillouin resonance and probe pulse frequency. As temperature increases, the gain peak wavelength increases. Therefore, the probe at longer Brillouin gain peak wavelength will have increased delay. Inversely, temperature drop indicates a decreased delay amount. The deduction that is obtained from the slow light experiment is that the delay between pump and probe can be changed to monitor certain parts of the FUT. This selection of spatial measurement indicates the usefulness for distributed sensing and dynamic profiling, especially in long range fibers.

Sensitivity improvement are also shown when slow light is used in tandem with other systems such as fiber laser sensor and FBGs. In the fiber laser sensor, the interrogation is conducted using a Mach-Zehnder interferometer. The change in vibration was detected to be at 408kHz. In order to further improve the sensitivity, slow light was introduced to the upper arm of the interferometer, which shown an improvement of 1.57 times compared to the system without slow light (Qian *et al.*, 2019). FBG slow light sensing also showed that the group velocity can be reduced to 2360km/s and achieve a sensitivity of 3.14×10^5 strain^{-1} (Wen *et al.*, 2011).

For the aforementioned researches, none of them are addressing the possibility of using higher order Brillouin scattering to improve the SBS slow light system. Higher order Brillouin gain spectrum that experiences multiples of Brillouin frequency shift might lead to greater frequency changes due to small temperature or strain variations.

2.5 Conclusion

The different sensing technologies are presented and discussed. With the small-scale slow light devices being researched, the capability of slow light sensing will be greatly enhanced. Hence, slow light is strongly recommended as a good candidate in optical sensing. Higher order Brillouin gain spectrum is investigated for the enhancement of Brillouin slow light and hence Brillouin slow light sensing.

CHAPTER 3

RESEARCH METHODOLOGY

3.1 Introduction

In this chapter, the techniques of slow light sensing will be explained. The fundamentals of the Brillouin slow light generation are based on the nonlinear process stimulated Brillouin scattering. The entirety of the approach used in this research is experimental investigation with analysis. In order to affirm the set objectives, the experiments are carried out using the configured setups that are proposed.

Experimental studies had been performed accordingly as follows:

1. Characterization of the first order Brillouin Stokes.
2. Characterization of the second order Brillouin Stokes.
3. Characterization of the first and second order Brillouin slow light.
4. Characterization of the temperature sensing performance for the first and second order Brillouin slow light.

3.2 Research Approach

Figure 3.1 shows the summary of the methodologies of slow light generation as studied in Chapter 2. In this work, the technique being used is based on coincidence of pump and probe signals derived from nonlinear SBS effect in the optical fibers. The two approaches are adopted side-by-side to produce Brillouin slow light. The first step is to generate Brillouin Stokes signals, where the first order and second order signals are produced. Then, the next step is to launch the pump and probe in opposite directions and coincide them in the tested fiber to produce SBS slow light. The procedure is repeated for the second order pump and probe signals to obtain second order slow light. Figure 3.2 shows the division between different optical fiber sensing methodologies. Point or discrete sensing comprises of the FBG, while for distributed sensing, there is BOTDA, BOCDA, BOFDA and BOTDR. As for slow light sensing, it is divided into first order and second order system.

Each and every section of this chapter is accompanied with a diagram of the experimental setup, and also the flow chart explaining the experiment flow. The aim of the conducted experiments is to validate the feasibility of the sensing setup. The structures in the setup are characterized by changing the parameters: input power, pump power, probe power, fiber length, modulation frequency, modulation scheme and temperature. After those parameters are changed and optimized, the final performance of the sensing setup is evaluated by comparing the delay produced by the first order setup and the second order setup to obtain the temperature sensitivity difference.

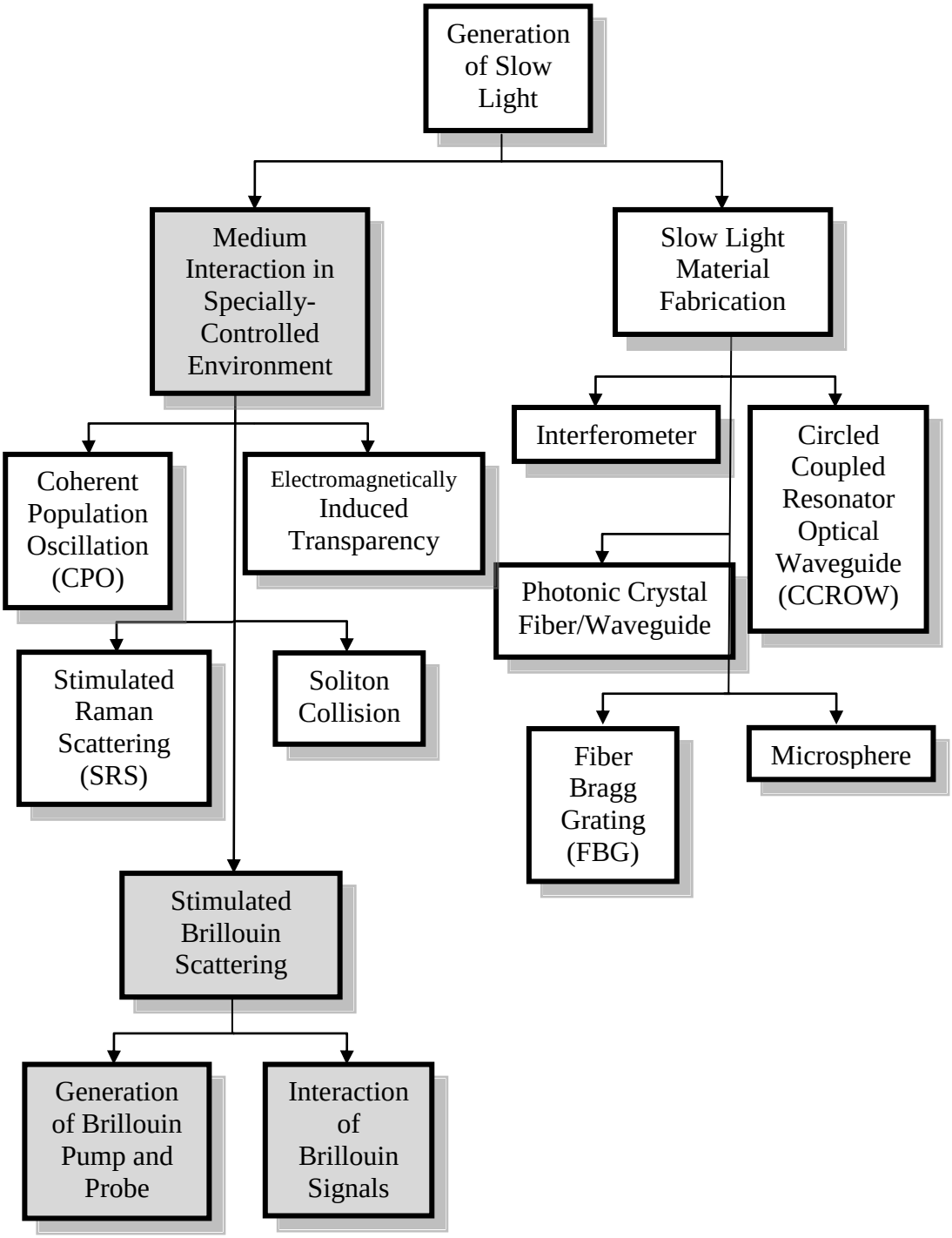

Figure 3.1: Research methodology chart

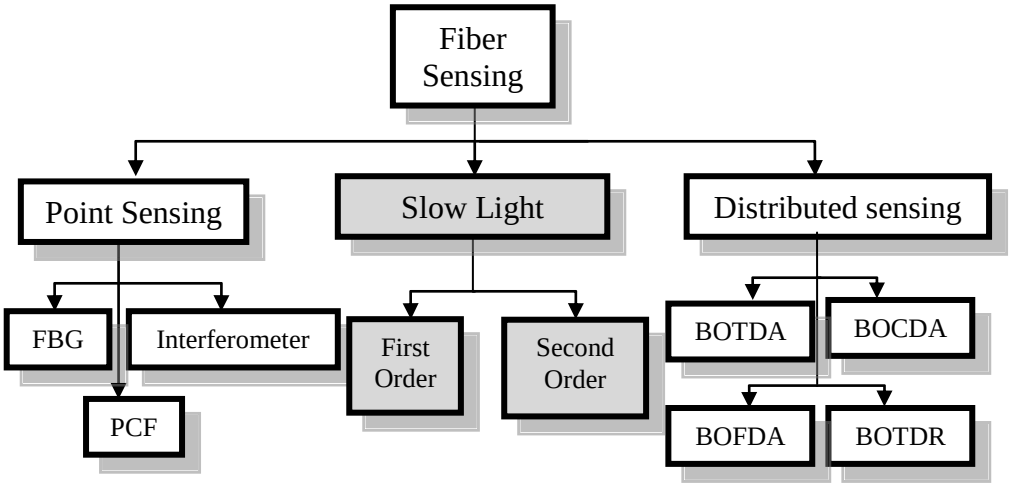

Figure 3.2: Fiber sensing classification

3.3 Characterization of first order Brillouin Stokes

As shown in some of the previous works, the nonlinearity of a medium contributes to the occurrence of Brillouin scattering (Edwards *et al.*, 2016; Mishra, Varun and Pant, 2019).

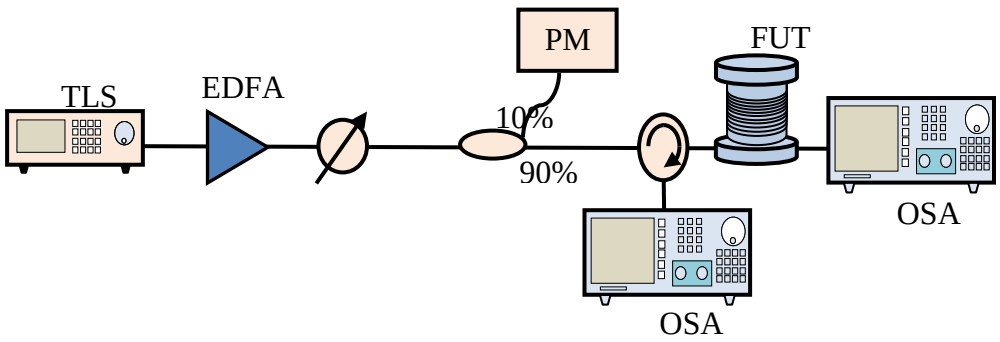

Figure 3.3: Operating setup for the generation of first order Brillouin Stokes

As shown in Figure 3.3, the TLS is a Santec WSL-100 with linewidth<100kHz and the EDFA is Keopsys CEFA-C-PB-HP. The first order

Brillouin Stokes characterization consists of the Brillouin pump, optical attenuator, 3-port circulator, fiber under test and OSA. The pump wave is injected into the system as the main light source, amplified by a high-power EDFA. Due to the nonlinearities of the optical fiber, there is a natural tendency for the optical fiber to produce backscattered waves travelling in the opposite direction to the pump wave, known as Brillouin Stokes signal.

This experiment aims to determine the first order Brillouin Stokes signal (BS1) threshold for different single mode fiber (SMF) lengths. With the increase in Brillouin pump (BP) power, the properties are recorded by measuring the power of the Brillouin threshold that is needed to instigate the BS1. Before this, we have discussed in the literature review that the Brillouin threshold is the power required for SBS to begin. The BS1 shows exponential growth as the threshold for BS1 is exceeded.

According to Figure 3.4, the changes in Brillouin shift, threshold and spectrum are recorded by increasing the BP power. After the results are analysed, we re-run the experiment by changing the fiber spool with different lengths.

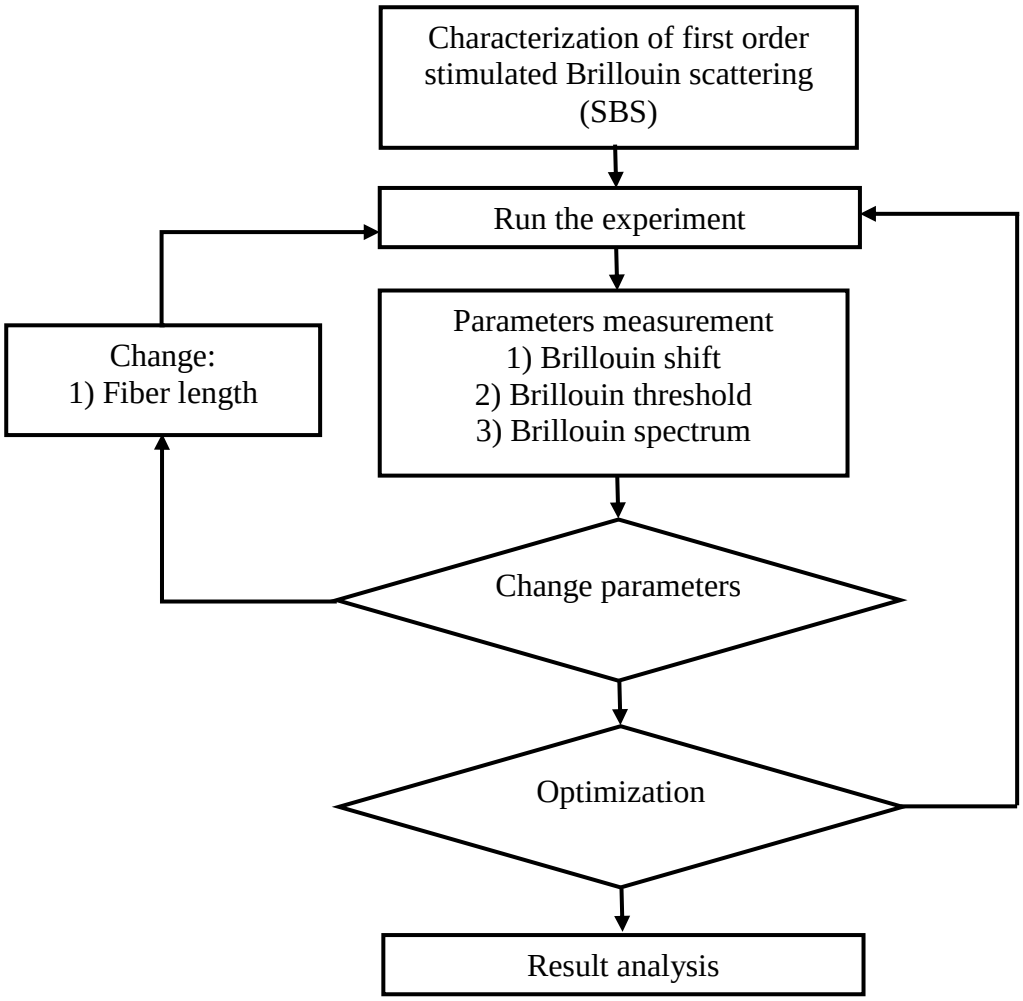

Figure 3.4: Flow chart for first order Brillouin Stokes

3.4 Characterization of Second Order Brillouin Stokes

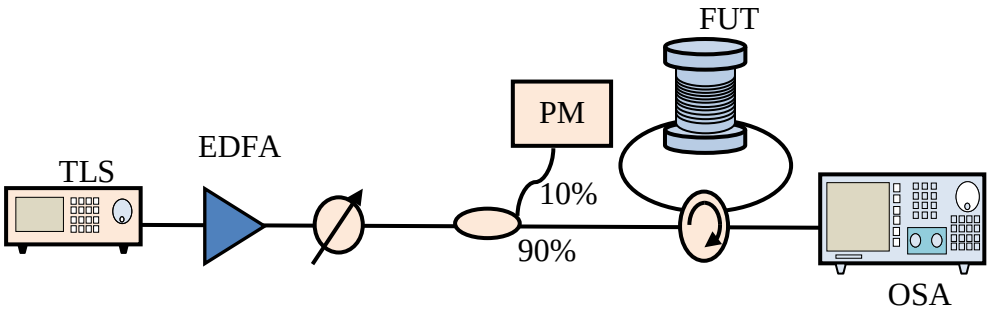

Figure 3.5: Operating concept for the generation of second order Brillouin Stokes

For the generation of the second order Stokes, we used a technique known as double Brillouin frequency shifting, which is an efficient method of generating higher order Brillouin Stokes, as shown in Figure 3.5 (Shee *et al.*, 2010). In order to achieve this, a 4-port circulator is used instead of a 3-port circulator to form a ring cavity, which is required for the vestigial power to circulate within the gain medium.

In the ring cavity, BS2 generation is initiated by circulation of odd order Stokes signal, which produces even order Stokes signal which is the desired output. When the first order Brillouin threshold is exceeded, the BS1 that travels opposite to the input signal will be generated. The generated BS1 travels through the circulator to reach the other end of the fiber and acts as a BP which is emitted from port 3. BS1 circulation is in a counterclockwise direction, where the energy is being supplied by BP. As the BS1 signal exceeds the SBS threshold, BS2 will be produced. The end-product will then go from port 3 to 4 and is analysed at the receiver. The receiver used is the OSA. The peak power of the BS2 is shown in the spectrum. This experiment aims to determine the second order Brillouin threshold for different SMF lengths.

Flow chart for the BS2 generation is depicted in Figure 3.6. The test structure is similar to the first order setup.

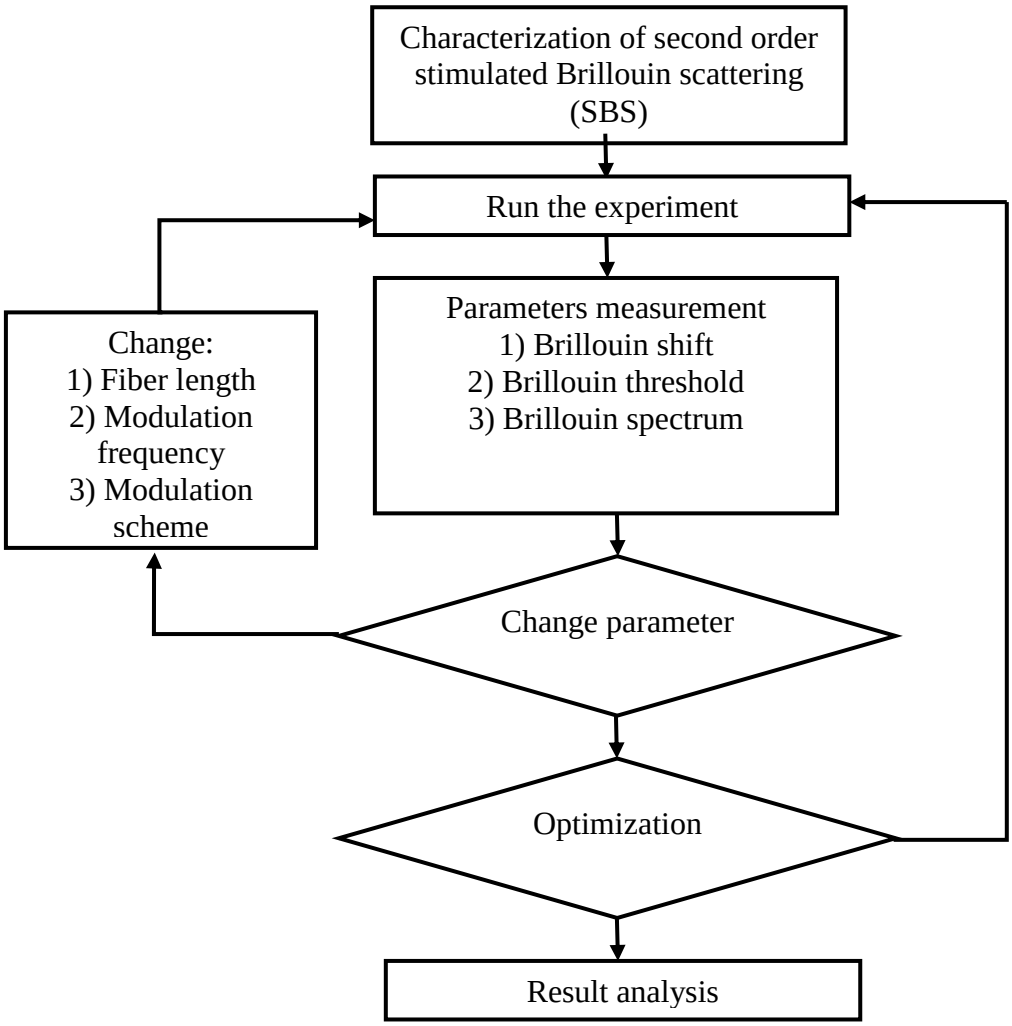

Figure 3.6: Flow chart for second order Brillouin Stokes

3.5 Characterization of First and Second Order Brillouin Slow Light

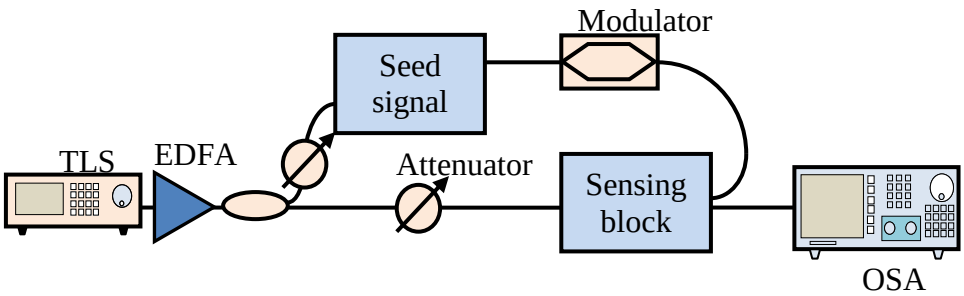

Figure 3.7: General setup for first and second order Brillouin slow light

Analysis on section 3.5 and section 3.6 will be referred to Figure 3.7. This figure shows the general setup of the Brillouin slow light experiment for both first order and second order. It comprises of an amplified laser split into two paths, namely the pump and probe path. The pump wave refers to the wave going through sensing block path, while the probe wave refers to the wave through the seed signal generator. The conceptual setup from Figure 3.3 is inserted into both the seed signal generator and sensing block for the first order slow light. Likewise, the setup from figure 3.5 is also inserted into the same sections of the slow light sensor for the second order slow light.

The scattering processes in optical fibers, whether spontaneous or stimulated, are categorised into Rayleigh, Raman, and Brillouin scattering (Zou, Long and Chen, 2015). This scattering phenomenon will occur in optical fibers regardless of the input power of the injected light. Typically, Brillouin Stokes wave produced by Brillouin scattering travels backwards to the direction of the incident light. In SBS slow light, the delaying of the optical pulse is achieved when the pump and probe are in resonance. This resonance effect is produced at the Brillouin frequency. Under the same Brillouin frequency, the coincidence of pump and probe wave in the fiber under test caused the modulated pulse to be delayed.

The laser source power is adjusted using the two optical attenuators placed after the 3dB coupler. According to Figure 3.8, we fix the power in the probe path, while the power in the pump path is varied. The results are plotted

and analysed. After analysis, we chose the most suitable pump power to proceed with the temperature sensing test.

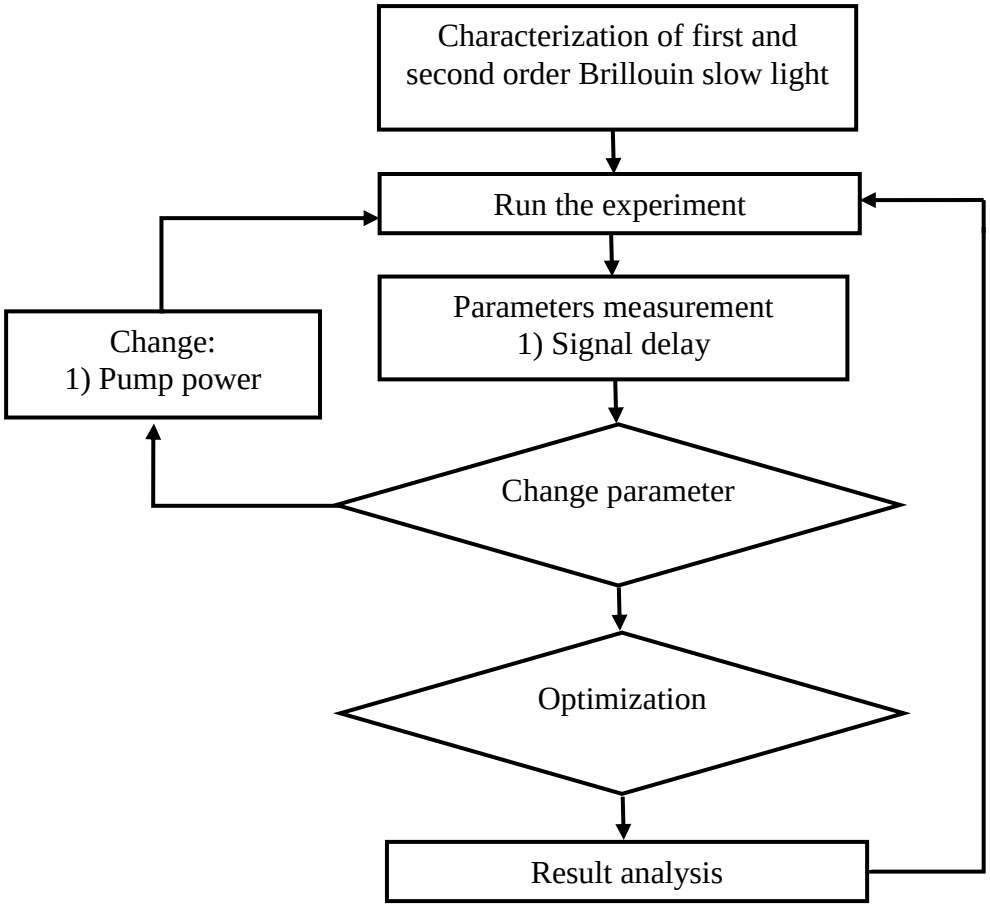

Figure 3.8: Flow chart for first order and second order Brillouin slow light

3.6 Characterization of Temperature Sensing Performance for the First and Second Order Brillouin Slow Light

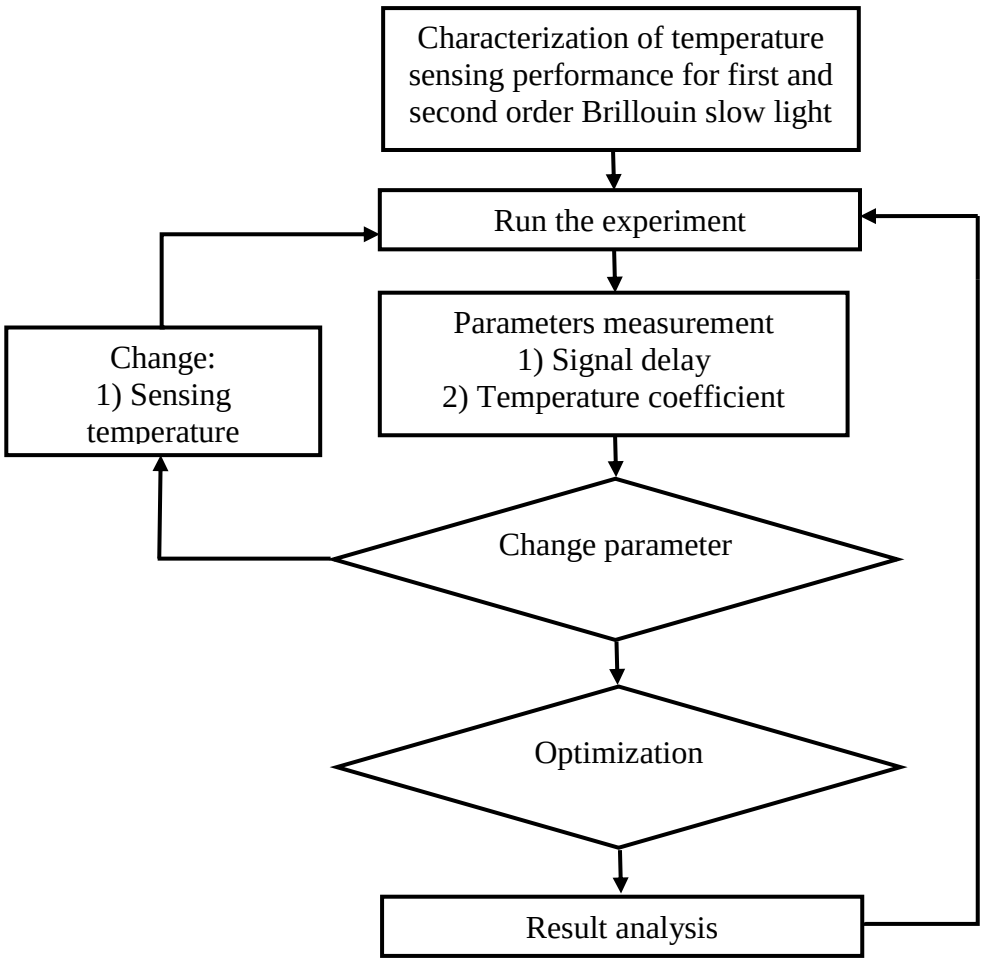

Figure 3.9: Flow chart for temperature sensing performance for the first and second order Brillouin slow light

As previously stated, Figure 3.7 is also used in section 3.6. For us to vary the temperature, part of the sensing block is encased in a laboratory convection oven. Resultant from the refractive index change of silica due to change of temperature, the temperature change will also affect the delay of the slow light pulse due to the dependency on the refractive index. This brings us back to one of the earliest formulae regarding speed of light in a medium:

$$n = \frac{c}{v} \tag{3.1}$$

where n is the refractive index, *v* is the group velocity of light in the medium and *c* is the velocity of light in free space.

Prod'homme provided explanations on the temperature-refractive index relationship (Prod'homme, 1960). There are two variables that are considered: volume expansion coefficient, β and polarizability coefficient, Φ. They are represented in the following equations:

$$\beta = \frac{1}{V}\frac{dV}{dT} = -\frac{1}{\rho}\frac{d\rho}{dT} \tag{3.2}$$

$$\Phi = \frac{1}{\alpha}\frac{d\alpha}{dT} \tag{3.3}$$

By differentiating the Lorentz-Lorenz equation,

$$\frac{dn}{dT} = \frac{(n^2-1)(n^2+2)}{6n}(\Phi - \beta) \tag{3.4}$$

which concluded that density of glass does not depend on the mean polarizability.

By using another approach, the temperature dependence of refractive index of silica glass has been revised (Tan, 1998). In this explanation, the independence of the mean polarizability towards the glass density has been debunked. Two equations could be used to describe the refractive index change due to temperature,

$$n^2 - 1 = \frac{N_A \rho}{\varepsilon_O W}\alpha \tag{3.5}$$

$$\frac{n^2-1}{n^2+2} = \frac{N_A \rho}{3\varepsilon_O W}\alpha \tag{3.6}$$

which are the Newton-Drude formula and the Lorentz-Lorenz equation respectively. N_A is the Avogadro number, W is the molecular weight, ρ is the density and α is the mean polarizability. In this relation, α has been proved to be a function of both density and temperature (Mueller, 1935; Tan, Arndt and Xie, 1998). The importance of proving α's relation with the density is because of the density's association with the resonance frequency or acoustic frequency.

Referring to Figure 3.9, the temperature change against delay curve is plotted and analysed to obtain the sensitivity of the setup. The temperature sensitivities of the first order and second order slow light sensing setup are measured up against each other to prove that the theory matches with the results.

3.7 Conclusion

To sum up this chapter, the research work in this thesis is based on the methodologies presented. The designed methodologies are displayed in the form of flow charts and are explained accordingly. The generation of Brillouin slow light for sensing are characterised based on parameters that dictate the performance of the setup. The performance of the proposed experimental setups are modified and assessed using these parameters as a benchmark.

CHAPTER 4

GENERATION OF FIRST AND SECOND ORDER SLOW LIGHT BASED ON STIMULATED BRILLOUIN SCATTERING FOR TEMPERATURE SENSING

4.1 Introduction

In this work, the temperature sensing is based on slow light mechanism, Brillouin gain medium shall be characterized to understand the parameters, consisting of the Brillouin frequency shift and Brillouin threshold. The performance of the second order system is benchmarked against the first order system. The Brillouin frequency shift and Brillouin threshold are being measured as part of the Brillouin parameters. Then, different waveforms and modulating frequencies are used.

For the temperature sensing experiment, the performance of the second order system is benchmarked against the first order system. The delay of the first and second order are recorded with increasing temperature. Then, a reliability test is conducted.

4.2 Brillouin Parameters Characterization

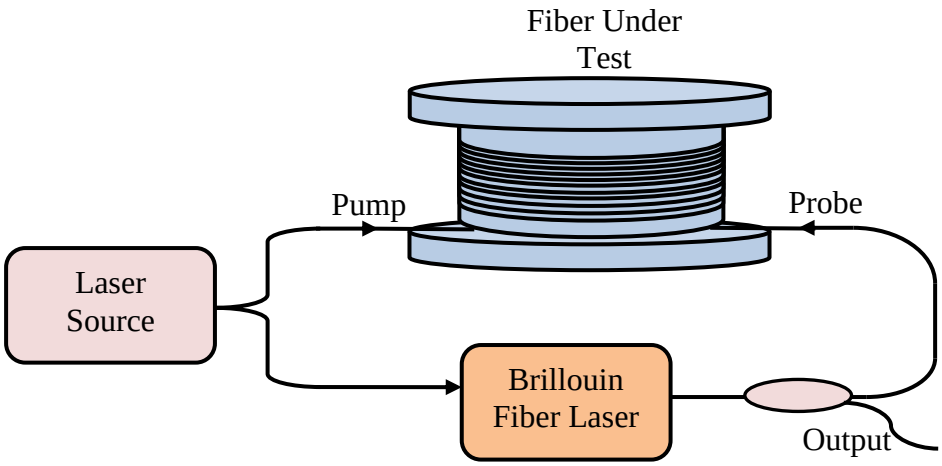

Figure 4.1: Simplified Representation of the Slow Light Model

Slow light is said to be achieved when the group velocity of the incident light source is effectively slowed down, by using any means listed in the literature review. Hereinafter, the method that is employed is based on SBS. Basically, SBS slow light is generated by using a coherent light source branching out into two paths as shown in Figure 4.1, which cross each other in the fiber under test. For any given light source, the resultant spectrum could be observed by the use of an OSA. With today's technology, the laser acting as the light source has narrow spectral width, which is usually referred to as single frequency laser. The operating wavelength resolution is in the order of 10^{-11}m. As the frequency downshift/wavelength upshift exhibits changes in such a small magnitude, the temperature difference incurred in the step size of 2°C cannot be properly observed using the OSA (Jung *et al.*, 1999).

For that reason, modulation schemes have to be used to assist in the measurement of delay. By modulating the signal produced using an electro-optic modulator (EOM), the element added is a time-domain component of the desired input signal. The modulator is able to project the frequency of the electrical signal produced from the signal generator, as well as the shape of the electrical signal, into the optical signal. Noise is added to the output signal as it travels along the optical fiber system, which is an inevitable factor (Bottacchi, 2008). However, noise compensation can be done by averaging techniques either at the oscilloscope or via post-processing (Fager and Andersson, 2006; Bishop, 2010).

In the output, a photodetector or optical-electrical converter is used to convert the optical signal into electrical signal. This conversion is done in order to facilitate the signal reading at the oscilloscope, since the oscilloscope can only read electrical signals. At the oscilloscope, the results are showed in time-domain instead of spectra, where the delay of the signal can be observed. This methodology of reading data is applied the same as BOTDA, with some differences in the optical setup. Conventionally, if a continuous wave laser is input into a photodetector, the noise floor shown in the oscilloscope will rise in accordance of the power of the output laser. Once the laser is being modulated, the signal alongside with the information being carried by it will be shown in the oscilloscope. The significance of this is that the unmodulated signal does not have a time component while the modulated signal has it. The time component is useful to detect any phase and amplitude change in the produced signal. A splitter is also used to compare the signals of the original

modulating electrical signal from the signal generator and the produced output signal. The modulating signal is used as a reference to determine how much delay is produced by the experiment being conducted at the time. Since the oscilloscope has multiple probes, the signals can be compared in real time, which means that time can be saved.

The Brillouin frequency shift and threshold are important parameters. The BFS gives information on the wavelength where Brillouin gain occurs. Since the pump and probe coincide each other in the FUT, the characterization of the BFS is needed to ensure that the wavelength of the Brillouin Stokes signals are exactly the same at different BP power for the signals produced at both FUT and seed signal fiber spools. On the other hand, when the Brillouin threshold power is exceeded, most of the power of the generated SBS signal are reflected. Therefore, the BFS and Brillouin threshold of the first order and second order will be measured and compared.

4.2.1 Brillouin Frequency Shift and Threshold Measurement

The Brillouin frequency shift occurs during the SBS process, where the reflected wave frequency is lower than the incident wave. This is known as the frequency difference between the incident wave and the reflected wave, ν_B and corresponds to the frequency of acoustic/emitted phonons. The Brillouin threshold power is the power level where the Brillouin Stokes signal power starts to increase exponentially. Knowing the Brillouin shift and threshold is important as it is part of the step of characterizing the slow light setup.

4.2.1.1 First Order Characterization

Referring to Figure 3.3, the tunable laser source (TLS) Santec WSL-100 is set to emit laser of around 1550nm. The input power is monitored at the splitter after the attenuator by using a power meter. The beam path then is circulated by a 3-port circulator, whereby the port 2 redirects the light path into the FUT. The output that is emitted through that path is monitored by an OSA, which is of the model Yokogawa AQ6370C. Due to the process of SBS, when the threshold of SBS is reached, part of the light emitted from the FUT which are the result of the Brillouin process are transmitted into the port 2 of circulator, which is redirected to port 3. Again, the output from the port 3 of circulator is monitored using an OSA. The Brillouin threshold is said to be achieved when the peak power of the Stokes wave increases exponentially. As the input power of the light source exceeds that particular threshold power, the excess power is transferred to generating the higher order Brillouin Stokes.

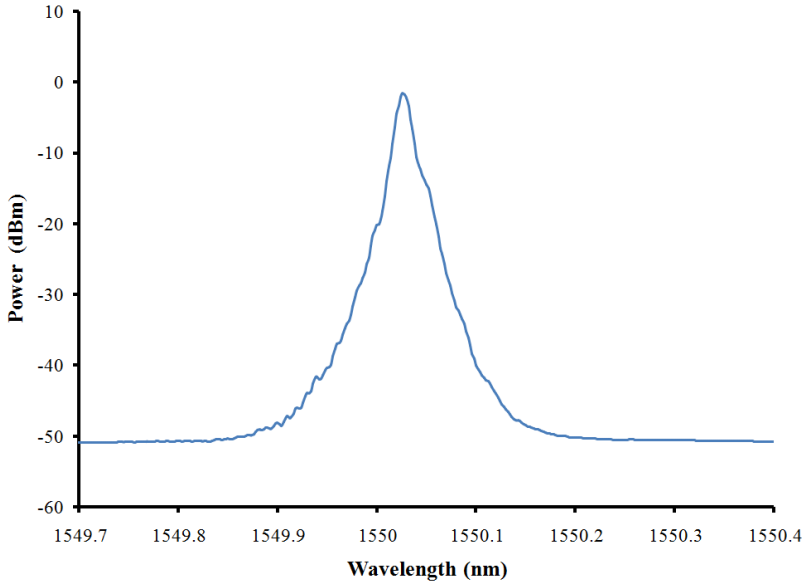

Figure 4.2: Tunable Laser Source Input Spectrum

The input spectrum from the TLS is shown in Figure 4.2. The peak power of the input spectrum is at 1550.026nm with a -1.62dBm peak power. This is used in both first and second order setup.

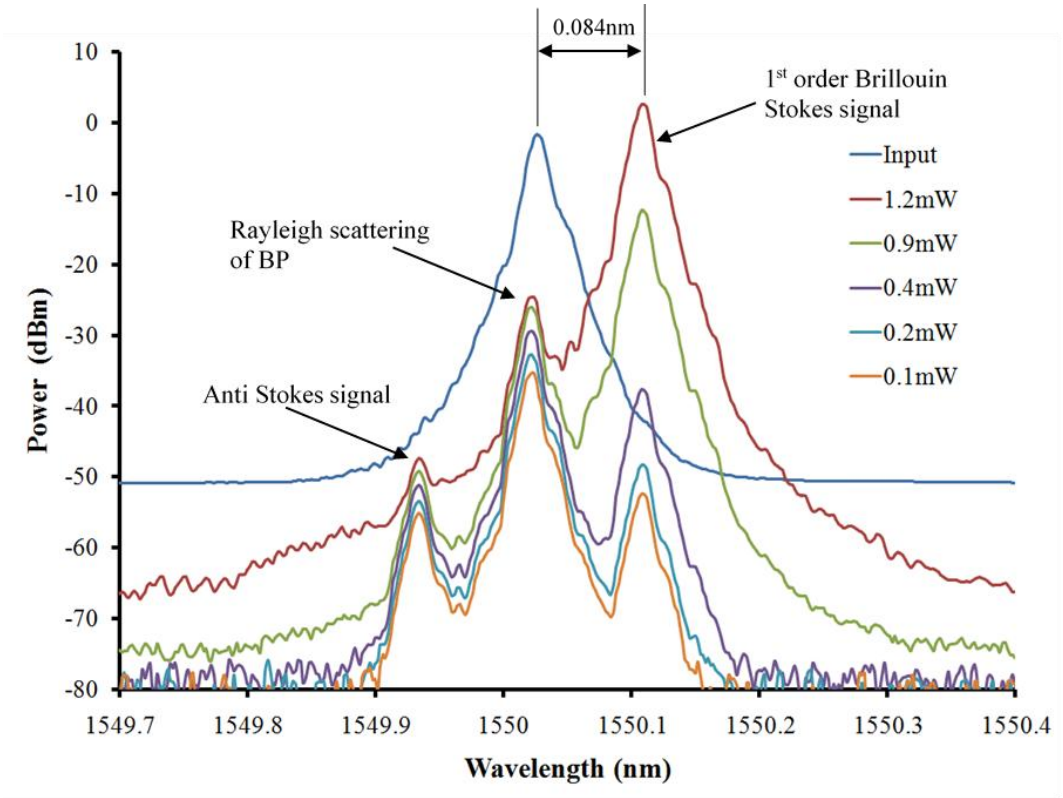

Figure 4.3: First Order Brillouin Stokes for 2km Fiber Spool

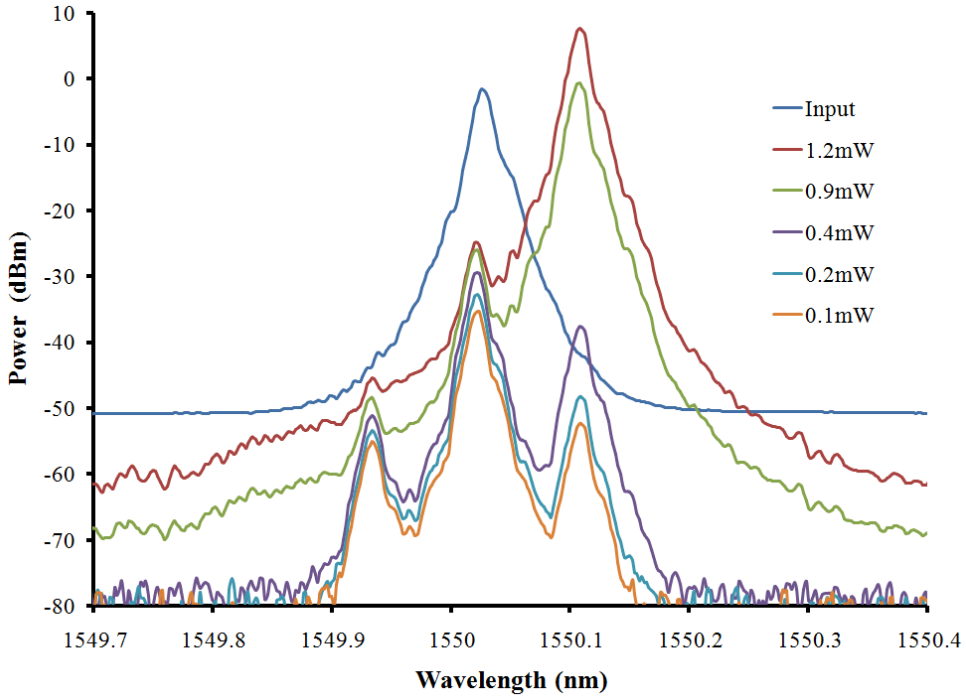

Figure 4.4: First Order Brillouin Stokes for 5km Fiber Spool

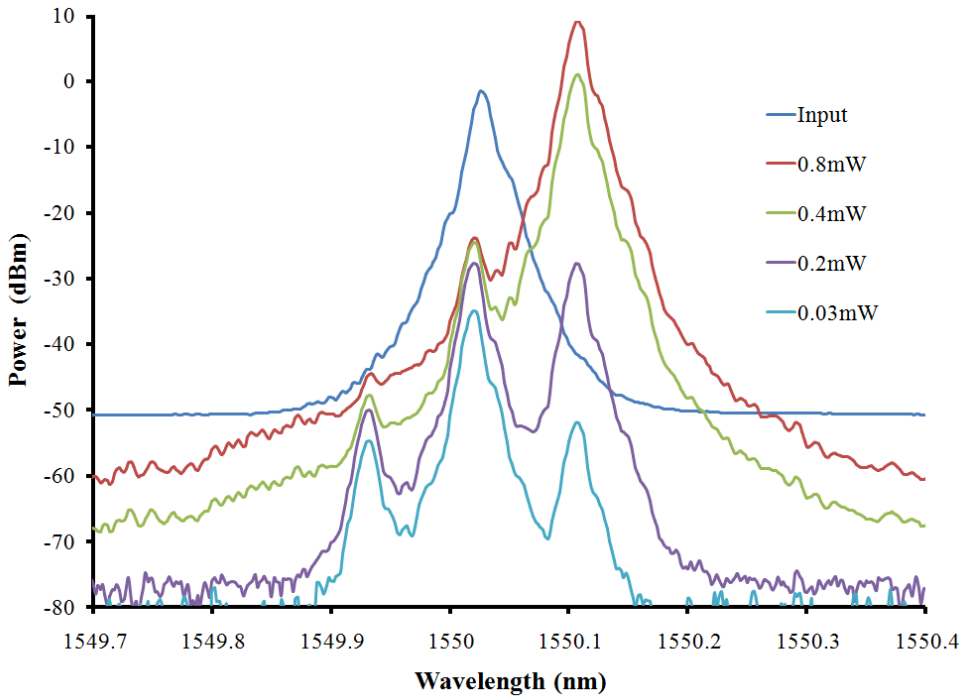

Figure 4.5: First Order Brillouin Stokes for 10km Fiber Spool

The first order Brillouin Stokes for the 2km, 5km and 10km fibers are as shown as in Figure 4.3, 4.4 and 4.5 respectively. Note that there are three

peaks that are important in this experiment. As pointed out in Figure 4.3, the leftmost peak is called the anti-Stokes peak, the middle peak is the reflected BP due to Rayleigh scattering, and the rightmost is the first order Brillouin Stokes signal. As the power of BP is increased, the increment of the peak power of these three peaks have different rate of progression, with the Stokes peak having higher progressive rate. It is observed that the anti-Stokes signal power increases as the BP is increased. However, it is negligible as its power is >40dB below the desired signal which is BS1. The Brillouin Stokes for all three lengths of fiber peaked at 1550.11nm, meaning that a frequency shift of 0.084nm has taken place. The value of the frequency downshift is the same due to the SMF for the three fibers are the same.

As can be seen from the spectrum figures, when the BP power is increased, the BS1 peak power also increased, alongside with some increase in the peak power of the signal that is of the same wavelength as the BP, which is the reflected signal due to Rayleigh scattering. The increase in BP power only increased the reflected Rayleigh signal peak power slightly, as most of the power is transferred to generating the BS1. In order to obtain the frequency downshift value from the Brillouin pump wavelength value itself, the expression below is used:

$$v_B = \frac{2nv_A}{\lambda} \tag{4.1}$$

which gives us a value of 11.14GHz downshift, from the general equation. For calculation purposes, the values in Table 4.1 are referred:

Table 4.1: Typical Values for SMF

Parameters	Symbols	Values
Refractive index	n	1.44
Pump wavelength	λ(nm)	1550.11
Acoustic velocity	v_A (m/s)	5996
Brillouin linewidth at FWHM	v_{BW}(MHz)	30
Speed of light	c (m/s)	299 792 458

A comparison is to be made using the following simplistic expression, which is derived as follows (Boyd, 2019):

$$f = \frac{c}{\lambda} \tag{4.2}$$

In order to obtain the change in frequency, i.e. frequency downshift, the change in frequency and wavelength is applied:

$$\Delta f = \frac{-c}{\lambda^2}\Delta\lambda \tag{4.3}$$

using the values obtained from Table 4.1,the frequency downshift obtained is 10.98GHz, which is a more precise value representation where Δf is the downshift frequency.

The Brillouin threshold is measured as shown in Figure 4.6. The Brillouin threshold is affected by various factors such as the Brillouin gain media length and effective area mode. The threshold value is obtained when the power of the BS increases exponentially. For the 2km, 5km and 10km fiber, the threshold power are 101mW, 61mW and 26mW respectively.

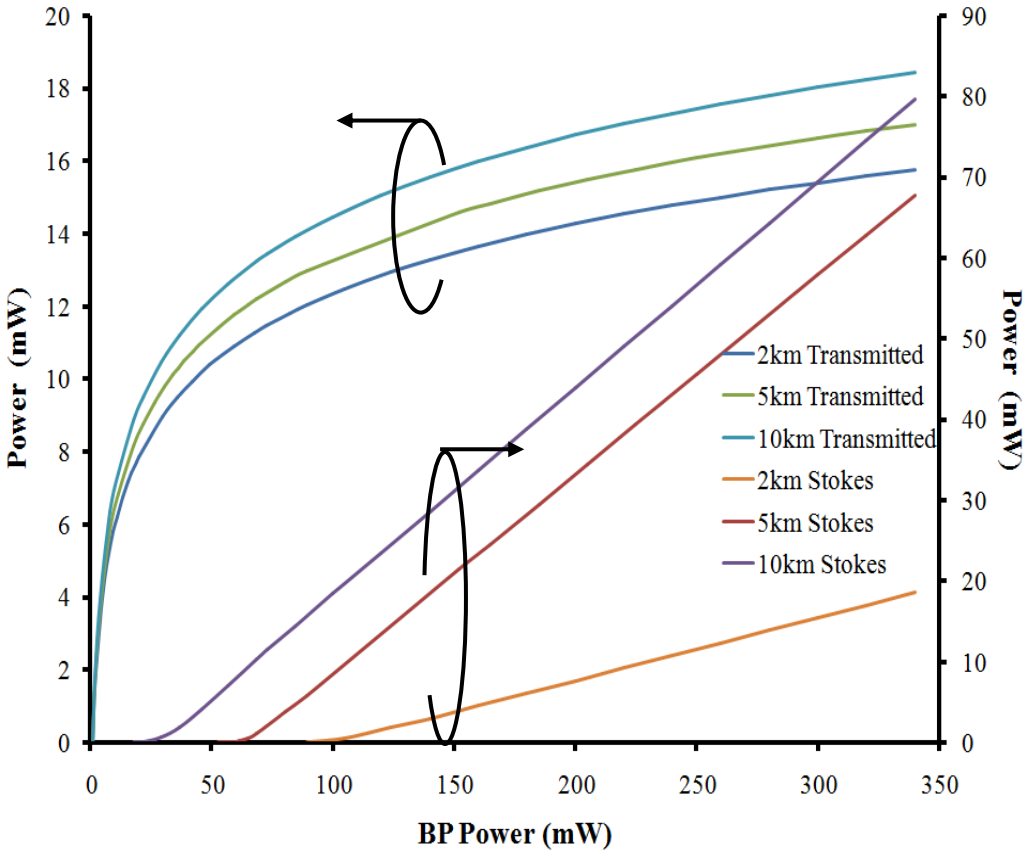

Figure 4.6: Plotted BP and Stokes Peak Power

4.2.1.2 Second Order Characterization

Referring to Figure 3.5, the measurement setup for the second order Brillouin Stokes signal characterization. The power requirement of the second order Brillouin process is higher compared to first order, so the number of components is kept at a minimal. This step is taken to ensure that the limited power of the laser source can be transferred as much as possible to the fiber under test.

This method of producing higher order Brillouin Stokes signal relies on the mechanism where the earlier order Stokes signal are needed to produce

the next order Stokes signal. To put this into perspective, we focus on the 4-port circulator part. The first order Brillouin Stokes signal is generated as the Brillouin pump enters port 2 via port 1. The first order Stokes signal is generated at the FUT as pump power exceeds the threshold. Since this signal is in the opposite direction of the pump, it travels to port 3 via port 2 and reaches the rear end of the FUT. Here, we could assume that the first order Stokes signal acts as a 'pump' to excite the generation of the second order Stokes signal, referring to the similar way on how the first order signal is generated. In this process, the power of the first order signal is also required to exceed the second order Brillouin threshold.

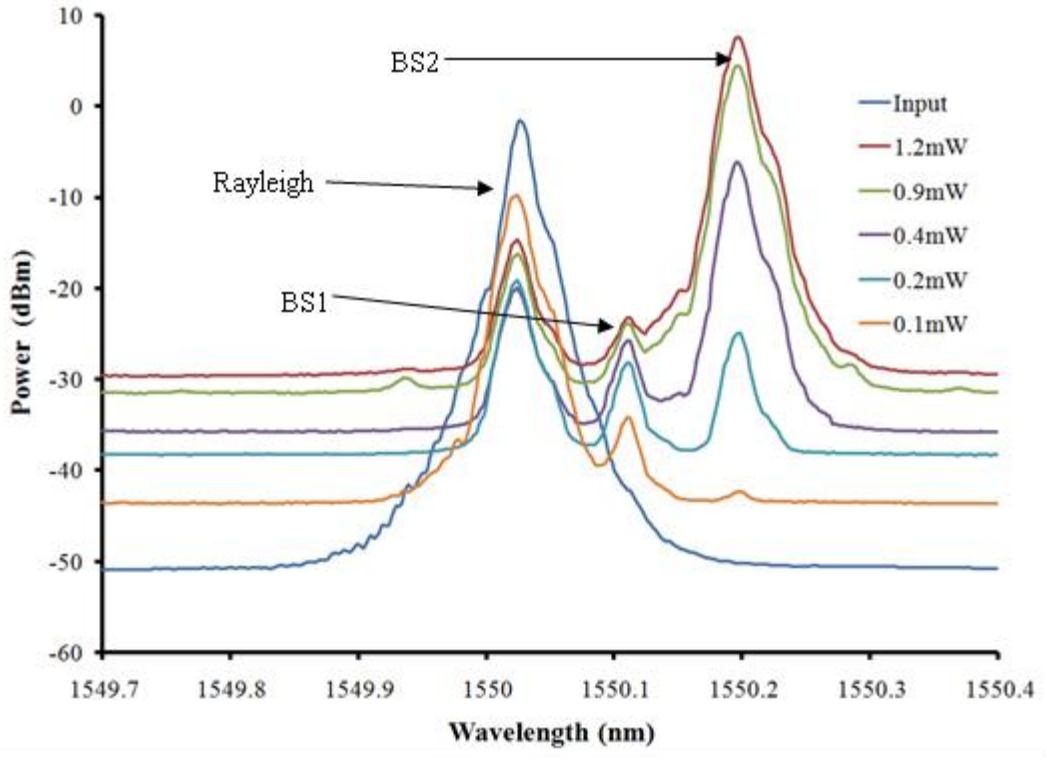

Figure 4.7: Second Order Brillouin Stokes for 2km Fiber Spool

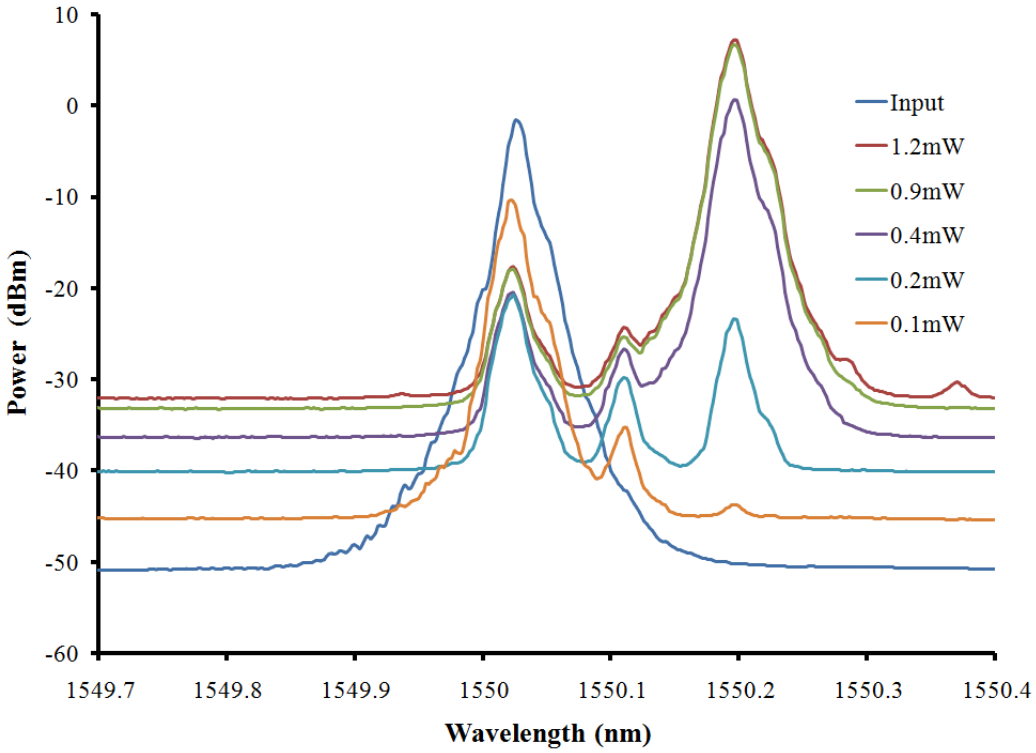

Figure 4.8: Second Order Brillouin Stokes for 5km Fiber Spool

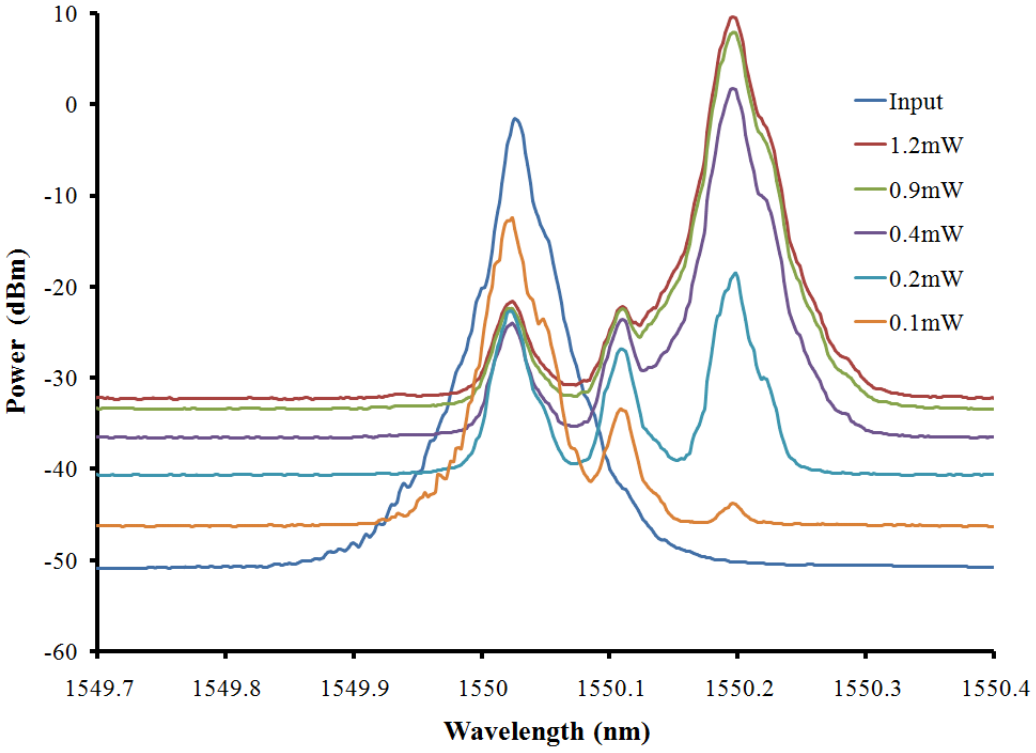

Figure 4.9: Second Order Brillouin Stokes for 10km Fiber Spool

The second order Brillouin Stokes for the 2km, 5km and 10km fibers are as shown as in Figure 4.7, 4.8 and 4.9 respectively. The power of the entering signal is tuned the same way as in the first order characterization. The remnant BP signal, Rayleigh scattering of BS1 and the second order Brillouin Stokes signal (BS2) are observed. In this experiment, the second order Brillouin Stokes for all three lengths of fiber peaked at 1550.196nm, meaning that a frequency shift of 0.170nm has taken place. The value of the frequency downshift is doubled compared to the first order experiment.

The second order Brillouin threshold is plotted as shown in Figure 4.10. For the 2km, 5km and 10km fiber, the threshold power are 124mW, 89mW and 53mW respectively.

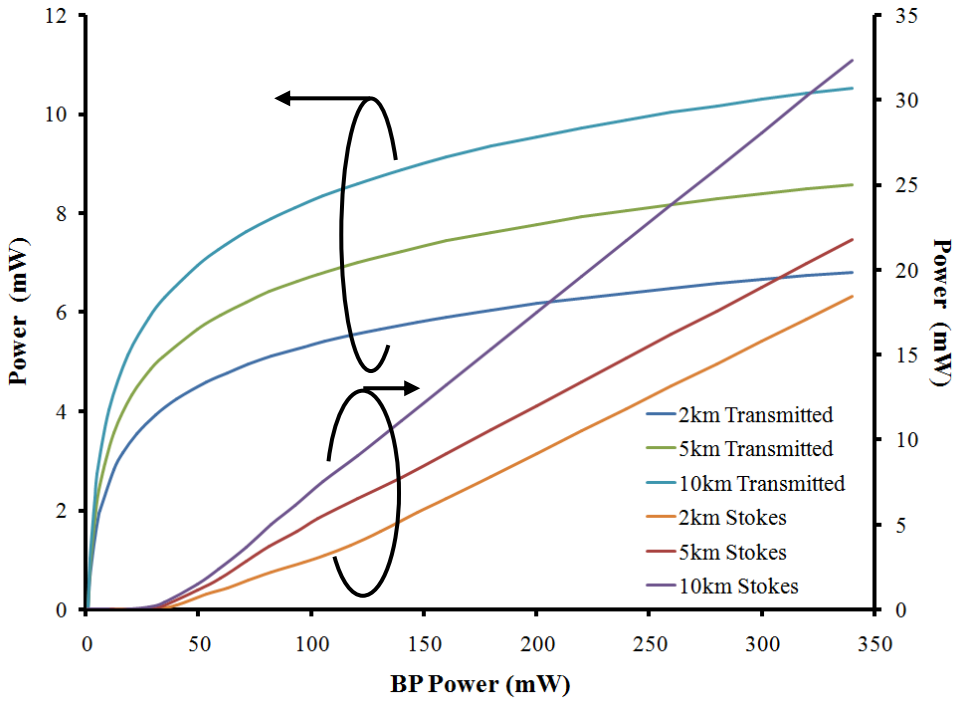

Figure 4.10: Plotted BP and Stokes Peak Power

4.3 Slow Light Characterization

For the slow light characterization, the delay values obtained based on the BP applied are measured by using 10MHz sine wave modulation of the first and second order signals. In the next experiment, the modulating schemes are also varied and the results are recorded. The modulating signals are sine wave and square wave, with 5MHz, 10MHz, 15MHz and 20MHz applied.

The range of the FWHM is a function of $f(x)$, which is correlated with the noisiness of the data given. Outside the range of the FWHM, the signal becomes distorted. Typical value of Brillouin gain FWHM is 30-40MHz (Song, Herráez and Thévenaz, 2005).

4.3.1 First and Second Order Slow Light Delay Values by increasing Brillouin Pump

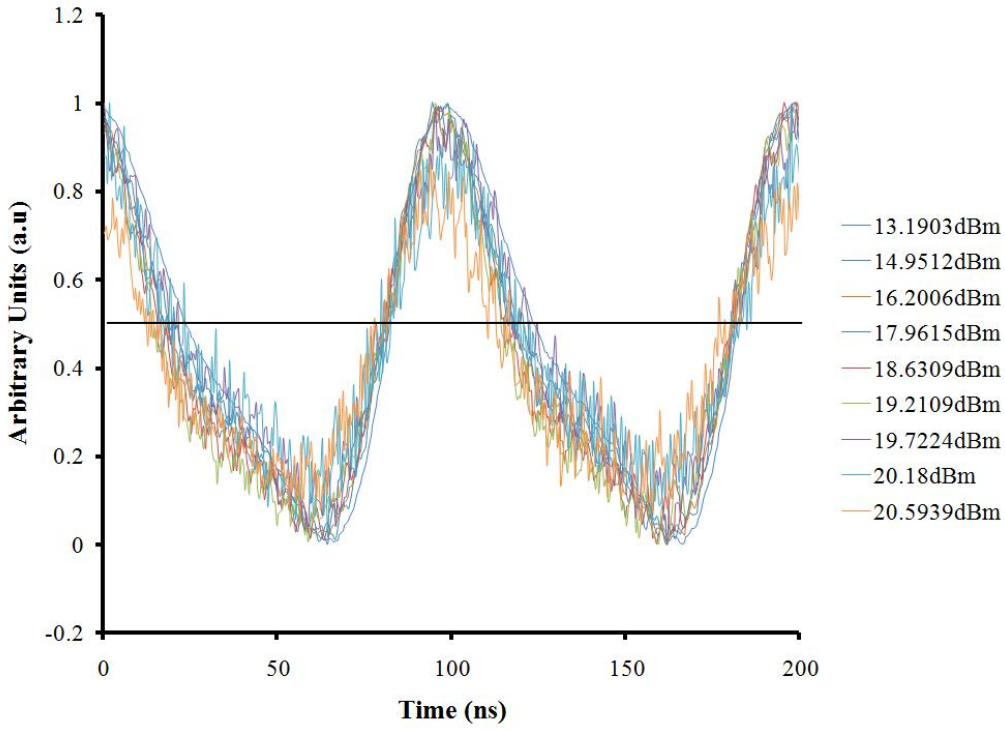

Figure 4.11: 1st Order Slow Light with Increasing BP

By increasing the BP power from 13.2 to 20.6dBm, the first order slow light signal shifted to the left. The signal becomes more and more distorted when the BP is increased, which showed the shifting of the signal away from the center of the FWHM. Initially, the generated signal is within the Brillouin gain bandwidth. The generated signal deteriorates as it shifts away from the maximum value. The delay is measured at the zero crossing at 0.5a.u..

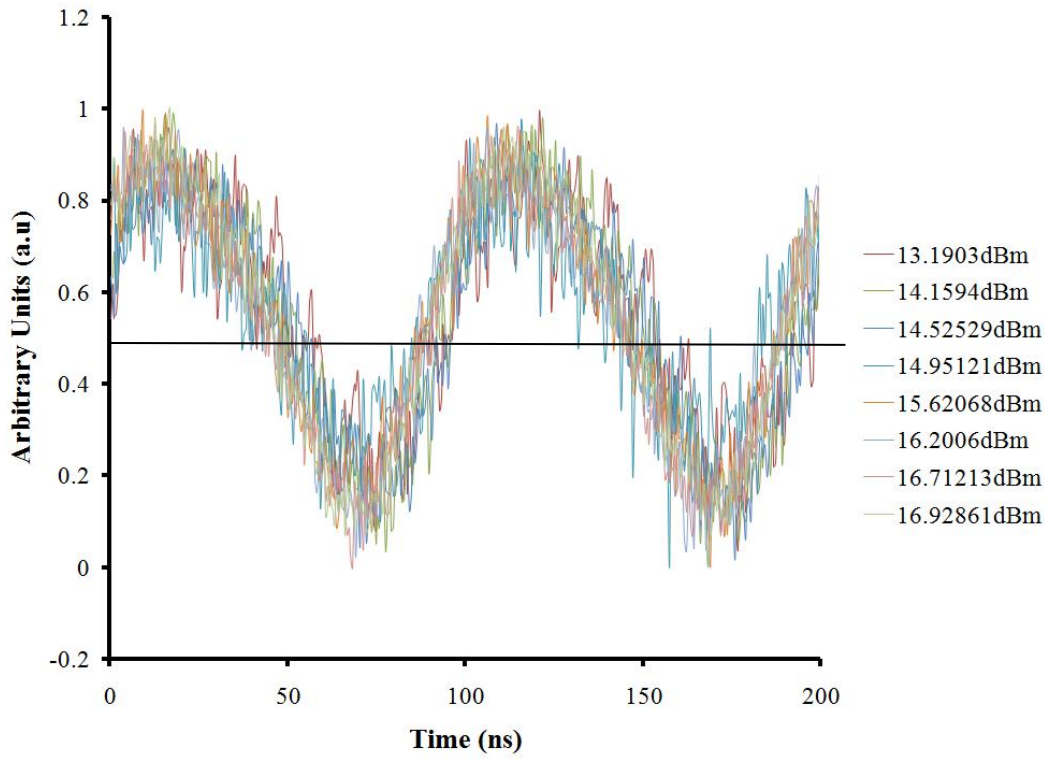

Figure 4.12: 2nd Order Slow Light with Increasing BP

For the second order experiment, the BP power is increased from 13.2 to 16.9dBm. The range of the signal is decreased for the second order results because the sensitivity is increased. When the sensitivity of the system increases, the signal shifts away from the center of the FWHM at a higher rate. In this experiment, the signal is highly distorted due the relationship of the signal power with the FWHM. Post-processing is needed in order to make the results discernible.

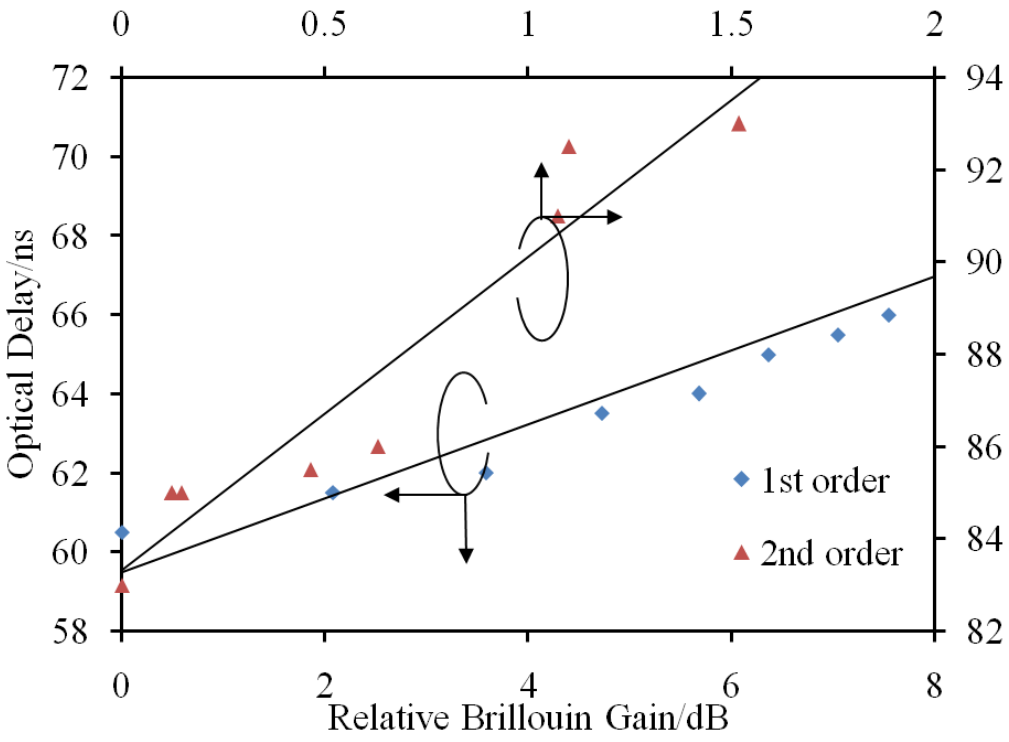

Figure 4.13: Optical Delay Versus Relative Brillouin Gain for First and Second Order Slow Light

The relative Brillouin gains for each of the optical delays are shown in Figure 4.13, which is the difference between current and initial Brillouin Stokes peak power. The values are compared with the initial pump power at 13.2 dBm for first and second order setup. Optical delays increase linearly with Brillouin gain as shown by Song *et al.*(Song and Hotate, 2007a).The range for the first order signal power is 7.5dB for delay values between 60.5ns to 69.5ns, and the range is 1.5dB between 83ns to 93ns for second order. Due to the dependence of the Brillouin gain on the state of polarization of the pump and probe signals, a polarization scrambler is suggested to be used to improve gain distribution (Xie *et al.*, 2012).

4.4 Comparison of Different Waveforms and Modulating Frequencies

Compared to the previous subsection, the different waveforms with different modulating frequencies are averaged 20 times to smoothen the signal. The frequency adjustment of 5MHz, 10MHz, 15MHz and 20MHz is done for sine and square wave modulation respectively. The output signal is obtained and the signal distortion is compared.

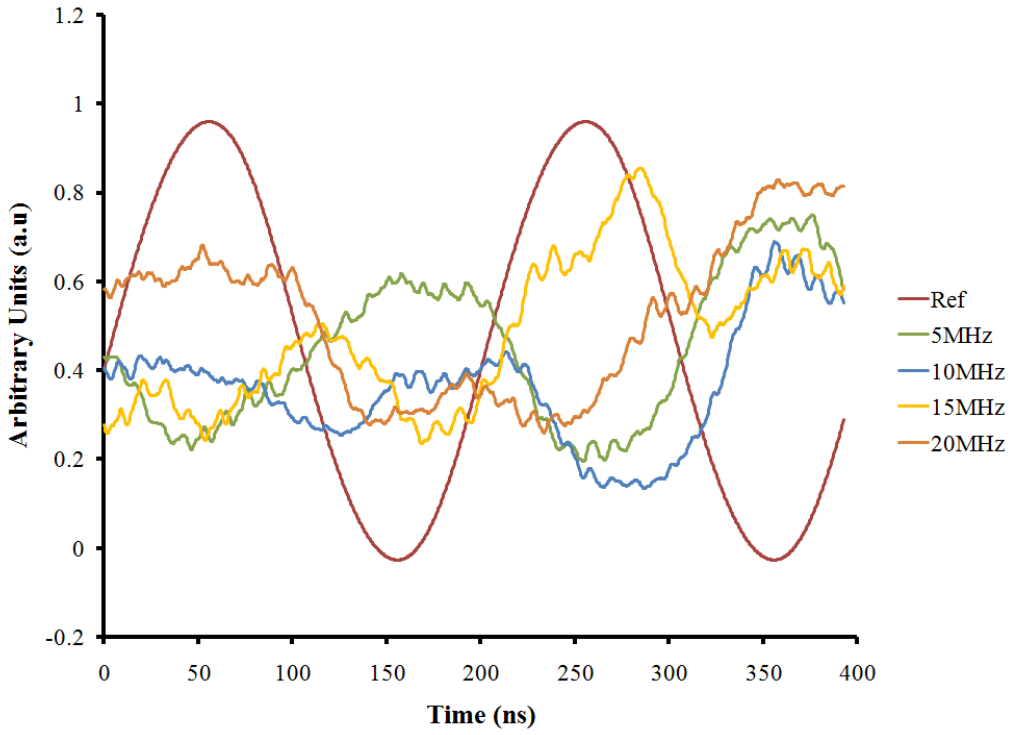

Figure 4.14: Sine Wave Modulation Frequencies at 10dBm BP power

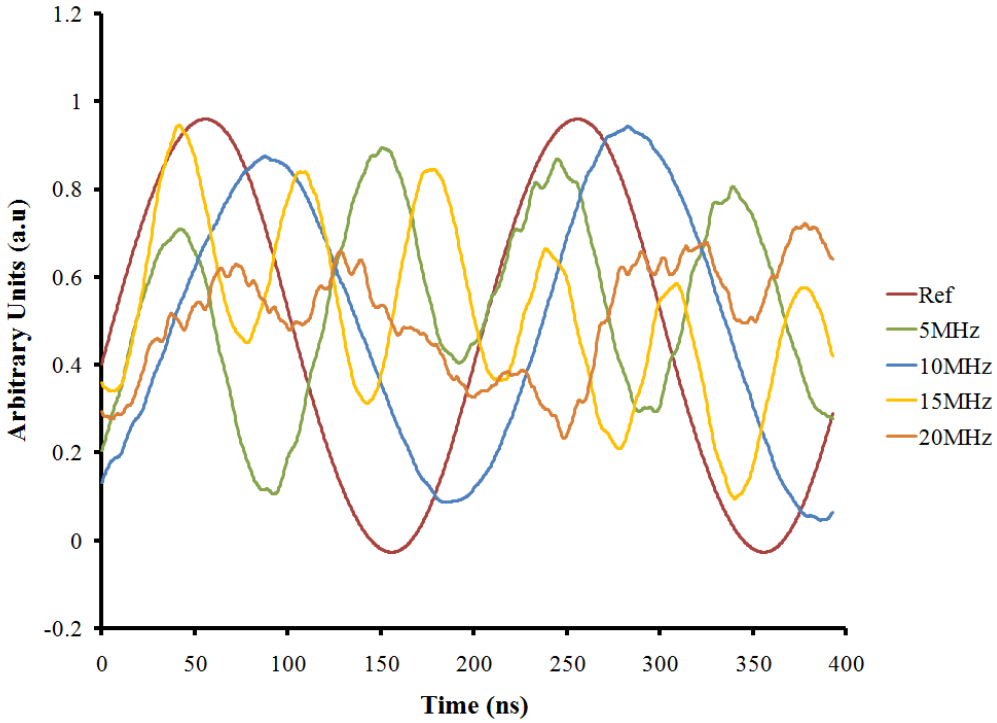

Figure 4.15: Sine Wave Modulation Frequencies at 15dBm BP power

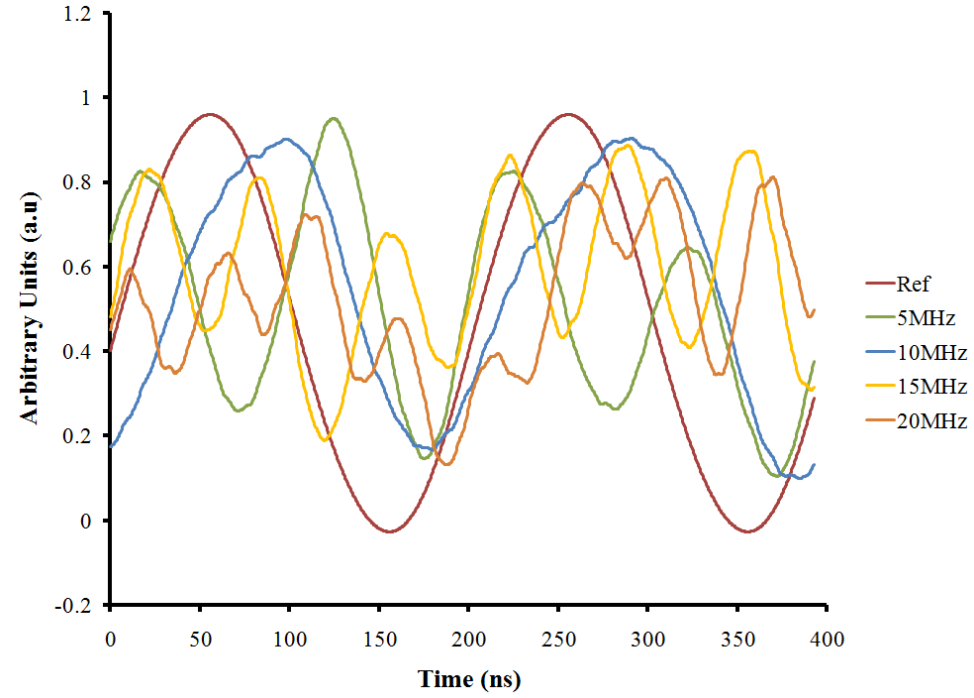

Figure 4.16: Sine Wave Modulation Frequencies at 20dBm BP power

As observed in Figure 4.14 to Figure 4.16, the reference sine wave signal from the signal generator is compared to the signals received at the oscilloscope with increasing BP power. The distortion that is observed for the 10MHz sine signal is the least compared to the others.

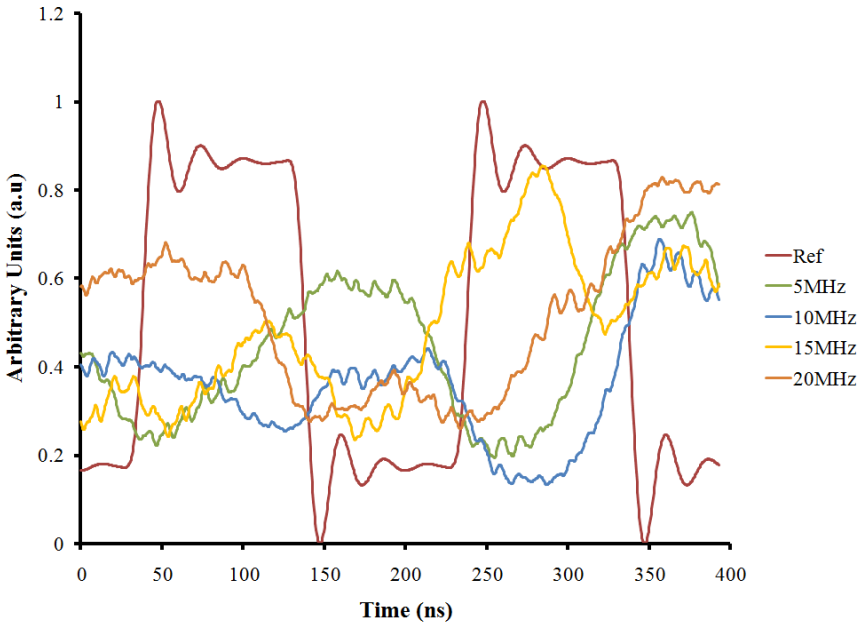

Figure 4.17: Square Wave Modulation Frequencies at 10dBm BP power

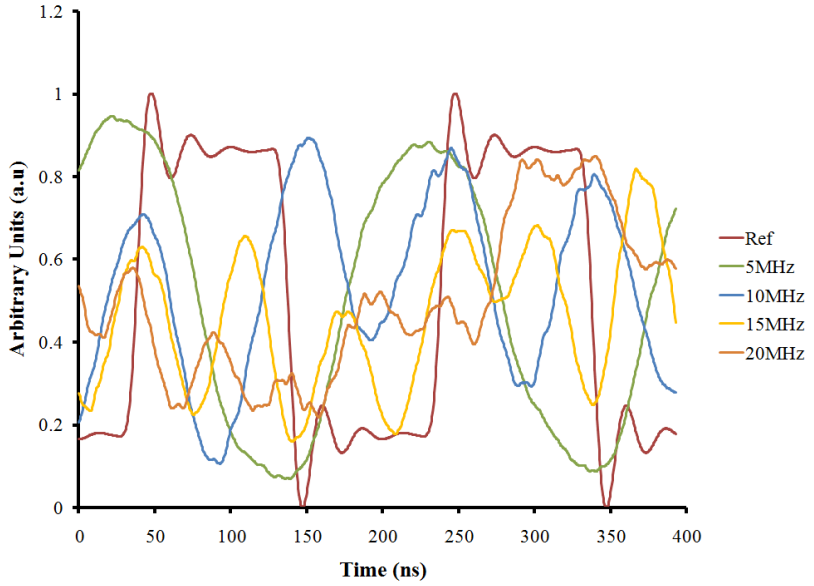

Figure 4.18: Square Wave Modulation Frequencies at 15dBm BP power

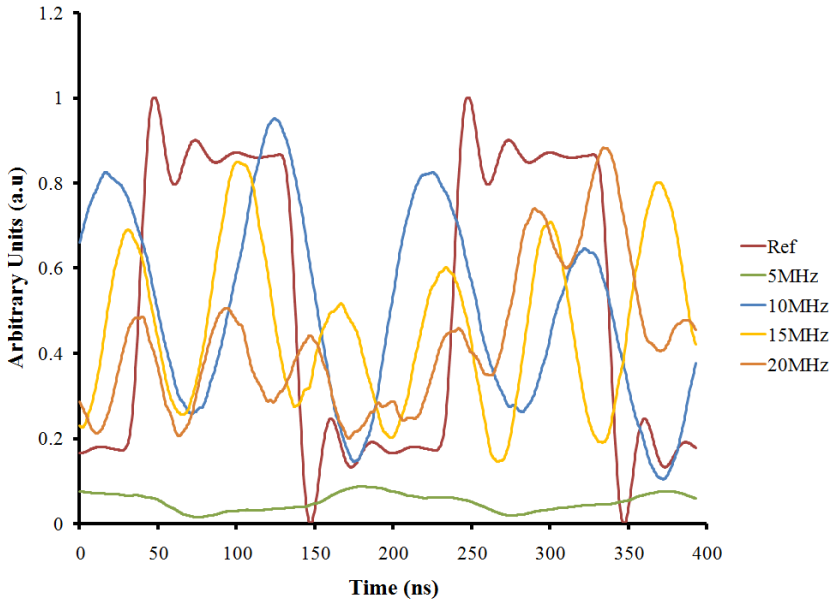

Figure 4.19: Square Wave Modulation Frequencies at 20dBm BP power

As observed in Figure 4.17 to Figure 4.19, the reference square wave signal from the signal generator is compared to the signals at the oscilloscope with increasing BP power. The resultant signal is not detected as a square wave as intended. This is because the occurrence of self phase modulation of the optical signal causes the resultant signal to experience distortion due to material dispersion (Shen and Yang, 2016). This causes the optical signal to assume the Gaussian waveform instead of the intended square waveform when detection occurs at the receiver.

4.5 First Order Temperature Sensing

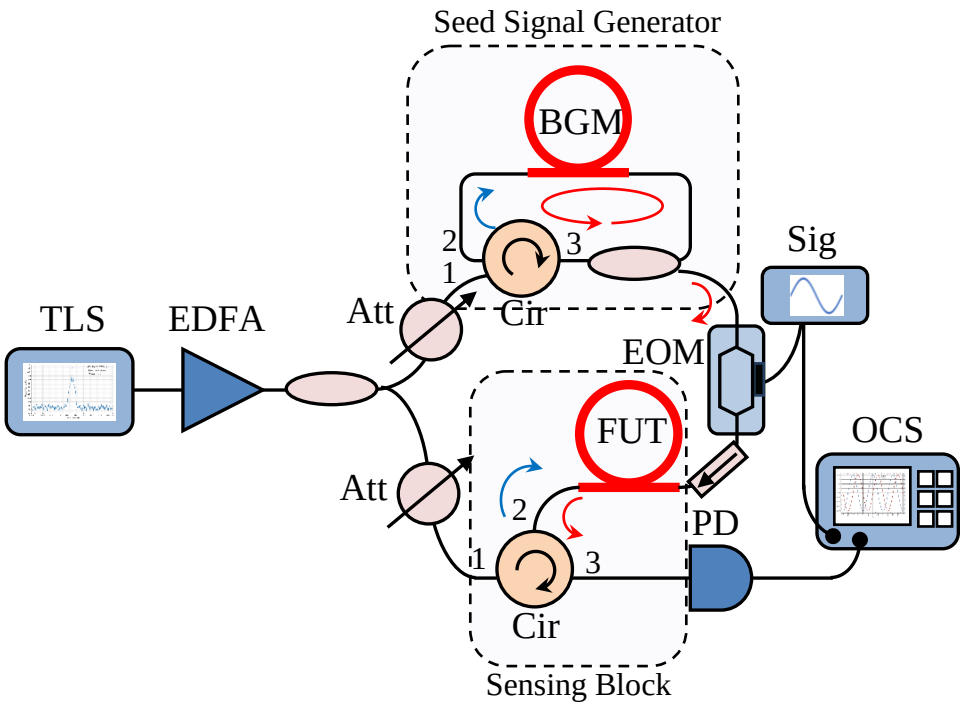

Figure 4.20: First order SBS slow light sensing setup

As shown in Figure 4.20, the sensing setup comprised of a Santec WSL-100 that has a linewidth of less than 100kHz. The TLS signal is amplified by a Keopsys CEFA-C-PB-HP EDFA. The incoming signal is then split by using a 3dB coupler to the upper and lower arm of the setup. The upper arm comprises of the seed signal generator, while the lower arm comprises of the sensing block. The seed signal generator and sensing block consist of a 90/10 coupler, a 4-port circulator and a SMF spool which are lengths of 2km and 10km respectively. First order Stokes is generated when the light passes through the circulator into the fiber spool, and then first order Stokes wave is generated in the reverse propagating direction, which will then exit via the circulator port 3. The 90/10 coupler is used to feedback the signal

into the fiber laser cavity and hence stabilizing the output. The light produced at the seed signal generator will be the probe signal, while the sensing block light will be named as the pump signal. The probe is modulated by a Lucent 2623NA EOM using a 10MHz sine wave RF signal. The probe is transmitted into the sensing block setup to coincide with the pump signal to produce SBS slow light. The produced slow light is fed into the photodetector, connected to the oscilloscope to be monitored.

To measure the sensitivity of the system, the temperature of the sensing block is controlled via the Venticell 55 oven, which encases the fiber under test and applies homogeneous temperature and maintain the temperature, as long as the setting is maintained. The results are recorded in a step size of 2°C.

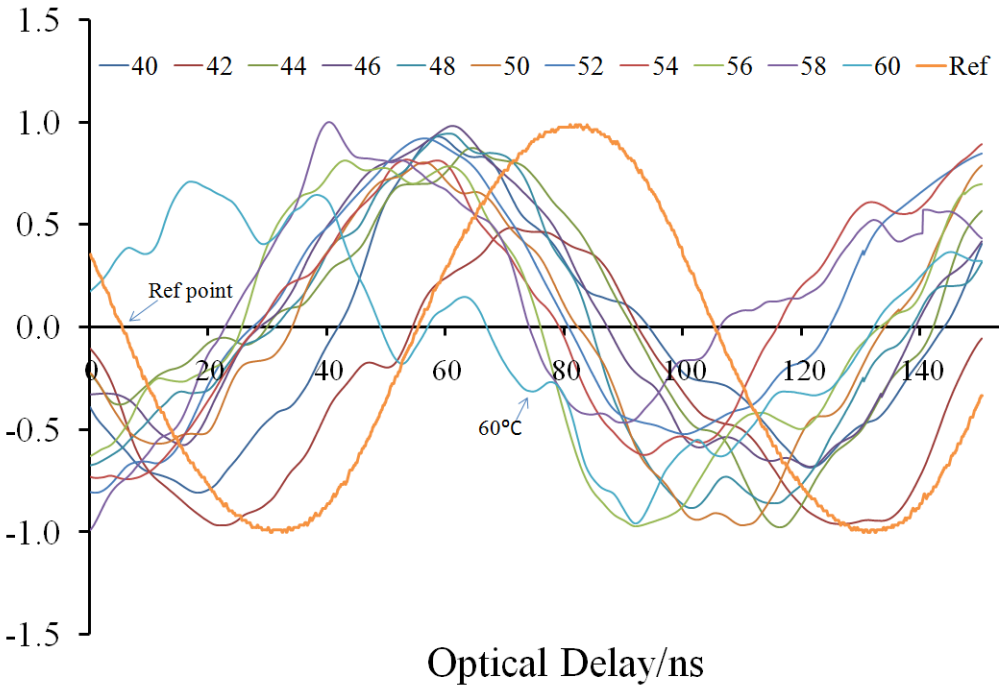

Figure 4.21: First Order Slow Light Oscilloscope Signal

The reference point functions as the initial point where the delay is to be derived. The optical delay changes as temperature changes since SBS is a process that is highly dependent on strain and temperature (Okawachi *et al.*, 2005). The Figure 4.21 shows the electrical signal displayed at the oscilloscope for the first order slow light setup. In order to obtain pulse signals at different ambient temperatures, the output pulse waves are beamed into a PP-10G photodetector, which is connected via a SubMiniature version A-Bayonet Neill–Concelman (SMA-BNC) cable to the oscilloscope. The frequency of the modulating signal is fixed at 10MHz.To reduce the amount of noise contained in the pulse signals, a total of 4096 averages are done on each output, with addition of post processing. As observed, the signal starts to deteriorate at 60°C. This could be attributed to the full width at half maximum of the standard telecommunication optical fiber's Brillouin gain spectrum. The FWHM is measured at around 30-35MHz (Boyd, Gauthier and Gaeta, 2006; Schulz *et al.*, 2017). Given that the temperature dependent characteristic of the Brillouin frequency shift is at 1.7MHz/°C, a shift of 18°C as in this experiment will shift the frequency by 30.6MHz. Temperature shifts beyond that will greatly attenuate the output pulse signal, thus degrading the SNR. The signals are then normalized to values residing between +1 and -1. The zero crossing value, which is the magnitude of the signal as it coincides with the x-axis, are compared and the delay values are attained and plotted.

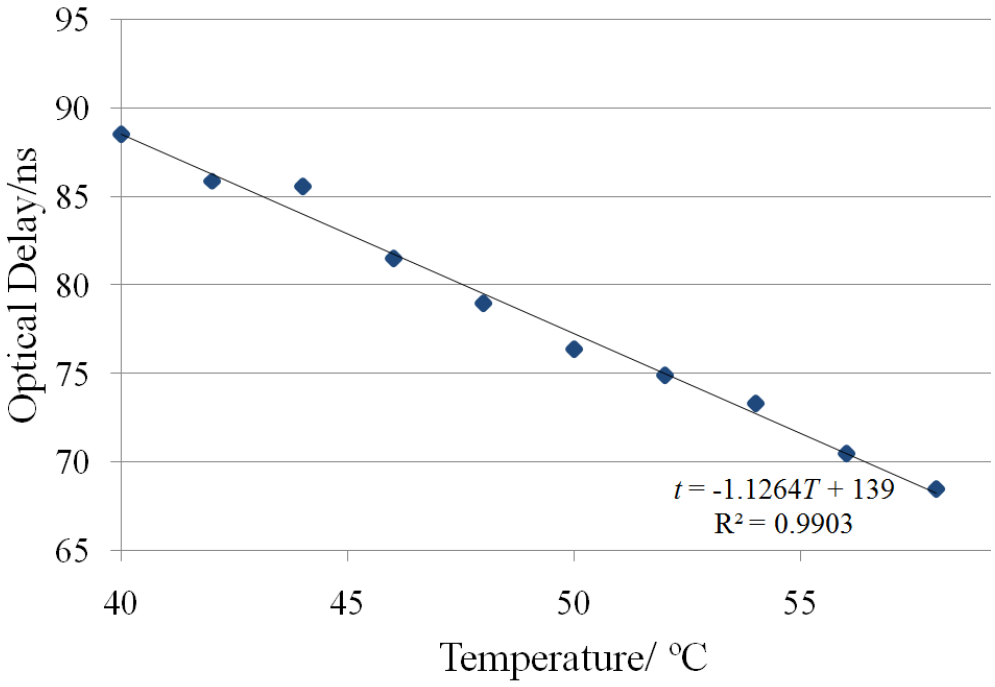

Figure 4.22: Sensitivity of First Order Brillouin Slow Light Temperature Sensing

For the ambient temperature ranging between 40-58°C, the step size being 2°C , delay values are 93.9ns, 91.3 ns, 91 ns, 86.9 ns, 84.4 ns, 81.8 ns, 80.3 ns, 78.7 ns, 75.9 ns and 73.9ns respectively. As Figure 4.22 suggests, the average delay per degree Celcius is at 1.126ns/°C. The coefficient of determination, or more well-known as the R-squared value, used to determine the proximity of the fitted trendline with the actual data, is at 0.990. As this number is getting closer to 1, the more relevant the actual data is with the regression line.

4.6 Second Order Temperature Sensing

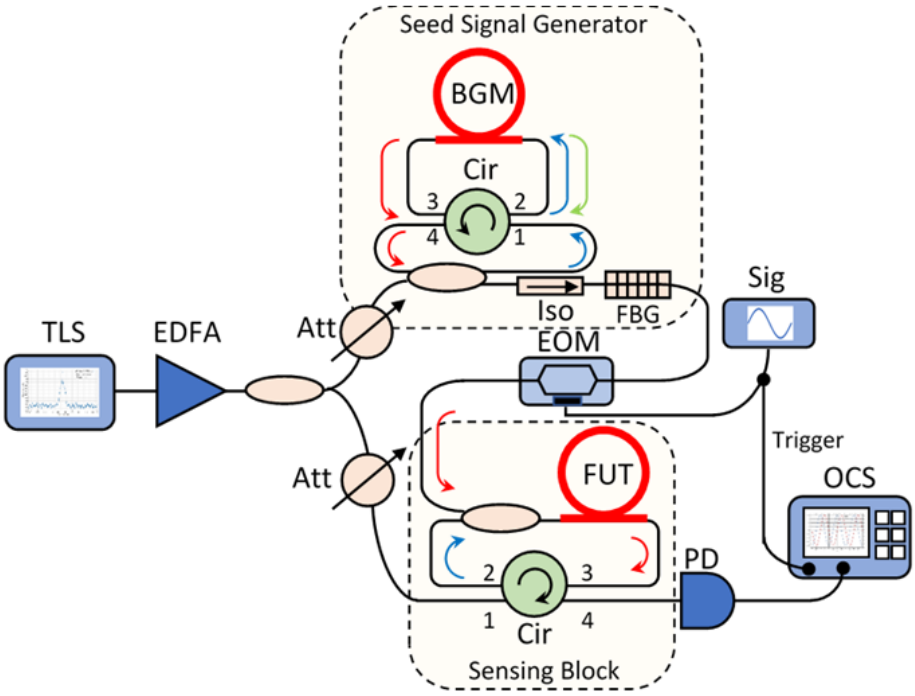

Figure 4.23: Second order SBS slow light sensing setup

In Figure 4.23, the active components such as the tunable laser source, erbium doped fiber amplifier, signal generator, photodetector and oscilloscope, as well as the passive components such as the attenuator, isolator, electro-optic modulator are maintained. The difference is that a 4-port circulator is used in the Brillouin gain setup for both the seed signal generator and sensing block. The first order Stokes signal is transmits back into the port 2 of the 4 port circulator and goes out of the port 3 into the back end of the fiber. When the second order Brillouin threshold is achieved by the first order Stokes in this path, the second order Stokes signal with be generated and exits the setup via the port 4.

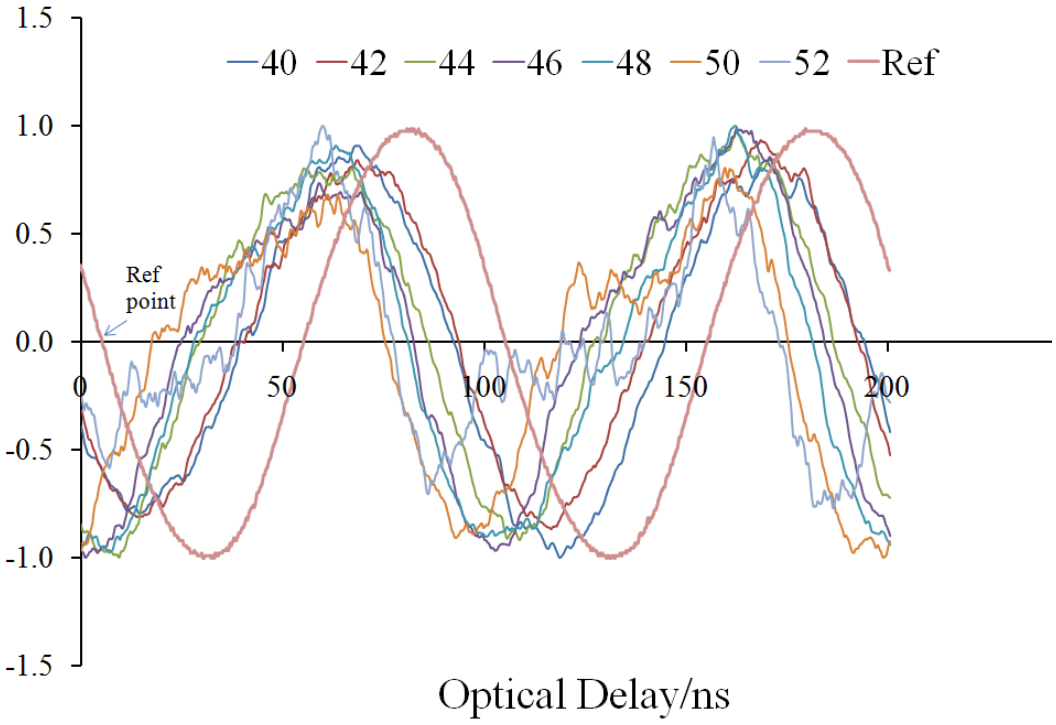

Figure 4.24: Second Order Slow Light Oscilloscope Signal

Figure 4.24 represents the electrical signal displayed at the oscilloscope for the second order slow light setup. The output of the system is detected by the photodetector connected to the oscilloscope to obtain this signal trace.

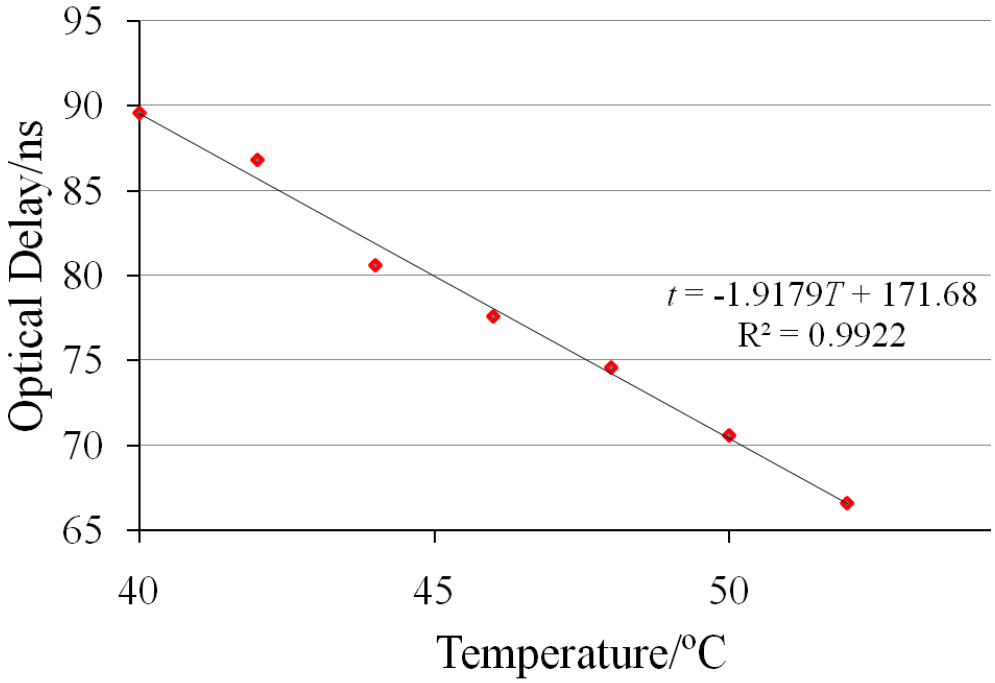

Figure 4.25: Sensitivity of Second Order Brillouin Slow Light Temperature Sensing

For the ambient temperature ranging between 40-52°C, the step size being 2°C, delay values are 95ns, 92.2ns, 86ns, 83ns, 80ns, 76ns and 72ns respectively. The average delay per degree Celcius is at 1.918ns/°C, which is almost double of the value of the first order experiment. The R-squared value is at 0.99.

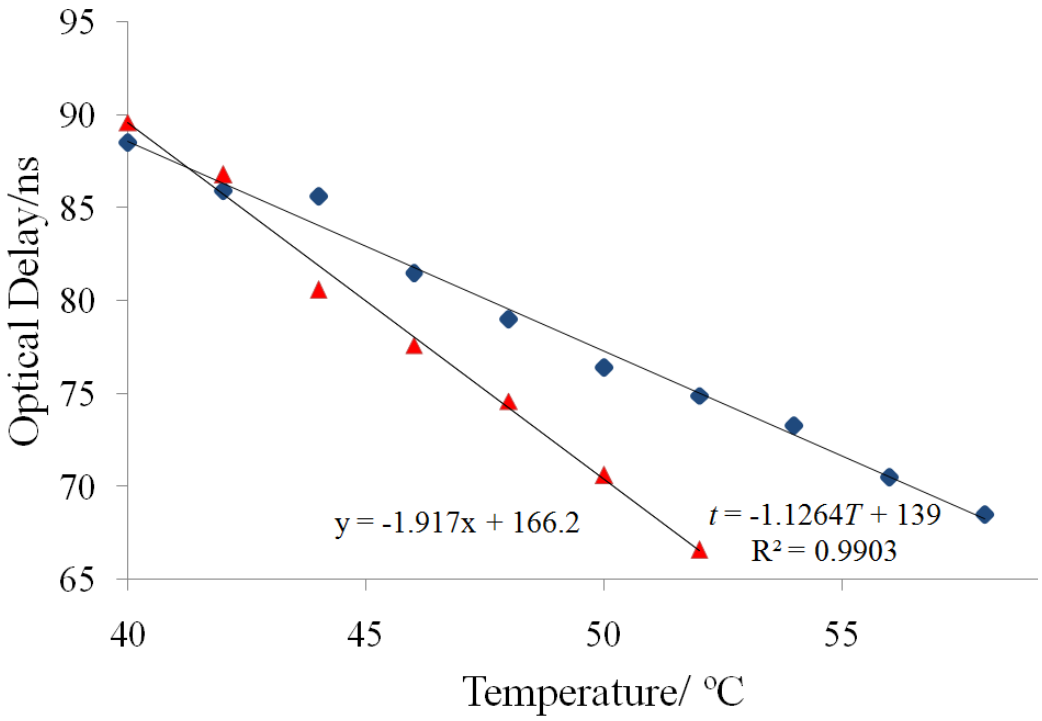

Figure 4.26: Sensitivity of First and Second Order Brillouin Slow Light Temperature Sensing

The first and second order SBS slow light setup exhibited sensitivities of 1.126ns/°C and 1.9179ns/°C respectively. The R^2values are 0.9903 and 0.9922, showing that the measured optical delay linearly increases with the temperature. This sensitivity enhancement is attributed to the Brillouin shift of the higher order Brillouin spectrum. The Brillouin effect was cascaded as the looping of the signal in the sensing fiber takes place. When there are changes to the ambient temperature, the change in optical delay for a measured temperature is doubled due to the cascading Brillouin effect.

4.7 Reliability T-test

The T-test is used to test the reliability and determines whether a sample mean is different from a known or hypothesized mean. A sample size of 20 have been collected and tabulated for both first and second order sensor parameters. A two tailed test is used because the sample size is small (N<20).

Table 4.2: Delay values for 20 iterations of the first order sensing setup

Iteration	Delay Value, ns									
	40°C	**42°C**	**44°C**	**46°C**	**48°C**	**50°C**	**52°C**	**54°C**	**56°C**	**58°C**
1	88.6	86.7	86.6	80.9	79.2	75.6	75.8	73.7	70.4	68.6
2	88.4	86.2	84.6	81.2	80	75.8	74.9	73.5	70.5	68.5
3	88.5	85.4	85	80.1	78.3	77	75.4	73.7	70.6	68.3
4	88.4	85	85.6	81.1	78.9	75.7	75.8	73.5	70.4	68.2
5	88.5	86.9	86.3	81.7	78.7	75.7	74.9	73	70.8	68.7
6	88.6	84.9	86.4	82.1	78.2	76.4	75.1	73.7	70.6	68.8
7	88.4	85.9	84.8	80.3	78.9	76.1	74.4	72.8	70.5	68.9
8	88.6	86.8	85.6	81.6	78.5	76.4	74.6	72.8	70.8	68.9
9	88.6	86.4	85.6	80.9	78.8	77.1	74.4	73.4	70.1	68.4
10	88.5	85.8	85.8	82.1	79.1	76.1	74.8	73.3	70.5	68.5
11	88.4	85.4	85.7	81.5	78.6	76.9	75.3	73.5	70.4	68.1
12	88.5	86.2	85.6	81.6	79.6	77.3	74.5	73.7	70.6	68.3
13	88.4	85	86.2	82.4	78.2	76.6	74.8	73.7	70.6	69
14	88.4	85.7	85.2	82.3	79.2	76	74.5	73.1	70.6	68
15	88.6	85.3	85.8	81.3	78.1	77.5	74.3	73	70.5	67.9
16	88.5	84.9	85.4	82.4	79.9	76.1	74.6	73.7	70.2	68.7
17	88.5	86.3	84.7	81.8	79.3	76.5	75.4	73.3	70.8	68.4
18	88.4	86.6	85.3	82.1	79.3	76.5	74.7	72.9	70.5	68.8
19	88.7	86.9	85.5	81.7	79.7	77.2	74.8	72.9	70.2	68.6
20	88.6	85.8	86	81.4	79.9	75.7	75.2	73.3	70.6	69
Mean, x	88.505	85.905	85.585	81.525	79.02	76.41	74.91	73.325	70.51	68.53
Standard Deviation, s	0.0944	0.6908	0.5546	0.6463	0.6014	0.5946	0.4494	0.3338	0.1916	0.3278
μ	88.5	85.9	85.6	81.5	79	76.4	74.9	73.3	70.5	68.5

Taking 40°C as an example for the first order, the hypotheses set would be:

Null hypothesis, H_0: μ=88.5

Alternative hypothesis: H_1: μ≠88.5

The null hypothesis will be rejected if the sample mean is too small or too big. The significance value used is a standard 0.05.

Using the formulae below, the standard error (SE), degree of freedom (DF), t-score and P-value are plotted.

$$SE = \frac{s}{\sqrt{N}}$$
$$DF = N - 1$$
$$t = \frac{x - \mu}{SE}$$

Table 4.3: T test values for 20 iterations of the first order sensing setup

Temperature, °C	**40**	**42**	**44**	**46**	**48**	**50**	**52**	**54**	**56**	**58**
SE	0.0211	0.1544	0.1240	0.1445	0.1344	0.1329	0.1004	0.0746	0.0428	0.0733
DF	19	19	19	19	19	19	19	19	19	19
T	0.2367	0.0323	0.6853	0.1729	0.1487	0.0752	0.0995	0.3349	0.2333	0.4092
$P_{(ONE\ SIDED)}$	0.4076	0.4872	0.2507	0.4322	0.4416	0.4704	0.4608	0.3706	0.4090	0.3434
P_{-VALUE}	0.8152	0.9745	0.5014	0.8644	0.8833	0.9408	0.9217	0.7413	0.8180	0.6869

For the case of 40°C, the p value is the probability of the t-score having 19 degrees of freedom, which is less than -0.2367 or more than 0.2367. The mathematical terms will be P(t<-0.2367)=0.4076 and P(t>0.2367)=0.4076. The P_{-VALUE}=0.4076+0.4076=0.8152. Since this P_{-VALUE} is greater than the significance value, which is 0.05, the null hypothesis cannot be rejected. Applying the same analysis for 42°C, 44°C, 46°C, 48°C, 50°C, 52°C, 54°C, 56°C, 58°C, their $P_{-VALUES}$ are 0.9745, 0.5014, 0.8644, 0.8833, 0.9408, 0.9217,

0.7413, 0.8180, 0.6869 respectively, showing that this methodology is reliable for all the measured temperature.

Table 4.4: Delay values for 20 iterations of the second order sensing setup

Iteration	Delay Value, ns						
	40°C	**42°C**	**44°C**	**46°C**	**48°C**	**50°C**	**52°C**
1	89.9	86.3	81.1	77.7	74.6	70.3	66.9
2	89.8	87.2	80.8	77.6	75	71	67
3	89.5	86.6	81.2	77.5	74.4	70.7	66.3
4	89.7	87.3	80.5	77.4	74.9	70.4	66.3
5	89.2	86.9	81.1	77.3	74.6	70.4	66.8
6	89.7	86.8	80.1	77.9	74.5	70.6	66.4
7	89.7	86.6	79.9	77.6	75	70.2	66.2
8	89.8	87	80	78	74.6	70.8	66.9
9	89.5	86.6	81	77.7	74.9	70.9	66.7
10	89.7	86.7	81.1	77.4	74.6	70.7	66.2
11	89.8	86.9	80.2	77.3	74.2	70.8	66.7
12	89.9	86.6	81.1	77.3	75	70.4	66.4
13	89.2	86.8	80.8	77.2	74.5	70.5	66.8
14	89.7	86.6	80.9	77.8	74.5	70.4	66.6
15	89.6	86.6	80.4	77.6	74.6	70.8	66.7
16	89.9	87.3	80.3	77.6	74.4	70.9	66.8
17	89.4	86.9	81	77.7	74.7	70.6	66.7
18	89.6	87.1	80	78	74.9	70.6	66.9
19	89.3	86.9	80.7	77.7	74.5	70.6	66.3
20	89.2	86.7	79.9	78	74.3	70.8	66.7
Mean, x	89.605	86.82	80.605	77.615	74.635	70.62	66.615
Standard Deviation, s	0.237254	0.264774	0.465069	0.247673	0.241214	0.221478	0.25808
μ	89.6	86.8	80.6	77.6	74.6	70.6	66.6

Table 4.5: T test values for 20 iterations of the second order sensing setup

Temperature, °C	**40**	**42**	**44**	**46**	**48**	**50**	**52**
SE	0.05305	0.05920	0.10399	0.05538	0.05393	0.04952	0.05770
DF	19	19	19	19	19	19	19
T	0.09424	0.33780	0.04808	0.27084	0.64890	0.40384	0.25992
$P_{(ONE\ SIDED)}$	0.46295	0.36960	0.48107	0.39471	0.26208	0.34541	0.39885
P_{-VALUE}	0.92589	0.73921	0.96215	0.78942	0.52416	0.69083	0.79771

As for the second order setup, 20 iterations of the results are also plotted as in the table above. The $P_{-VALUES}$ are 0.92589, 0.73921, 0.96215, 0.78942, 0.52416, 0.69083, 0.79771 for 40°C, 42°C, 44°C, 46°C, 48°C, 50°C, 52°C respectively. Due to the probability of the results being higher than 0.05, the reliability of this method is also confirmed.

4.8 Conclusion

In this chapter, the Brillouin parameters characterization for the first order and second order frequency shift and threshold measurement are recorded. Then, for the slow light characterization, the delay values are measured by increasing the Brillouin pump. Furthermore, the square and sine wave modulated signals are presented, which have different modulating frequencies. Sine wave was used as modulating signal with less distortion to ease the delay measurement.

The temperature sensing regime presented are for the first order and second order SBS slow light setup. The sensitivity of the second order SBS slow light temperature sensing setup is 1.918ns/°C, which is almost double of the value of the first order setup at 1.111ns/°C. The reliability t-test that is conducted also confirmed that the p-values for the first and second order results are greater than 0.05.

CHAPTER 5

CONCLUSION AND RECOMMENDATIONS FOR FUTURE WORKS

5.1 Conclusion

The advantages of fiber optic sensors highlighted in these few decades are low loss, long distance transmission and high speed. Fiber optic sensing provides environmental resilience, electrical immunity and also the capability of distributed sensing compared to electrical sensing (Turner *et al.*, 1990). Brillouin slow light sensing shows compatibility with existing devices, room temperature operation, large potential for high bandwidth signal, simplicity of measurement and tunable resonance (Boyd, Gauthier and Gaeta, 2006).

In this dissertation, SBS slow light characterization and temperature sensing has been demonstrated. For the SBS characterization, the first and second order Brillouin Stokes are plotted for the 2km, 5km and 10km SMF, which peaked at 1550.11nm and 1550.196nm respectively. BS1 and BS2 wavelength remained unchanged for different lengths of fiber with the same material composition. SBS slow light is characterized by increasing the BP power and the delay was obtained for each of the relative Brillouin gains, where a linear increase is observed. The range for the first order signal power is 7.5dB for delay values between 60.5ns to 69.5ns, and the range is 1.5dB

between 83ns to 93ns for second order.The SBS threshold power is also obtained. For the first order, the values for the 10km, 5km and 2km SMF are 26mW, 61mW and 101mW; for the second order, the values are 53mW, 89mW and 124mW. For the slow light experiment, the BP power was tuned from 0 to 20.6dBm for the first order. Whereas for the second order, the BP power was tuned from 13.2 to 16.9dBm. Sine wave and square wave are also used to modulate the signal for frequencies of 5MHz, 10MHz, 15MHz and 20MHz.The modulated 10MHz sine wave signal has better signal integrity and matching.

Then, the temperature sensing experiment was conducted for both first and second order SBS slow light. The sensing setup was subdivided into two sections, the seed signal generator and the sensing block. The seed signal generator is responsible to generate the probe signal, while the sensing block is where the amplified pump from the BP coincides with the probe and the temperature was applied to this section. The step size used is 2°C, starting from 40°C. The temperature sensing range that is determined from this experiment is 40°C to 58°C for the first order, and 40°C to 52°C for the second order. This produced a sensitivity of 1.918ns/°C for the second order setup, which is a significant improvement compared to the first order value 1.111ns/°C. Finally, a t-test model was produced and the findings show that SBS slow light sensing method is sufficiently reliable with all the results passing the 0.05 p-value. This work is a proof of concept to show that sensitivity of slow light sensor can be increased by few folds depending on the generated higher order Brillouin Stokes signal. This could potentially be used

in harsh environments where sensitivity, temperature, EMI and remote location are concerned, such as oil rigs, bridges, dams and power plants.

5.2 Recommendations for Future Works

As a fiber optic based sensor, the second order slow light temperature sensor can be potentially used in aerospace applications, oil rigs, pipelines, geothermal, automotive, and energy sector. Remote monitoring of civil structures of a few kilometers due to accessibility issues can be overcome because of fiber optic is inherently low loss. The usage of the second order slow light sensor for distributed sensing is also recommended, whereby the first order SBS slow light strain sensor setup is shown by Wang *et al*. (L. Wang *et al.*, 2013). The pump-probe pulse relative delay can be controlled to set the crossover point that indicates the region being measured.

In order to improve the stability and reliability of Brillouin slow light sensing, a polarization scrambler can be used to distribute the Brillouin gain so that the signal distortion could be further reduced. Due to limited funding we are not able to have a polarization scrambler. Fourth, sixth order and higher order SBS can also be explored to obtain further enhanced sensitivity and delay for the slow light sensor. The sensing range issue due to FWHM bandwidth limitation can also be solved by using different techniques such as in (Yoshizawa and Imai, 1993; Song and Hotate, 2007a). Yoshizawa and Imai

extended the bandwidth from 50MHz to 400Mhz using double stranded cabling, while Song and Hotate demonstrated a 25GHz bandwidth enlargement using a Brillouin double pump. Applications with special fibers such as polymer, plastic and perfluorinated graded index polymer optical fibers should also be explored (Ishigure *et al.*, 2003; Koike and Ishigure, 2006; Lethien *et al.*, 2011).

LIST OF REFERENCES

Agrawal, G. P. (2000) 'Nonlinear fiber optics', in *Nonlinear Science at the Dawn of the 21st Century*. Springer, pp. 195–211.

Alvarez-Botero, G. *et al.* (2017) 'Optical sensing using fiber Bragg gratings: fundamentals and applications', *IEEE Instrumentation & Measurement Magazine*. IEEE, 20(2), pp. 33–38.

Arora, A. *et al.* (2018) 'High-resolution slow-light fiber Bragg grating temperature sensor with phase-sensitive detection', *Optics letters*. Optical Society of America, 43(14), pp. 3337–3340.

Azman, M. F. *et al.* (2019) 'Design and fabrication of copper-filled photonic crystal fiber based polarization filters', *Applied optics*. Optical Society of America, 58(8), pp. 2068–2075.

Baiatu, T. (2000) 'PTC thermistor and a current limiter device having at least one PTC thermistor'. Google Patents.

Bang, H.-J., Kim, H.-I. and Lee, K.-S. (2012) 'Measurement of strain and bending deflection of a wind turbine tower using arrayed FBG sensors', *International journal of precision engineering and manufacturing*. Springer, 13(12), pp. 2121–2126.

Barnoski, M. *et al.* (1977) ‘Optical time domain reflectometer’, *Applied optics*. Optical Society of America, 16(9), pp. 2375–2379.

Basov, N. G. *et al.* (1966) ‘Nonlinear amplification of light pulses’, *Sov. Phys. JETP*, 23(1), pp. 16–22.

Bishop, C. (2010) ‘Effects of averaging to reject unwanted signals in digital sampling oscilloscopes’, in *2010 IEEE AUTOTESTCON*. IEEE, pp. 1–4.

Bottacchi, S. (2008) *Noise and signal interference in optical fiber transmission systems: an optimum design approach*. John Wiley & Sons.

Boyd, R. W. (2019) *Nonlinear optics*. Academic press.

Boyd, R. W., Gauthier, D. J. and Gaeta, A. L. (2006) ‘Applications of slow light in telecommunications’, *Optics and Photonics News*. Optical Society of America, 17(4), pp. 18–23.

Chan, T. H. T. *et al.* (2006) ‘Fiber Bragg grating sensors for structural health monitoring of Tsing Ma bridge: Background and experimental observation’, *Engineering structures*. Elsevier, 28(5), pp. 648–659.

Chaudhary, V. S., Kumar, D. and Kumara, S. (2021) ‘Gold-immobilized Photonic Crystal Fiber-based SPR Biosensor for Detection of Malaria Disease in Human Body’, *IEEE Sensors Journal*. IEEE.

Chauhan, J. and Neelakantan, U. (2016) ‘An experimental approach for precise temperature measurement using platinum RTD PT1000’, in *2016 International Conference on Electrical, Electronics, and Optimization Techniques (ICEEOT)*. IEEE, pp. 3213–3215.

Chen, Y. *et al.* (2012) ‘Structural health monitoring of wind turbine blade using fiber Bragg grating sensors and fiber optic rotary joint’, in *Sensors and Smart Structures Technologies for Civil, Mechanical, and Aerospace Systems 2012*. International Society for Optics and Photonics, p. 834534.

DeMiguel-Soto, V. *et al.* (2017) ‘Interferometric vs wavelength selective optical fiber sensors for cryogenic temperature measurements’, in *2017 25th Optical Fiber Sensors Conference (OFS)*. IEEE, pp. 1–4.

Digonnet, M. J. F. *et al.* (2012) ‘Slow light in fiber sensors’, in *Advances in Slow and Fast Light V*. International Society for Optics and Photonics, p. 82730W.

Dong, J. *et al.* (2020) ‘A Novel Mach–Zehnder Interferometric Temperature Sensor Based on a Symmetrical Double-Grooved Structure’, *IEEE Sensors Journal*. IEEE, 20(24), pp. 14850–14856.

Dong, Y. *et al.* (2012) ‘2 cm spatial-resolution and 2 km range Brillouin optical fiber sensor using a transient differential pulse pair’, *Applied optics*. Optical Society of America, 51(9), pp. 1229–1235.

Edwards, M. R. *et al.* (2016) ‘Short-pulse amplification by strongly coupled stimulated Brillouin scattering’, *Physics of Plasmas*. AIP Publishing LLC, 23(8), p. 83122.

Fager, C. and Andersson, K. (2006) ‘Improvement of oscilloscope based RF measurements by statistical averaging techniques’, in *2006 IEEE MTT-S International Microwave Symposium Digest*. IEEE, pp. 1460–1463.

Fraden, J. (2004) *Handbook of modern sensors: physics, designs, and applications*. Springer Science & Business Media.

Garcus, D. *et al.* (1997) 'Brillouin optical-fiber frequency-domain analysis for distributed temperature and strain measurements', *Journal of lightwave technology*. IEEE, 15(4), pp. 654–662.

Garret, K. (2012) 'Solve sensing challenges with optical sensor', *Electrical Design News*.

Gifford, D. K. *et al.* (2005) 'Distributed fiber-optic temperature sensing using Rayleigh backscatter', in *Optical Communication, 2005. ECOC 2005. 31st European Conference on*. IET, pp. 511–512.

Goldfarb, F. *et al.* (2009) 'Electromagnetically-induced transparency, slow light, and negative group velocities in a room temperature vapor of 4He∗ ', *Comptes Rendus Physique*. Elsevier, 10(10), pp. 919–926.

Guo, N. *et al.* (2018) 'Averaging-free Vector BOTDA assisted by a Reference Probe Lightwave', in *CLEO: Science and Innovations*. Optical Society of America, pp. SM3K-3.

Guo, Y. L. *et al.* (2012) 'Performance evaluation of Canton Tower under winds based on full-scale data', *Journal of Wind Engineering and Industrial Aerodynamics*. Elsevier, 104, pp. 116–128.

Gupta, N. *et al.* (2013) 'Structural health monitoring of composite aircraft structures using fiber Bragg grating sensors', *Journal of the Indian Institute of Science*, 93(4), pp. 735–750.

de Györgyfalva, G. D. C. C. and Reaney, I. M. (2001) ‘Decomposition of NiMn2O4 spinel: an NTC thermistor material’, *Journal of the European Ceramic Society*. Elsevier, 21(10–11), pp. 2145–2148.

Hamilton, W. R. (1839) ‘Researches respecting vibration, connected with the theory of light’, in *Proc. Roy. Irish Acad*, pp. 341–349.

Hau, L. V. *et al.* (1999) ‘Light speed reduction to 17 metres per second in an ultracold atomic gas’, *Nature*. Nature Publishing Group, 397(6720), pp. 594–598.

Hill, K. O. and Meltz, G. (1997) ‘Fiber Bragg grating technology fundamentals and overview’, *Journal of lightwave technology*. IEEE, 15(8), pp. 1263–1276.

Hirsch, M. *et al.* (2017) ‘Low-coherence interferometric fiber-optic sensors with potential applications as biosensors’, *Sensors*. Multidisciplinary Digital Publishing Institute, 17(2), p. 261.

Hisham, H. K. (2018) ‘Optical fiber sensing technology: Basics, classifications and applications’, *American Journal of Remote Sensing*. Science Publishing Group, 6(1), pp. 1–5.

Hocker, G. B. (1979) ‘Fiber-optic sensing of pressure and temperature’, *Applied optics*. Optical Society of America, 18(9), pp. 1445–1448.

Horiguchi, T., Kurashima, T. and Koyamada, Y. (1994) ‘1 m spatial resolution measurement of distributed Brillouin frequency shift in single-mode fibers’, in *Tech. Dig. Symp. Opt. Fiber Meas.*, pp. 73–76.

Horiguchi, T. and Tateda, M. (1989) ‘BOTDA-nondestructive measurement of single-mode optical fiber attenuation characteristics using Brillouin interaction: Theory’, *Journal of lightwave technology*. IEEE, 7(8), pp. 1170–1176.

Hotate, K. (2014) ‘Recent achievements in BOCDA/BOCDR’, in *SENSORS, 2014 IEEE*. IEEE, pp. 142–145.

Hotate, K. and Abe, K. (2005) ‘BOCDA fiber optic distributed strain sensing system with a polarization diversity scheme for enlargement of measurement range’, in *17th International Conference on Optical Fibre Sensors*. International Society for Optics and Photonics, pp. 591–594.

Ishigure, T. *et al.* (2003) ‘High-bandwidth graded-index polymer optical fiber enabling power penalty-free gigabit data transmission’, *Journal of lightwave technology*. IEEE, 21(11), pp. 2923–2930.

Jung, J. *et al.* (1999) ‘Fiber Bragg grating temperature sensor with controllable sensitivity’, *Applied optics*. Optical Society of America, 38(13), pp. 2752–2754.

Kapa, T., Schreier, A. and Krebber, K. (2018) ‘63 km BOFDA for Temperature and Strain Monitoring’, *Sensors*. Multidisciplinary Digital Publishing Institute, 18(5), p. 1600.

Kapa, T., Schreier, A. and Krebber, K. (2019) ‘A 100-km bofda assisted by first-order bi-directional raman amplification’, *Sensors*. Multidisciplinary Digital Publishing Institute, 19(7), p. 1527.

KERSEY, A. D. (2018) ‘Fiber-Optic Sensing: Leveraging three decades of fiber Bragg grating sensing technology’.

Kersey, A. D., Berkoff, T. A. and Morey, W. W. (1993) ‘Fiber-optic Bragg grating strain sensor with drift-compensated high-resolution interferometric wavelength-shift detection’, *Optics letters*. Optical Society of America, 18(1), pp. 72–74.

Khurgin, J. B. and Tucker, R. S. (2008) *Slow light: Science and applications*. CRC press.

Kim, H.-J., Thukral, A. and Yu, C. (2018) ‘Highly sensitive and very stretchable strain sensor based on a rubbery semiconductor’, *ACS applied materials & interfaces*. ACS Publications, 10(5), pp. 5000–5006.

Koike, Y. and Ishigure, T. (2006) ‘High-bandwidth plastic optical fiber for fiber to the display’, *Journal of Lightwave Technology*. IEEE, 24(12), pp. 4541–4553.

Koyamada, Y. *et al.* (2009) ‘Fiber-optic distributed strain and temperature sensing with very high measurand resolution over long range using coherent OTDR’, *Journal of Lightwave Technology*. IEEE, 27(9), pp. 1142–1146.

Kraeh, C. *et al.* (2018) ‘Slow light enhanced gas sensing in photonic crystals’, *Optical Materials*. Elsevier, 76, pp. 106–110.

Krauss, T. F. (2008) ‘Why do we need slow light?’, *Nature photonics*. Nature Publishing Group, 2(8), pp. 448–450.

Kroll, N. M. (1965) ‘Excitation of Hypersonic Vibrations by Means of

Photoelastic Coupling of High-Intensity Light Waves to Elastic Waves', *Journal of Applied Physics*. American Institute of Physics, 36(1), pp. 34–43.

Lengyel, B. A. (1962) 'Lasers: generation of light by stimulated emission'. Wiley.

Lethien, C. *et al.* (2011) 'Exploit the bandwidth capacities of the perfluorinated graded index polymer optical fiber for multi-services distribution', *Polymers*. Molecular Diversity Preservation International, 3(3), pp. 1006–1028.

Li, C. *et al.* (2008) 'Monitoring second lining of tunnel with mounted fiber Bragg grating strain sensors', *Automation in Construction*. Elsevier, 17(5), pp. 641–644.

Li, D. S. *et al.* (2012) 'Structural health monitoring of a tall building during construction with fiber Bragg grating sensors', *International Journal of Distributed Sensor Networks*. SAGE Publications Sage UK: London, England, 8(10), p. 272190.

Li, Z. *et al.* (2018) 'Temperature and Strain Discrimination in BOTDA Fiber Sensor by Utilizing Dispersion Compensating Fiber', *IEEE Sensors Journal*. IEEE, 18(17), pp. 7100–7105.

Li, Z. *et al.* (2019) 'A high sensitivity temperature sensing probe based on microfiber Fabry-Perot interference', *Sensors*. Multidisciplinary Digital Publishing Institute, 19(8), p. 1819.

Li, Z., Askim, J. R. and Suslick, K. S. (2018) 'The optoelectronic nose:

colorimetric and fluorometric sensor arrays', *Chemical reviews*. ACS Publications, 119(1), pp. 231–292.

Liao, C. R. and Wang, D. N. (2013) 'Review of femtosecond laser fabricated fiber Bragg gratings for high temperature sensing', *Photonic Sensors*. Springer, 3(2), pp. 97–101.

Lorentz, H. A. (1916) *The Theory of Electrons and Its Applications to the Phenomena of Light and Radiant Heart: A Course of Lectures Delivered in Columbia University, New York in March and April, 1906*. Teubner.

Lu, P. *et al.* (2019) 'Distributed optical fiber sensing: Review and perspective', *Applied Physics Reviews*. AIP Publishing LLC, 6(4), p. 41302.

MacDonald, D. K. C. (2006) *Thermoelectricity: an introduction to the principles*. Courier Corporation.

Maiman, T. H. (1960) 'Stimulated optical radiation in ruby', *nature*. Nature Publishing Group, 187(4736), pp. 493–494.

Al Mamun, M. A. and Yuce, M. R. (2019) 'Sensors and systems for wearable environmental monitoring toward iot-enabled applications: A review', *IEEE Sensors Journal*. IEEE, 19(18), pp. 7771–7788.

Marini, D., Iuliano, M., *et al.* (2018) 'BOTDA sensing employing a modified Brillouin fiber laser probe source', *Journal of Lightwave Technology*. IEEE, 36(4), pp. 1131–1137.

Marini, D., Rossi, L., *et al.* (2018) 'Tunable lower-RIN Brillouin fiber ring laser for BOTDA sensing', in *CLEO: QELS_Fundamental Science*. Optical

Society of America, pp. JW2A-166.

Matsumoto, T., Kishi, M. and Hotate, K. (2014) 'Discriminative and distributed measurement of temperature and strain with time-division pump-probe-read light generation by single laser diode in simplified BOCDA system', in *23rd International Conference on Optical Fibre Sensors*. International Society for Optics and Photonics, p. 91573W.

Mishra, A., Varun, M. K. and Pant, R. (2019) 'Stimulate Brillouin scattering based slow light at 2μm', in *Frontiers in Optics*. Optical Society of America, pp. JTu4A-61.

Mohammed, N. A. *et al.* (2020) 'Malaria biosensors with ultra-sensitivity and quality factor based on cavity photonic crystal designs', *The European Physical Journal Plus*. Springer, 135(11), pp. 1–22.

Mueller, H. (1935) 'Theory of the photoelastic effect of cubic crystals', *Physical review*. APS, 47(12), p. 947.

Okawachi, Y. *et al.* (2005) 'Tunable all-optical delays via Brillouin slow light in an optical fiber', *Physical review letters*. APS, 94(15), p. 153902.

Prod'homme, L. (1960) 'A new approach to the thermal change in the refractive index of glasses', *Phys. Chem. Glasses*, 1(4), pp. 119–122.

Qian, K. *et al.* (2019) 'Enhanced sensitivity of fiber laser sensor with Brillouin slow light', *Optics express*. Optical Society of America, 27(18), pp. 25485–25492.

Qiao, X. *et al.* (2017) 'Fiber Bragg grating sensors for the oil industry',

Sensors. Multidisciplinary Digital Publishing Institute, 17(3), p. 429.

Rakow, N. A. and Suslick, K. S. (2000) 'A colorimetric sensor array for odour visualization', *Nature*. Nature Publishing Group, 406(6797), pp. 710–713.

Rayleigh, Lord (1877) 'Theory of Sound f 109', *Ed*, 1, p. 93.

Ren, L. *et al.* (2006) 'Health monitoring system for offshore platform with fiber Bragg grating sensors', *Optical Engineering*. International Society for Optics and Photonics, 45(8), p. 84401.

Ruiz-Lombera, R. *et al.* (2018) 'Feasibility Study of a Fiber Ring Laser Working on the SLM Regime in a BOTDA Sensor', *IEEE Sensors Journal*. IEEE, 18(12), pp. 4947–4953.

Rush, R. M. and Yoe, J. H. (1954) 'Colorimetric Determination of Zinc and Copper with 2-Carboxy-2-hydroxy-5-sulfoformazylbenzene', *Analytical Chemistry*. ACS Publications, 26(8), pp. 1345–1347.

Schulz, S. A. *et al.* (2017) 'Photonic crystal slow light waveguides in a kagome lattice', *Optics letters*. Optical Society of America, 42(16), pp. 3243–3246.

Shafkat, A. *et al.* (2021) 'Design and analysis of a single elliptical channel photonic crystal fiber sensor for potential malaria detection', *Journal of Sol-Gel Science and Technology*. Springer, 98(1), pp. 202–211.

El Shamy, R. S., Khalil, D. and Swillam, M. A. (2020) 'Mid infrared optical gas sensor using plasmonic Mach-Zehnder interferometer', *Scientific reports*. Nature Publishing Group, 10(1), pp. 1–9.

Shee, Y. G. *et al.* (2010) ‘All-optical generation of a 21 GHz microwave carrier by incorporating a double-Brillouin frequency shifter’, *Optics letters*. Optical Society of America, 35(9), pp. 1461–1463.

Shen, Y. R. and Yang, G.-Z. (2016) ‘Theory of self-phase modulation and spectral broadening’, in *The Supercontinuum Laser Source*. Springer, pp. 1–32.

Shupe, D. M. (1980) ‘Thermally induced nonreciprocity in the fiber-optic interferometer’, *Applied optics*. Optical Society of America, 19(5), pp. 654–655.

Silva-Muñoz, R. A. and Lopez-Anido, R. A. (2009) ‘Structural health monitoring of marine composite structural joints using embedded fiber Bragg grating strain sensors’, *Composite Structures*. Elsevier, 89(2), pp. 224–234.

Song, K. Y., Herráez, M. G. and Thévenaz, L. (2005) ‘Observation of pulse delaying and advancement in optical fibers using stimulated Brillouin scattering’, *Optics Express*. Optical Society of America, 13(1), pp. 82–88.

Song, K. Y. and Hotate, K. (2007a) ‘25 GHz bandwidth Brillouin slow light in optical fibers’, *Optics letters*. Optical Society of America, 32(3), pp. 217–219.

Song, K. Y. and Hotate, K. (2007b) ‘Distributed fiber strain sensor with 1-kHz sampling rate based on Brillouin optical correlation domain analysis’, *IEEE Photonics Technology Letters*. IEEE, 19(23), pp. 1928–1930.

Soto, M. A. *et al.* (2012) ‘Optimization of a DPP-BOTDA sensor with 25 cm spatial resolution over 60 km standard single-mode fiber using Simplex codes

and optical pre-amplification', *Optics express*. Optical Society of America, 20(7), pp. 6860–6869.

Suthar, H. A. and Gadit, J. J. (2012) 'Low Cost Signal Conditioning Technique for RTD Measurement.', *International Journal of Nano Device, Sensor and Systems*. IAES Institute of Advanced Engineering and Science, 1(1), p. 19.

Szabó, R., Gontean, A. and Lie, I. (2012) 'Surface temperature measurement with thermocouple matrix using a switch control unit', in *2012 IEEE 18th International Symposium for Design and Technology in Electronic Packaging (SIITME)*. IEEE, pp. 283–288.

Tam, H. Y. *et al.* (2007) 'Utilization of fiber optic Bragg Grating sensing systems for health monitoring in railway applications', *Struct. Health Monitoring, Quantification, Validation, Implementation*, 1(2).

Tan, C. H. *et al.* (2016) 'Fiber Bragg grating based sensing system: Early corrosion detection for structural health monitoring', *Sensors and Actuators A: Physical*. Elsevier, 246, pp. 123–128.

Tan, C. Z. (1998) 'Review and analysis of refractive index temperature dependence in amorphous SiO2', *Journal of non-crystalline solids*. Elsevier, 238(1–2), pp. 30–36.

Tan, C. Z., Arndt, J. and Xie, H. S. (1998) 'Optical properties of densified silica glasses', *Physica B: Condensed Matter*. Elsevier, 252(1–2), pp. 28–33.

Tang, M. *et al.* (2018) 'SNR Enhanced fast BOTDA Combining Channel

Estimation Technique with Complementary Pulse Coding', *IEEE Photonics Journal*. IEEE.

Tennyson, R. C. *et al.* (2001) 'Structural health monitoring of innovative bridges in Canada with fiber optic sensors', *Smart materials and Structures*. IOP Publishing, 10(3), p. 560.

Thames, L. and Schaefer, D. (2017) 'Industry 4.0: an overview of key benefits, technologies, and challenges', in *Cybersecurity for Industry 4.0*. Springer, pp. 1–33.

Thévenaz, L. (2008) 'Slow and fast light in optical fibres', *Nature photonics*. Nature Publishing Group, 2(8), p. 474.

Tong, M., Tham, L. G. and Au, F. T. K. (2002) 'Extreme thermal loading on steel bridges in tropical region', *Journal of Bridge Engineering*. American Society of Civil Engineers, 7(6), pp. 357–366.

Turkani, V. S. *et al.* (2018) 'Nickel based printed resistance temperature detector on flexible polyimide substrate', in *2018 IEEE SENSORS*. IEEE, pp. 1–4.

Turner, R. D. *et al.* (1990) 'Fiber-optic strain sensors for smart structures', *Journal of Intelligent Material Systems and Structures*. Sage Publications Sage CA: Thousand Oaks, CA, 1(1), pp. 26–49.

Wang, F. *et al.* (2013) 'Improvement of spatial resolution for BOTDR by iterative subdivision method', *Journal of lightwave technology*. IEEE, 31(23), pp. 3663–3667.

Wang, F. *et al.* (2019) ‘Improved spectral performance of fiber sensor using Brillouin slow light’, in *2019 18th International Conference on Optical Communications and Networks (ICOCN)*. IEEE, pp. 1–3.

Wang, L. *et al.* (2011) ‘Stimulated Brillouin scattering slow-light-based fiber-optic temperature sensor’, *Optics letters*. Optical Society of America, 36(3), pp. 427–429.

Wang, L. *et al.* (2013) ‘Distributed Temperature Sensing Using Stimulated-Brillouin-Scattering-Based Slow Light’, *IEEE Photonics Journal*. IEEE, 5(6), p. 6801808.

Weber, H., Thiel, U. and Bauschke, D. W. (2011) ‘High vibration thin film RTD sensor’. Google Patents.

Wen, H. *et al.* (2011) ‘Sensing with slow light in fiber Bragg gratings’, *IEEE Sensors Journal*. IEEE, 12(1), pp. 156–163.

Wosniok, A. *et al.* (2013) ‘L-BOFDA: a new sensor technique for distributed Brillouin sensing’, in *Fifth European Workshop on Optical Fibre Sensors*. International Society for Optics and Photonics, p. 879431.

Woyessa, G. *et al.* (2016) ‘Temperature insensitive hysteresis free highly sensitive polymer optical fiber Bragg grating humidity sensor’, *Optics express*. Optical Society of America, 24(2), pp. 1206–1213.

Woyessa, G. *et al.* (2017) ‘Zeonex microstructured polymer optical fiber: Fabrication friendly fibers for high temperature and humidity insensitive Bragg grating sensing’, *Optical Materials Express*. Optical Society of

America, 7(1), pp. 286–295.

Wu, Hao *et al.* (2018) ‘Real-Time Denoising of Brillouin Optical Time Domain Analyzer with High Data Fidelity Using Convolutional Neural Networks’, *Journal of Lightwave Technology*. IEEE.

Wu, Huan *et al.* (2018) ‘Support Vector Machine based Differential Pulse-width Pair Brillouin Optical Time Domain Analyzer’, *IEEE Photonics Journal*. IEEE, 10(4), pp. 1–11.

Xie, S. *et al.* (2012) ‘Polarization dependence of Brillouin linewidth and peak frequency due to fiber inhomogeneity in single mode fiber and its impact on distributed fiber Brillouin sensing’, *Optics express*. Optical Society of America, 20(6), pp. 6385–6399.

Xie, Y., Zhang, M. and Dai, D. (2020) ‘Design rule of Mach-Zehnder interferometer sensors for ultra-high sensitivity’, *Sensors*. Multidisciplinary Digital Publishing Institute, 20(9), p. 2640.

Xu, Y. L. *et al.* (2010) ‘Monitoring temperature effect on a long suspension bridge’, *Structural Control and Health Monitoring*. Wiley Online Library, 17(6), pp. 632–653.

Yamauchi, T. and Hotate, K. (2004) ‘Distributed and dynamic strain measurement by BOCDA with time-division pump-probe generation scheme’, in *Conference on Lasers and Electro-Optics*. Optical Society of America, p. CWA57.

Yan, S. Z. and Chyan, L. S. (2010) ‘Performance enhancement of BOTDR

fiber optic sensor for oil and gas pipeline monitoring', *Optical Fiber Technology*. Elsevier, 16(2), pp. 100–109.

Yoshizawa, N. and Imai, T. (1993) 'Stimulated Brillouin scattering suppression by means of applying strain distribution to fiber with cabling', *Journal of Lightwave Technology*. IEEE, 11(10), pp. 1518–1522.

Yuan, W. *et al.* (2011) 'Humidity insensitive TOPAS polymer fiber Bragg grating sensor', *Optics express*. Optical Society of America, 19(20), pp. 19731–19739.

Zadok, A., Eyal, A. and Tur, M. (2011) 'Stimulated Brillouin scattering slow light in optical fibers', *Applied Optics*. Optical Society of America, 50(25), pp. E38–E49.

Zan, M. S. D. Bin and Horiguchi, T. (2012) 'A dual Golay complementary pair of sequences for improving the performance of phase-shift pulse BOTDA fiber sensor', *Journal of lightwave technology*. IEEE, 30(21), pp. 3338–3356.

Zeldovich, I. A. *et al.* (1985) 'Mathematical theory of combustion and explosions'. Consultants Bureau, New York, NY.

Zhang, J., Hernandez, G. and Zhu, Y. (2008) 'Slow light with cavity electromagnetically induced transparency', *Optics letters*. Optical Society of America, 33(1), pp. 46–48.

Zhang, S. *et al.* (2008) 'Plasmon-induced transparency in metamaterials', *Physical review letters*. APS, 101(4), p. 47401.

Zhao, Y. *et al.* (2009) 'New mechanisms of slow light and their applications',

Optics & Laser Technology. Elsevier, 41(5), pp. 517–525.

Zhao, Y., Qin, C. and Wang, Q. (2014) 'Principles of structural slow light and its applications for optical fiber sensors: a review', *Instrumentation Science & Technology*. Taylor & Francis, 42(1), pp. 72–94.

Zhao, Y., Zhang, Y. and Wang, Q. (2012) 'High sensitivity gas sensing method based on slow light in photonic crystal waveguide', *Sensors and Actuators B: Chemical*. Elsevier, 173, pp. 28–31.

Zhou, Z. *et al.* (2003) 'Techniques of advanced FBG sensors: Fabrication, demodulation, encapsulation, and their application in the structural health monitoring of bridges', *Pacific Science Review*, 5(1), pp. 116–121.

Zhu, T. *et al.* (2007) 'Strain sensor without temperature compensation based on LPFG with strongly rotary refractive index modulation', *Electronics Letters*. IET, 43(21), pp. 1132–1134.

Zou, W., Long, X. and Chen, J. (2015) 'Brillouin Scattering in Optical Fibers and Its Application to Distributed Sensors', *Intech: Advances in Optical Fiber Technology: Fundamental Optical Phenomena and Applications*, pp. 1–53.

LIST OF PUBLICATIONS

International Journals

Pang, W.S., Shee, Y.G., Rahman, F.A., Adikan, F.R.M. and Mahdi, M.A., 2020. Enhanced sensitivity temperature sensing based on second order Brillouin slow light. Optik, 228, p.166146.

Conference Papers

Pang, W.S., Shee, Y.G., Rahman, F.A., Adikan, F.M. and Mahdi, M.A., 2018, November. Post-Amplified Reversed S-shaped Brillouin-erbium Fiber Laser. In 2018 IEEE Student Conference on Research and Development (SCOReD) (pp. 1-4). IEEE.